THE RELATIVE DEGREE OF CONTROLLABILITY OF SOLAR SAILS IN ARTIFICIAL LAGRANGIAN ORBITS

MEENA FARAG

A THESIS SUBMITTED TO
THE FACULTY OF GRADUATE STUDIES
IN PARTIAL FULFILLMENT OF THE REQUIREMENTS FOR THE DEGREE OF
MASTER OF SCIENCE

GRADUATE PROGRAM IN EARTH AND SPACE SCIENCE
YORK UNIVERSITY
TORONTO, ONTARIO

NOVEMBER 2017

© MEENA FARAG, 2017

Abstract

The problem of orbital controllability of solar sails in artificial Lagrangian orbits (ALOs) has received little attention from academics in the field of control. As a result, an important property for missions involving ALOs has not yet been investigated; namely, the degree of controllability (DOC). This thesis examines the relative degree of orbital controllability of solar sails in artificial Lagrangian orbits using the singular values of the controllability Gramian. The relative degree of controllability is determined by comparing the condition number of the controllability Gramian corresponding to individual ALOs. The finite time controllability Gramian is computed for the unstable system, and the magnitude of the individual singular values are used to determine the relative potential for control. Regions of potential for control are revealed for the Earth-Sun system; particularly near the Earth. No conclusions are made regarding absolute controllability, nor is an exact measure of controllability computed for arbitrary ALOs.

Acknowledgements

The research presented in this thesis is the product of two years worth of efforts geared towards learning about solar sails and control systems. Prior to meeting my supervisor, Dr. George Vukovich, I did not have much familiarity with either subject. Dr. Vukovich's remarkable knowledge of control systems is what first sparked my interest in the field. Over the past several years he has been extremely supportive and helpful to a capacity in which I could not have expected from any professor. I would like to thank Dr. Vukovich for all his efforts towards guiding me through my graduate research, and for the opportunity to learn about control theory from a true expert in the field.

I would also like to thank Dr. Regina Lee, who did not hesitate to join my supervisory committee on very late notice. Dr. Lee has always been willing to step in and help with any matters she could; for this I am very grateful.

My fellow colleague and friend, Lucien Gatien, has been a great help throughout my graduate studies. We have both benefited greatly through our shared interest of control systems and developed a great friendship. I am thankful for all his support and wish him the best of luck in all his future endeavors.

Finally, I would like to thank my family, who have encouraged me to pursue a higher education without any pressure. Their support over the years has been a strong motivation for me to further my education through higher learning.

Table of Contents

List of Tables

List of Figures

1. Introduction

Solar sails are unique, propellantless spacecraft which use the pressure from light to accelerate and traverse through space. The idea of a spacecraft gaining thrust from light is an old one, but solar sails are not a mature technology. Though real difficulties exist due to the design complexity of sailcraft, their photon induced thrust makes them serious candidates for missions that are currently impossible with conventional spacecraft. The constant solar radiation pressure (SRP) from the Sun – though vanishingly small – is large enough to perturb the orbits of conventional spacecraft[1]. This seemingly insignificant force is exploited by the highly reflective, lightweight satellite, and is capable of accelerating to unprecedented spacecraft velocities, or resting in a continuum of otherwise impossible equilibria. A solar sail performs orbital maneuvers by varying its orientation angles as well as furling and unfurling its large thin mirror-like film. This thesis examines the relative orbital controllability of sailcraft in artificial Lagrangian orbits (ALOs). ALOs are volumes of equilibrium points, which are extensions of the equilibria of the Circular Restricted Three-Body Problem (CRTBP). Attitude control is not examined in this study; some relevant papers on this subject are introduced for the reader in section 1.2 as a general background on solar sail development. The purpose of this study is to examine measures of assessing the potential for control, without consideration of methods of control, which is a vast subject on its own. The former study is a prerequisite for the latter.

1.1 A Brief History of Solar Sailing

Since the inception of spaceflight worldwide it has depended entirely on chemical propulsion systems, but the potential benefits of solar sail propulsion have caused the space community to take what was originally science fiction seriously. Despite the fact that solar sails are not yet a mature technology, they have been considered serious candidates for certain space missions for nearly half a century. As early as the 1970s, NASA considered using solar sails for a rendezvous mission with Halley's Comet in its 1986 flyby of Earth[2, 3]. However, this mission lacked sufficiently developed technology, so it was scrapped. More recent endeavors have confirmed the viability of solar sailing.

ZNAMYA

The Znamya project was conducted by the Russian Space Agency as a series of experimental orbital mirrors, designed to illuminate parts of the Earth by reflecting sunlight. Znamya-1 was a ground engineering test model that never flew in space, but Znamya-2 was successfully deployed on February 4th, 1993, next to the Russian Mir space station. The $20\ m$ round sail was able to produce a $5\ km$ wide bright spot, with a luminosity equivalent to that of a full moon over Europe for several hours before deorbiting in atmospheric re-entry over Canada[4]. The successful spin deployment and flight of Znamya-2 was a demonstration of one of the most vexing problems of solar sailing, namely, deployment. A $25\ m$ round sail called Znamya-2.5 was deployed on February 5th, 1999, and expected to produce a $7\ km$ wide bright spot with a luminosity of about eight moons. However, the mirror was torn after being caught on an antenna of the Mir space station. It was then deorbited and burned up on re-entry[4, 5].

IKAROS

Possibly the most successful demonstration of solar sailing technology comes from the Japan Aerospace Exploration Agency (JAXA) for their successful mission to Venus using their IKAROS solar sail. Launched by JAXA on May 21st, 2010, the $14\ m\ \times\ 14\ m$ square sail was successful in demonstrating solar photon pressure acceleration and control as it flew by Venus at an accumulated speed of $100\ m/s$ on December 8, 2010; roughly six months after its deployment[6]. Since the mission was completed, IKAROS has gone into hibernation mode, but has been waking up intermittently[7]. This interplanetary success story remains one of the most persuasive missions for solar sailing critics as it very strongly demonstrates the practicality of photon induced thrust for spacecraft.

NANOSAIL-D

The first flight demonstration of solar sails for Nanosatellites comes from NanoSail-D[8]. NanoSail-D was to have been operated in Low Earth Orbit (LEO), but was lost during launch due to rocket failure. More success came from NanoSail-D2, which was built as a ground spare for Nanosail-D. The $10\ m^2$ square sail was successfully launched on November 19, 2010 and

deployed on January 17, 2011[9]. The sail's purpose was to demonstrate deorbiting capabilities that could be used to bring down decommissioned satellites and space debris. NanoSail-D2 failed to separate from FASTSAT on the expected date, but was successfully ejected about a month later. After 240 days in LEO, NanoSail-D2 successfully completed its Earth orbiting mission and re-entered Earth's atmosphere, having demonstrated deorbiting capabilities of large low mass high surface area spacecraft.

DEORBITSAIL

Another LEO operating nanosail is the DeorbitSail; a 3U CubeSat using Carbon-Fibre Reinforced Plastic (CFRP) booms to deploy the $25\ m^2$ square sail[10]. The nanosail was designed and built by the Surrey Space Centre at the University of Surrey. As the name suggests, the purpose of this nanosail was to demonstrate a sailcraft's ability to rapidly deorbit using aerodynamic drag. The deorbiting device was expected to be effective at altitudes below $1000\ km$, whereas above $1000\ km$, the same design would be capable of using SRP as a deorbiting force[10]. DeorbitSail was successfully launched and put into orbit on July 10, 2015. Though some mission objectives were met, the Attitude Determination and Control System (ADCS) of the sail was unable to accurately determine the satellite's tumble rate, or get it under control. The satellite experienced very high initial spin rates which is believed to have been caused by inherent magnetic characteristics. Despite several attempts, deployment of the sail could not be achieved, which was believed to be due to a physical disconnection of the motor cables[10].

SUNJAMMER

The development of another NASA mission for a much larger sail, constructed by LGarde, was anticipated to launch in January, 2015 aboard a SpaceX Falcon 9 rocket. Sunjammer, named after the title of a short story written by Arthur C. Clarke in 1964, has a surface area of approximately $1200\ m^2$ and weighs only 32 kg[11]. Attitude control was to be achieved through the use of gimballed vanes located at the tips of each of the satellite's four booms. Sunjammer was the world's largest solar sail to date, and would have been the largest structure ever to have been deployed in space. It was intended to be a demonstration craft for studying the Sun, and to aid in future early-warning systems for space weather. Although successful (ground) deployment

of the sail was achieved, NASA abandoned the flight in 2015 due to a lack of confidence in its contractor's ability to deliver.

1.2 Contributions to Solar Sail Technology

There have been a number of contributions to the research and development of solar sailing technology in the past two decades. This thesis will only address one important aspect of solar sails – namely, orbital controllability of ALOs. Outside of this problem, there are many other applications of solar sails that have been explored; several examples follow:

SOLAR POLAR IMAGER

One of several studied Sun-Earth missions involving solar sails is the Solar Polar Imager (SPI) mission. The purpose of this mission is to explore the dynamics and structure of the solar corona and reveal information about the origins of solar activity and solar cycles. The proposed solar sail design in this study is a $160\ m\ \times\ 160\ m$ square sail with a total mass of $450\ kg$ and a sail film temperature limit of $100℃$ [12,13]. The target orbit for the SPI is a circular orbit at a solar distance of $0.48\ au$, which the study shows would take 6.7 years. Other trajectories in this study have been shown to approach the Sun closer (to about $0.4\ au$). It was also shown that increasing the limit of the sail temperature to $240℃$ means an optimal transfer trajectory approaches the Sun at about $0.22\ au$, resulting in an even shorter transfer duration of 4.7 years[14]. Sail orbits would be controlled by variations to the sail's orientation, allowing more or less incident light on the sail. Though many factors affect controllability, it is important to examine controllability as a function of solar distance, given that the source of its input – namely, SRP – is itself a function solar distance.

PERIODIC ORBITS ABOVE THE ECLIPTIC

Little of the work produced on solar sails deals with applications in artificial Lagrangian orbits since solar sailing is still very much in the concept development stage, i.e. proof of concept for sail propulsion, deployment, and control. Among the few exceptions is the work of Thomas J. Waters and Colin R. McInnes, who have considered orbits about equilibrium points in the Earth-Sun rotating frame, high above the ecliptic plane, for potential 'polesitter' missions. Such high latitude missions entail "parking" a solar sail at an ALO above the Earth for constant observation

of its poles. The authors were able to demonstrate that there is freedom in choosing the position and period of the sail orbit; this is particularly useful for a polar observer because the orientation of the Earth's axis of rotation varies over the course of a year. By choosing large amplitude periodic orbits for the sail, a continuous view of the poles is achieved. Their result was a closed orbit with a one year period for an ALO in the Earth-Sun rotating frame with positions $x = 0.9895\ au,\ z = 0.0078\ au$[15]. This ALO was chosen for its sail quality parameter, or sail lightness number; these are terms which will be defined later. In Chapter 3 it will be shown that this equilibrium point falls in a relatively controllable region as defined by the condition number of the controllability Gramian. This particular method for a polesitter mission is a significant improvement compared to orbital regulation of the sail.

SOLAR SAIL ATTITUDE CONTROL

An important prerequisite for the orbital controllability of solar sails is the assumption that the sail's attitude is highly controllable. The validation of sail attitude stability and thrust-vector pointing was investigated in a study by Bong Wie for a $160\ kg$, $40\ m \times 40\ m$ square sail configuration[16,17]. Though selecting a particular configuration is mission specific, a square sail is a likely candidate for various sail missions[18-22]. To control the attitude of a three-axis stabilized sailcraft, a two-axis gimballed control boom and control vanes were used to counter the significant solar-pressure disturbance torque. In this thesis, orbital controllability will be examined using both inputs to sail attitude as well as varying the sail area. Though the latter control element is more difficult to implement, it is not neglected in this investigation.

SOLAR SAIL TECHNOLOGY FOR NANOSATELITES

A fundamental consideration for sailing is the area-to-mass ratio for the momentum of electromagnetic radiation to produce significant thrust. The larger the area-to-mass ratio of the solar sail, the greater its acceleration. The sail size is to be as large as possible so as to compensate for the spacecraft's mass. However, the opposite has also been considered. Though less capable than conventional spacecraft, nanosatellites offer an attractive solution to the area-to-mass ratio problem by drastically reducing the payload mass, and thereby decreasing demands on sail size. For this reason, many of the solar sails which have been studied or developed recently are nanosails; e.g. Nanosail-D, DeorbitSail, CubeSail, LightSails-1&2, and SailSat.

Michael D. Souder and Matthew West introduced preliminary designs for a nanosail called SailSat, along with suggested applications including a Low Earth Orbit demonstration mission. SailSat is a 3U CubeSat intended for deployment from California Polytechnic State University's Poly Picosatellite Orbital Deployer (P-POD)[23]. The square sail – designed by the solar sailing nanosatellite group at Stanford University – was chosen over the heliogryo or spinning sail types due to its simplicity in control. Square sails are more difficult to deploy since they rely on unfurling booms, and not centripetal acceleration. Apart from sail size, extremely lightweight, thin, and highly reflective materials are desired to maximize momentum transfer. A Kapton-like film called CP1, having a density of only $5\ g/m^2$ is a polyimide that can incorporate both a highly reflective surface and rip stop properties, and has a thickness of only 2.5 microns[24]. The study also included an analysis of attitude control driven by magnetic torque coils and momentum wheels used to change sail orientation with respect to the Sun.

ELECTRON RADIATION EFFECTS ON CANDIDATE SOLAR SAIL MATERIAL

Another critical area of study regarding the development of sail technology is sail material. In this paper, an idealized perfectly reflecting solar sail is assumed for simplicity. In reality there are many factors to consider when deciding on the material of a sail. In studying such materials several characteristics should be considered, such as reflectivity, weight, thickness, resistance to heat, and rip stop properties. In one such study, Edwards et al. examined several candidate materials to determine which could best withstand the rigors of the space environment[25]. The materials investigated included 2.0 micron Mylar with aluminum coating, 2.0 micron Mylar without coating, and 2.0 Teonex with aluminum coating. These materials have an areal density of just a few grams per square meter. It was found that Mylar and Teonex were able to survive significant doses of electron radiation under high uniaxial stress, which concludes that survivable solar sail missions are at least possible from a materials survivability standpoint.

MARS MISSIONS

Most solar sails have been demonstration LEO nanosatellites, primarily because there is still much to learn about sailing. With the success of IKAROS, and the increased interest shown in Mars, it is not surprising that solar sails are being considered for the interplanetary mission. A study performed by Science Application International Corporation (SAIC) and British Aerospace

Marconi Electronic (BAE) Systems under contract with the NASA Marshall Space Flight Center (MSFC) explored possible Mars missions using sailcraft. Considering Earth-to-Mars trips, and taking into consideration characteristics of the solar sail, results favoured a ballistic trajectory over Hohmann-A transfers and Sundiver transfers[26,27]. Transfer times were shown to be shorter than most Hohmann type 1 trajectories used by current chemical systems. The study also addresses the issue of capture techniques at Mars using sail aerocapture, i.e. using solar sails for aerobraking. This study opens the door to a much broader band of possible missions for solar sails.

Though the validity of solar sailing has been confirmed by several successful flights, there are many aspects of solar sailing technology that have not yet been thoroughly examined. The analysis of a sail's degree of orbital controllability is an important characteristic that has received virtually no attention thus far. The degree of controllability is a rather nebulous area of control systems since there is no clearly defined scheme for determining such a property. There has been a significant amount of development on various measures of controllability – which will be introduced in Chapter 3. After exploring some of these methods, it will be shown that the singular values of the controllability Gramian can provide a physically meaningful interpretation of relative controllability, particularly for the orbital control of solar sails in ALOs. An understanding of a sail's degree of controllability is indispensable for any practical application. Whether it's controlling a halo orbit or chasing a comet, knowledge of controllability is essential to all space missions.

Chapter 2 investigates the Modified Circular Restricted Three-Body Problem (MCRTBP) for the Earth-Sun system. Unlike the five classical Lagrange points resulting from two primaries, the acceleration due to SRP on the third (infinitesimal) mass – caused by a single luminous body – creates an infinite set of new solutions known as the artificial Lagrangian orbits. This infinite set of solutions is represented by a continuum of equilibria with various degrees of instability. The local behavior of the system is then determined by first developing a simple linear model. Simulations are produced using initial conditions based on the linear approximation, which accurately describes the local behavior of the nonlinear system, and reveals that the equilibria are generally unstable[28]. Chapter 3 introduces various methods for determining controllability, and

shows that although ALOs are unstable, they are completely controllable via the rank test on the controllability matrix using variations to the sail's attitude and area. These control elements are used to produce various control configurations for planar ALOs to demonstrate controllability using the binary definition of control. For example, determining if the controllability matrix is full rank (completely controllable) using only one, two, or three inputs to the system. However, the validity of the rank test on determining whether or not a system is controllable is further examined by considering the system's nearness to rank deficiency. Definitions for the degree of controllability are examined to verify that given a finite period of time, the system can be driven from some arbitrary initial state to an arbitrary final state. The binary definition of controllability does not include any information regarding the time and energy required for the state transfer; which are two of the most important factors in any practical application. A measure for the degree of controllability is examined using the singular values of the controllability Gramian. The merit of using certain control configurations is evaluated by comparing the minimum energy required to transfer states. Also examined is the controllability, or reachability, of the system along various directions in state-space, beginning from a zero-state initial condition. In Chapter 4 simulations are produced using a minimum energy controller to show the impact of the diverging singular values on control difficulty, and confirm the relative degree of controllability proposed in the previous chapter. Concluding remarks on the presented material, as well as suggested directions of research for future work are presented in Chapter 5.

1.3 Previous Work

This thesis straddles and draws on primarily two areas: controllability measures from system theory, and solar sail dynamics. As mentioned earlier, there has been a substantial amount of work on the first, and the relevant literature from this area is reviewed in Chapter 3. The dynamics of solar sails is an area that still requires much work. Colin R. McInnes is a pioneer in the research and development of solar sails, and has covered many aspects of solar sailing, including solar sail dynamics and construction. Colin R. McInness has investigated the existence, as well as the nature, of the artificial Lagrangian orbits using the MCRTBP– introduced in Chapter 2. This was done using an ideal perfectly reflecting solar sail and a linearized model of the equations of motion for the Earth-Sun system. McInnes was able to demonstrate that there is an infinite set of equilibrium solutions to the circular restricted three-body problem when the

acceleration due to solar radiation pressure from the first primary is included in the equations of motion. Furthermore, McInnes showed that the artificial Lagrangian orbits are generally unstable through the application of the Routh-Hurwitz critereon. He has also shown that these equilibria are completely controllable through the application of the rank test on the controllability matrix using inputs to the sails attitude.

The main subject of this thesis is the degree of controllability of solar sail spacecraft. There is no review of previous work in this area because, to the best of the author's knowledge, there has been no substantial work on this subject prior to this thesis.

1.4 Problem Statement

The degree of orbital controllability of solar sails in the artificial Lagrangian orbits is a difficult problem to resolve due to the nature of the problem itself. There are volumes of ALOs in the Earth-Sun system as will be demonstrated in Chapter 2, which means there is an infinite set of equilibrium points to examine. Rather than arbitrarily selecting an ALO to investigate, the problem can be simplified by describing ALOs in terms their relative DOC. Some ALOs exist only as theoretical equilibrium points for sails with an area-to-mass ratio that is so large, they would be physically impossble to design, or control. Other ALOs exist in regions where solar sail flight is physically impossible, e.g. too close to the Sun; these examples are simply disregarded in this thesis. It is more meaningful to consider information regarding which – more seemingly practical – ALOs are feasible for solar sail flight.

The objective of this thesis is to demonstrate the relative degree of controllability of solar sails in various artificial Lagrangian orbits using an energy-related measure. A quantitative measure of controllability can be difficult to express for any dynamical system, but a meaningful measure is one which describes the difficulty of control in terms of energy. Various measures of controllability are described in the controllability literature review section of Chapter 3. The measure that will be used to accomplish the objective in this thesis is the energy-related measure derived from the controllability Gramian. This measure will be used to demonstrate the relative difficulty of control for ALOs in the Earth-Sun system.

First, the reliability of the rank test will be examined by considering various controllable configurations which are full rank. The condition number of the controllability Gramian will then

be used to provide information on rank deficiency based on each configuration. The condition number will also be used to demonstrate regions of equilibrium points that are theoretically more controllable than other regions of equilibria. Relative controllability will be defined through the Gramian's condition number, which will indicate the degree of controllability based on the location of each ALO in the Earth-Sun system. This is not a measure of absolute controllability, and no conclusions are made on whether or not solar sails are truly controllable at any ALO. A minimum energy controller will also be implemented to verify that the regulation of solar sails is possible using variations in sail attitude and area. In order to confirm the results, the minimum energy controller is implemented using arbitrarily selected ALOs – based on their corresponding controllability Gramian's condition number. Minimum energy controllers are controllers that use the minimum energy required to complete a specific control task. This means that given some bound on energy, the controller should fail at an ALO that requires more energy to regulate the sail. Since this thesis looks at controllability in a relative sense, the specific bound on minimum energy is not important and is also somewhat arbitrarily selected. The purpose of the simulations are to demonstrate the relative DOC of solar sails in terms of the minimum energy required for regulation.

1.5 Summary of Results

In Chapter 3, it is shown that a solar sail can be controlled using one, two, or three inputs in the xz plane (the plane perpendicular to the ecliptic in the Earth-Sun rotating frame). This is confirmed through the rank test on the controllability matrix. However, this test is a poor indicator of controllability. The condition number of the controllability Gramian is largely affected by the removal or addition of certain control elements (see Tables 3.2.2a-e). In the case where only one control element is used, the true rank of the controllability Gramian is arguably 4, i.e not full rank, which implies the system is not controllable. It was also shown that the minimum energy required to regulate a sail using two inputs is much greater than when using three inputs. This is demonstrated in Chapter 3 by plotting the minimum energy as a function of time (see Figure 3.4.1).

The condition number of the controllability Gramian is also used to demonstrate relative controllability as a function of the ALO's position in the rotating frame. It was found that ALOs near the primaries are more difficult to control; especially near the ecliptic plane (see Figures

3.3.1). This is likely due to gravitational effects near the primaries, which also increases the instability of ALOs in these regions. Figures (3.3.1) clearly illustrate the relative controllability of all ALOs in the Earth-Sun system based on the size of the controllability Gramian. In order to expand on these results, a minimum energy controllability ellipse was implemented for three arbitrarily selected ALOs. The minimum energy ellipse represents all possible states (in state space) that can be reached from a zero initial state, and is determined by a specified bound on energy and time. The relative size and shape of these ellipses reveal information about the system's degree of controllability in state space through the relative sizes of the controllability Gramian's singular values. The results shown in Figures 3.5.1 illustrate how controllability in state space is weakened near the primaries, and more energy is required to perform certain state transfers. The same control configurations were used for all three ALOs so that relative controllability could be determined based on ALO location, and not input.

Furthermore, simulations for regulating the sail at these ALOs are presented in Chapter 4 to confirm the results of the minimum energy ellipses. In these example, the same amount of energy and time are used for the minimum energy controller so that the relative controllability could be demonstrated as a function of ALO position, and not control configuration. The simulations are first presented for the natural response of a solar sail placed near an ALO. Since the ALOs are unstable, all three examples show an unbounded response. However, the instability of ALOs near the primaries cause the natural, unbounded response to grow much faster with time. The minimum energy controller was then implemented over a period of 200 days for all three examples. The forced response was more underdamped for ALOs near the primaries, which indicates that the system requires more energy to dampen the transient response. In all the examples shown, the results were consistent in favouring ALOs further away from the primaries as being relatively more controllable. A more detailed explanation of all the results summarised in this section are presented in their corresponding sections.

2. Solar Sails in ALOs

This chapter begins with an introduction to the Circular Restricted Three-Body Problem which will be used to derive the equilibrium conditions for solar sails using the nonlinear equations of motion in the rotating frame. An additional acceleration term caused by the solar radiation pressure on the sail will be included in the equations to reveal a new set of equilibrium solutions for the Earth-Sun system. A linearized model will then be derived in order to represent the system of second order differential equations of the dynamics as a system of first order differential equations in state space. The linear model reveals the local behavior of the system near an equilibrium point, thus revealing the stability of the ALOs. This is done by examining the system's eigenvalues on the complex plane.

2.1 Solar Sails and the Circular Restricted Three-Body Problem

The analysis begins with the derivation of the nonlinear system; a mathematical expression describing the motion of celestial bodies. This expression is generally very complex but can be greatly simplified under certain assumptions, which will be introduced throughout this chapter beginning with Newton's second law of motion, which describes the external force acting on a body given by the vector equation,

$$\boldsymbol{F} = m\ddot{\boldsymbol{r}}. \tag{2.1.1}$$

The vector $\boldsymbol{F}$ is the sum of all forces acting on a particle with the inertial position vector $\boldsymbol{r}$, given by the inertial time rate of change of the particle's linear momentum with constant mass, m. Bold letters used throughout this text denote vectors. The analysis begins with Newton's Law of Universal Gravitation, which describes the mutually attractive force between any two objects,

$$\boldsymbol{F_{21}} = \frac{Gm_1m_2}{|\boldsymbol{r_{12}}|^3}\boldsymbol{r_{12}}, \tag{2.1.2}$$

where $\boldsymbol{F_{21}}$ is the force that mass m_2 experiences due to m_1 at the relative position $\boldsymbol{r_{12}}$, and where G is the *Universal Gravitational Constant*. Since the gravitational force is conservative, it can be derived from a scalar potential energy function by applying the gradient operator

$$\boldsymbol{F}(\boldsymbol{r}) = -\nabla V(\boldsymbol{r}) \tag{2.1.3}$$

Where the potential energy function V is[18,29]

$$V(\boldsymbol{r}) = -\frac{Gm_1m_2}{r} \tag{2.1.4}$$

This scalar function describes the energy required to separate the two masses from a distance r to ∞. The gradient of the potential field is given by

$$-\nabla V(\boldsymbol{r}) = -\frac{Gm_1m_2}{|\boldsymbol{r}|^3}\boldsymbol{r} \tag{2.1.5}$$

Newton's laws allow one to accurately model attractive forces between spacecraft and planets in multi-body systems, which can sometimes be further simplified depending on the relative size of the masses. It's important to describe the positions of the masses with respect to an inertial frame $\boldsymbol{\mathcal{N}}$: $\{\hat{\boldsymbol{I}}, \hat{\boldsymbol{J}}, \hat{\boldsymbol{K}}\}$, since all derivatives taken in Newton's second law must be inertial time derivatives. The center of mass of the system will be the origin of the inertial frame $\boldsymbol{\mathcal{N}}$ as displayed in Figure 2.1.1. The assumption made under the circular restricted three-body problem is that there are two primary masses, m_1 & m_2 (where $m_1 > m_2$) in circular orbit about their common center of mass. The third mass, m_3 is assumed to be infinitesimal relative to the primaries ($m_1 > m_2 \gg m_3$) so that its gravitational effect on their Keplerian motion is negligible.

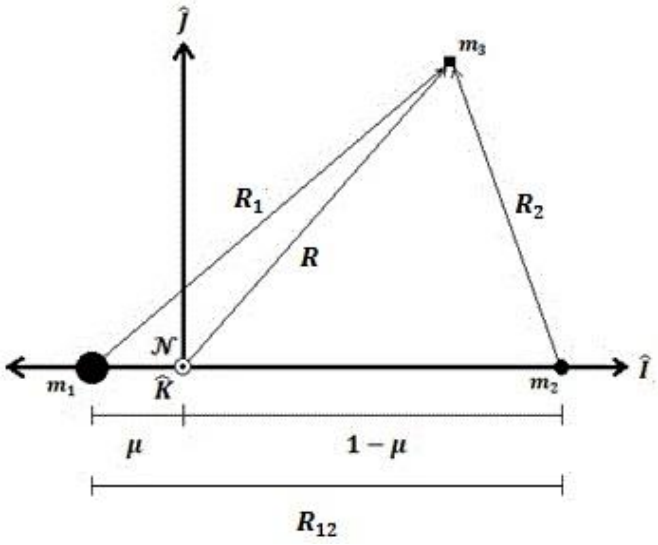

Figure 2.1.1. Inertial Frame of the Planet-Sun system

The sum of the forces acting on the solar sail which will be considered include the gravitational forces from the Sun and Earth at distances $\boldsymbol{R_1}$ and $\boldsymbol{R_2}$, respectively, the solar radiation pressure from $\boldsymbol{R_1}$, as well as a control term which will be derived later. The inertial acceleration of m_3 due to the external forces from the primaries is

$$^{\mathcal{N}}\ddot{\boldsymbol{R}} = -\frac{Gm_1}{R_1^3}\boldsymbol{R_1} - \frac{Gm_2}{R_2^3}\boldsymbol{R_2} + \frac{\boldsymbol{f}_{SRP}}{m_3}. \tag{2.1.6}$$

As previously discussed, the gravitational terms in equation 2.1.6 can be derived by taking the gradient of the scalar gravity potential energy function, ∇V. To represent the orbital motion of the primaries, the rotating frame $\boldsymbol{\mathcal{R}}$: $\{\hat{\boldsymbol{\imath}}, \hat{\boldsymbol{\jmath}}, \hat{\boldsymbol{k}}\}$, first introduced by Leonhard Euler in his formulation of the restricted three-body problem in 1772[30], is used. $\boldsymbol{\mathcal{R}}$ has its origin at the system's center of mass and rotates about its $\hat{\boldsymbol{k}}$ axis relative to the inertial frame $\boldsymbol{\mathcal{N}}$.

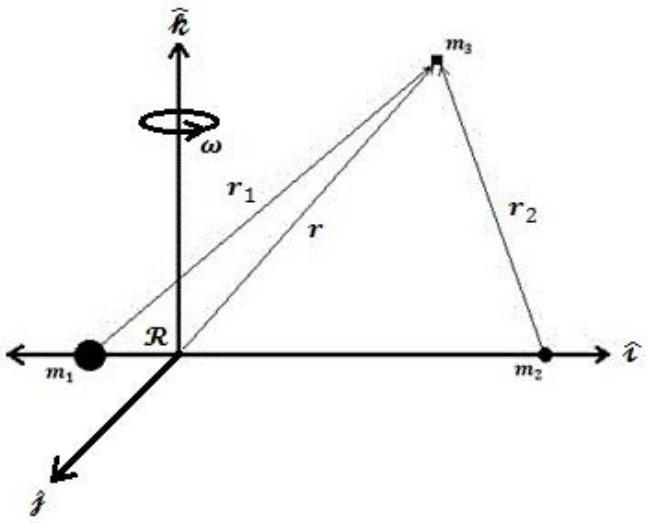

Figure 2.1.2. Rotating Frame

$\boldsymbol{r}$**,** the position of m_3 expressed in components of the rotating frame, is

$$\boldsymbol{r} = x\hat{\boldsymbol{\imath}} + y\hat{\boldsymbol{\jmath}} + z\hat{\boldsymbol{k}}. \tag{2.1.7}$$

The relationship between inertial and relative acceleration is well known and is derived by taking the second derivative of

$$^{\mathcal{N}}\boldsymbol{r} = {}^{\mathcal{R}}\boldsymbol{r} + \boldsymbol{r}_o, \tag{2.1.8}$$

which produces a five-term acceleration formula, but is reduced to three terms since both frames of reference share the same origin, $\boldsymbol{r}_0 = 0$, and the rotating frame has a constant angular velocity $\dot{\boldsymbol{\omega}} = 0$. Therefore the relationship between the absolute and relative accelerations is[31]

$$^{\mathcal{N}}\ddot{\boldsymbol{r}} = {}^{\mathcal{R}}\ddot{\boldsymbol{r}} + \boldsymbol{\omega} \times \left(\boldsymbol{\omega} \times {}^{\mathcal{R}}\boldsymbol{r}\right) + 2\boldsymbol{\omega} \times {}^{\mathcal{R}}\dot{\boldsymbol{r}}, \tag{2.1.9}$$

where $\boldsymbol{\omega} \times \left(\boldsymbol{\omega} \times {}^{\mathcal{R}}\boldsymbol{r}\right)$ and $2\boldsymbol{\omega} \times {}^{\mathcal{R}}\dot{\boldsymbol{r}}$ are the centrifugal and coriolis accelerations, respectively. The vector equation of motion for the solar sail can now be expressed in the rotating frame $\boldsymbol{\mathcal{R}}$ by combining equations 2.1.6 and 2.1.9 to produce

$$\ddot{\boldsymbol{r}} + \boldsymbol{\omega} \times (\boldsymbol{\omega} \times \boldsymbol{r}) + 2\boldsymbol{\omega} \times \dot{\boldsymbol{r}} = \boldsymbol{a}_{SRP} - \nabla V. \tag{2.1.10}$$

Because the centripetal term is conservative, it is convenient to define a new modified potential ∇U, so that a reduced equation of motion is obtained[28].

$$\nabla \phi = \boldsymbol{\omega} \times (\boldsymbol{\omega} \times \boldsymbol{r}). \tag{2.1.11}$$

$$\nabla U = \nabla V + \nabla \phi. \tag{2.1.12}$$

$$\ddot{\boldsymbol{r}} + 2\boldsymbol{\omega} \times \dot{\boldsymbol{r}} + \nabla U = \boldsymbol{a}_{SRP}. \tag{2.1.13}$$

The five classical Lagrange points are solutions to equation 2.1.13 for $\ddot{\boldsymbol{r}} = \dot{\boldsymbol{r}} = \boldsymbol{a}_{SRP} = 0$, and hence, $\nabla U = 0$. For a solar sail however, the addition of an acceleration term due to SRP introduces the set of infinite solutions called artificial Lagrangian orbits. Hence, it is sometimes referred to as the Modified Circular Restricted Three-Body Problem. The acceleration vector, $\boldsymbol{a}_{SRP}$ has the same direction as the sail attitude vector, $\boldsymbol{n}$. Therefore the cross product of $\boldsymbol{n}$ with $\nabla U = \boldsymbol{a}_{SRP}$ gives

$$\nabla U \times \boldsymbol{n} = \boldsymbol{0}. \tag{2.1.14}$$

The normalization condition $|\boldsymbol{n}| = \boldsymbol{1}$, reveals the sail attitude vector is equivalent to the unit vector of equal direction as ∇U,

$$\boldsymbol{n} = \frac{\nabla U}{|\nabla U|}. \tag{2.1.15}$$

The attitude vector can also be expressed in terms of two angles called the cone and clock angles, which are normally defined with respect to a co-ordinate triad attached to the center of the sail. However, only the cone angle is used in this thesis, and will be referred to as the *sail pitch angle*. Before continuing, it is beneficial to nondimensionalize the equations of motion. A scalar parameter, μ is introduced to nondimensionalize the system's mass quantities,

$$\mu = \frac{m2}{m1 + m2}. \tag{2.1.16}$$

Other dimensionless units are also used such that the distance between the primaries, the angular velocity of the rotating frame, and the gravitational constant are all taken to be unity. Nondimensionalizing, or rescaling, the system's model variables can help reduce the overall number of model parameters, but more importantly, improve the condition number of the linearized system's dynamics matrix. A *well-conditioned* matrix may reduce errors in accuracy which will prove vital when computing the singular values of the controllability Gramian in Chapter 3. Equation 2.1.10 is now rewritten using the nondimensional parameters,

$$\ddot{\boldsymbol{r}}_1 + 2\boldsymbol{\omega}^{\times}\dot{\boldsymbol{r}}_1 + \frac{(1-\mu)\boldsymbol{r}_1}{r_1^3} + \frac{\mu \boldsymbol{r}_2}{r_2^3} + \boldsymbol{\omega}^{\times}\boldsymbol{\omega}^{\times}\boldsymbol{r}_1 = \boldsymbol{a}_{SRP}, \tag{2.1.17}$$

where $\boldsymbol{\omega}^{\times}$ is the skew symmetric matrix, and the sail's position in the rotating frame is redefined as,

$$\boldsymbol{\omega}^{\times} = \begin{bmatrix} 0 & -1 & 0 \\ 1 & 0 & 0 \\ 0 & 0 & 0 \end{bmatrix}. \tag{2.1.18}$$

$$\boldsymbol{r_1} = [x + \mu, \quad y, \quad z]^{\mathrm{T}}. \tag{2.1.19a}$$

$$\boldsymbol{r_2} = [x - (1 - \mu), \quad y, \quad z]^{\mathrm{T}}. \tag{2.1.19b}$$

2.2 Force on a Sail

The existence of light pressure was known as early as 1873 and demonstrated theoretically by James Clerk Maxwell, and the suggestion of spacecraft being propelled by sunlight came decades later from Konstantin E. Tsiolkovsky's publication of *Extension of man into Outer Space* in 1921[32]. There are two forces exerted on a sail's surface which contribute to its acceleration; the force exerted on the sail due to incident photons and the force of reflected photons. An idealized perfectly reflecting solar sail, which makes equations 2.1.17 possible, is obtained by summing these two forces.

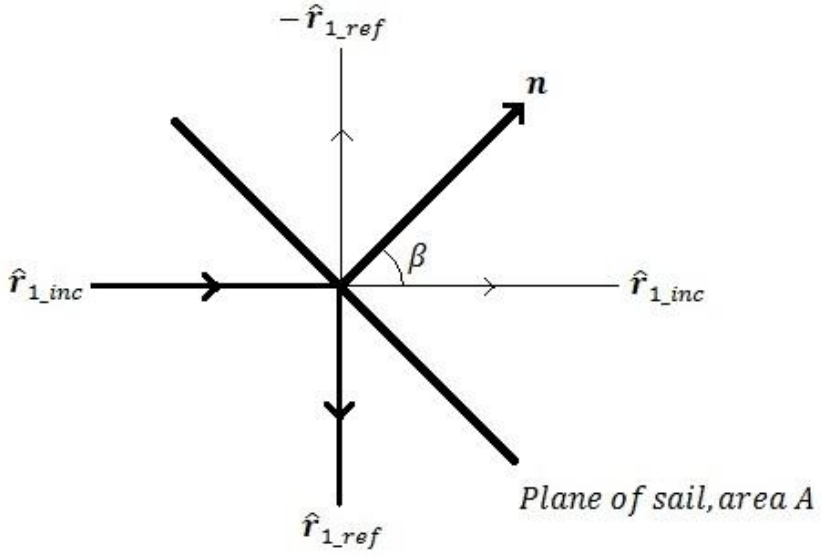

Figure 2.2.1. Solar Radiation Pressure on a Sail

The acceleration of the sail due to SRP is given by[28]

$$\boldsymbol{a}_{SRP} = 2P\frac{A}{m}cos^2\beta\boldsymbol{n}, \tag{2.2.1}$$

where the sail pitch angle, β, is the angle between the sail normal and the incident radiation.

$$cos\beta = \frac{1}{r_1}(\boldsymbol{n}\cdot\boldsymbol{r}_1). \tag{2.2.2}$$

The sail constants are gathered into one term, which will be referred to as the *sail quality* parameter,

$$\mathcal{B} \triangleq 2P\frac{A}{m}. \tag{2.2.3}$$

A/m is an important figure for solar sails and a key design parameter. Its inverse is sometimes called the sail loading parameter, and is denoted by σ (mass per unit area of the sail). Ideally, a solar sail is made as large and as light as possible in order increase thrust potential from solar

radiation pressure, this is reflected in the sail quality parameter. Figure 2.2.3 shows surfaces of ALOs characterized by demands on sail quality. The complexity involved with designing solar sails increases with increasing demands on this parameter. For example, impractical design requirements exist for ALOs closer to the Earth, and are represented by exceedingly large values of $\mathcal{B}$, which means that the sail must be made impractically large compared to its mass. Therefore, some ALOs are only theoretical because they exist for sails with impossible design requirements. The radiation pressure is given by P and is a function of solar distance. By defining P_0 to be the SRP at Earth's distance, the radiation pressure at the sail's distance can be expressed as

$$P(r_1) = P_o \frac{r_{12}^2}{r_1^2}. \tag{2.2.4}$$

The sail quality is now expressed as a function of distance from the Sun.

$$\mathcal{B}(r_1) = 2P_o r_{12}^2 \frac{\zeta}{r_1^2}, \tag{2.2.5}$$

where ζ is defined as

$$\zeta \triangleq \frac{A}{m}. \tag{2.2.6}$$

The solar sail acceleration due to SRP can now be rewritten in terms of the Sun's standard Gravitational parameter, which given the new non-dimensional parameters is written as

$$\boldsymbol{a}_{SRP} = \mathcal{B} \frac{1-\mu}{r_1^2} cos^2(\beta)\boldsymbol{n} \tag{2.2.7a}$$

or,

$$\boldsymbol{a}_{SRP} = \mathcal{B} \frac{1-\mu}{r_1^2} (\hat{\boldsymbol{r}}_1 \cdot \boldsymbol{n})^2 \boldsymbol{n}. \tag{2.2.7b}$$

The artificial Lagrange points are the solutions to the differential equation

$$\ddot{\boldsymbol{r}}_1 + 2\boldsymbol{\omega} \times \dot{\boldsymbol{r}}_1 + \nabla U = \mathcal{B}\frac{1-\mu}{r_1^2}(\hat{\boldsymbol{r}}_1 \cdot \boldsymbol{n})^2\boldsymbol{n}, \tag{2.2.8}$$

The equilibrium equation can now be obtained from the differential equation (2.2.8) where $\ddot{\boldsymbol{r}}_1 = \dot{\boldsymbol{r}}_1 = 0$.

$$\nabla U = \mathcal{B}\frac{1-\mu}{r_1^2}(\hat{\boldsymbol{r}}_1 \cdot \boldsymbol{n})^2\boldsymbol{n}, \tag{2.2.9a}$$

or,

$$\frac{(1-\mu)\boldsymbol{r}_1}{r_1^3} + \frac{\mu\boldsymbol{r}_2}{r_2^3} + \boldsymbol{\omega}^{\times}\boldsymbol{\omega}^{\times}\boldsymbol{r}_1 = \mathcal{B}\frac{1-\mu}{r_1^2}(\hat{\boldsymbol{r}}_1 \cdot \boldsymbol{n})^2\boldsymbol{n}, \tag{2.2.9b}$$

Figure 2.2.2 shows the planar equilibrium solutions to the MCRTBP under the constraint that the radiation pressure can only push, not pull. This constraint is defined by

$$(\hat{\boldsymbol{r}}_1 \cdot \boldsymbol{n}) \geq 0 \;\Rightarrow -90^\circ < \beta < 90^\circ \tag{2.2.10}$$

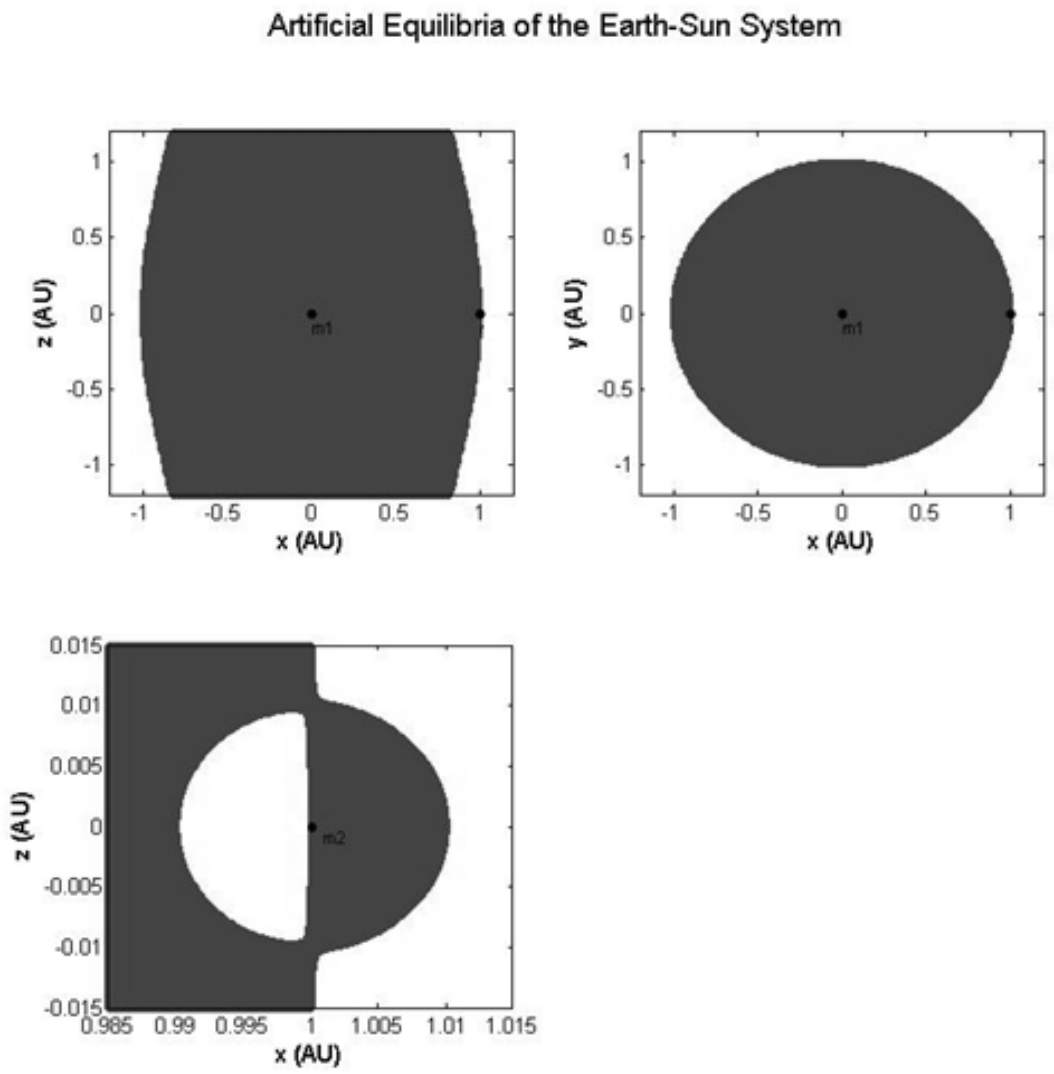

Figure 2.2.2. Artificial Lagrange Orbits of the Earth-Sun System

Figure 2.2.2 shows the existence of the artificial Lagrangian orbits in the rotating frame, where the xy plane represents the ecliptic plane of the Earth-Sun system, and the xz plane is perpendicular to ecliptic and passes through the center of the Earth and the Sun. The origin $(0, 0, 0)$ au represents the center of mass of the Earth-Sun system, and $(1, 0, 0)$ au represents the Earth's position . The two figures on top show the ALOs for the entire Earth-Sun system, while the bottom left figure shows ALOs near the Earth. The shaded area represents the continuum of points where the external net force acting on a solar sail is zero; outside this shaded surface is the region where equilibria are not possible. By simply changing the Planet-Sun mass ratio and

distance, ALOs for any Planet-Sun system can be derived. This set of infinite equilibrium solutions is a result of the solar radiation pressure acting on a sail, whereas the five classical Lagrange points do not include SRP. Even if the SRP term had been included, only a sail-type spacecraft that could make use of this additional force would generate the set of infinite solutions. Though Figure 2.2.2 reveals the existence of ALOs, design constraints reveal more practical solutions characterized by the sail quality parameter. Figure 2.2.3 is constructed from values of $\mathcal{B}$ which have been arbitrarily chosen[28,33] and present ALOs as a function of the design parameter. The same frame of reference used in Figure 2.2.2 is used in Figure 2.2.3. The five classical Lagrange solutions correspond to the sail quality $\mathcal{B} = 0$; these are places where the gravitational and centrifugal forces are balanced, but acceleration due to solar radiation pressure is ignored. The sail quality contour values used in Figure 2.2.3 are described in Tables 2.2.1-2.2.3. The contour lines represent regions of ALOs that exist only for solar sails with a specific sail quality parameter, and at each point on the contour, a specific sail orientation. For example, values represented in Table 2.2.1 show that in the top left plot of Figure 2.2.3, the contour line 8 represents a region of ALOs that exist only when the sail quality parameter has a value of 1.5. Figure 2.2.3 also shows the required sail pitch angle as short straight lines on/near the contours.

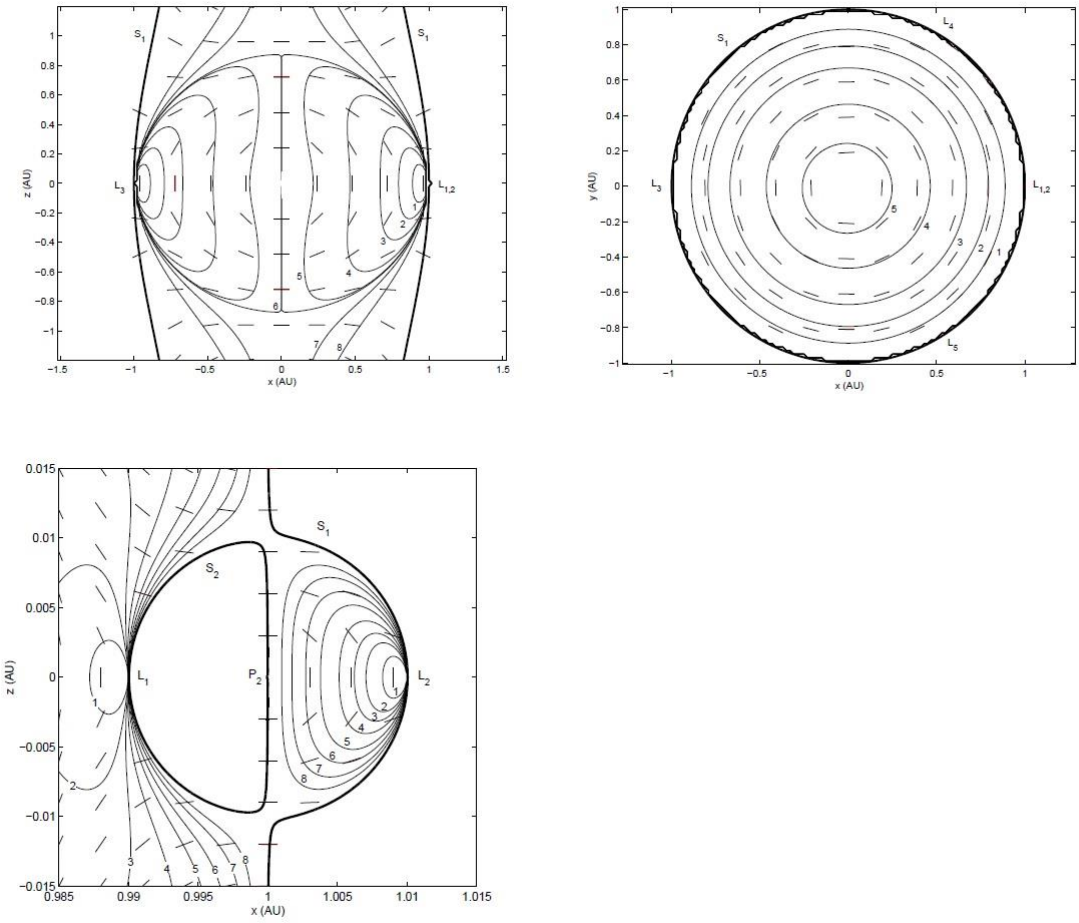

Figure 2.2.3. ALOs as a Function of Sail Quality[28,33]

Table 2.2.1. Sail Quality for Earth-Sun system ALOs (Fig 2.2.3: Top Left – xz plane)[28,33]

Contour line	1	2	3	4	5	6	7	8
$\mathcal{B}$	0.3	0.5	0.7	0.9	0.99	1.0	1.1	1.5

Table 2.2.2. Sail Quality for ALOs near Earth (Fig 2.2.3: Bottom Left – xz plane)[28,33]

Contour line	1	2	3	4	5	6	7	8
$\mathcal{B}$	0.02	0.04	0.06	0.1	0.2	0.4	1.0	3.0

Table 2.2.3. Sail Quality for Earth-Sun system ALOs (Fig 2.2.3: Top Right – xy plane)[28,33]

Contour line	1	2	3	4	5
$\mathcal{B}$	0.3	0.5	0.7	0.9	0.99

The nonlinear equations of motion for a solar sail in the artificial Lagrangian orbits have been derived, and stability properties of the system can now be explored. There are several methods to determining the nature of these ALOs. One simple and effective method is to linearize the system of equations about the equilibrium points – in order to obtain the local behaviour of the system – and represent the system in state space. All the methods that are used to determine controllability in this thesis are developed for linear systems in state space (see Chapter 3).

2.3 Linearized Force Model

All real physical elements behave nonlinearly. Whether the recovery of a spring following some displacement, or the spiraling away of the Moon from the Earth – all of nature is nonlinear. The local beviour of nonlinear systems can be modeled, often with good accuracy, by linearizing the system about some operating point. Linear systems are good approximations to nonlinear systems and are much simpler to deal with. The nature of the five classical Lagrange orbits is already known, as well as the continuum of artificial Lagrange points. The nature of these ALOs play a huge role in controllability. For example, regarding the regulation of a sail, an unstable ALO may require more control effort since the sail will drift from equilibrium following a disturbance. An asymptotically stable system will require much less control since regulation will come naturally near the vicinity of the equilibrium point.

In this section, the Taylor series expansion is used to linearize the nonlinear equations of motion at each artificial Lagrange point, since these are the points of interest. The nonlinear equations of motion expressed in the rotating frame are now expressed as perturbations about the equilibrium points;

$$\boldsymbol{r}_1(t) = \boldsymbol{r}_{1e} + \delta\boldsymbol{r}_1(t), \tag{2.3.1a}$$

$$\boldsymbol{r}_2(t) = \boldsymbol{r}_{2e} + \delta\boldsymbol{r}_2(t), \tag{2.3.1b}$$

$$r_1(t) = r_{1e} + \delta r_1(t), \tag{2.3.2a}$$

$$r_2(t) = r_{2e} + \delta r_2(t), \tag{2.3.2b}$$

$$\beta(t) = \beta_e + \delta\beta(t). \tag{2.3.3}$$

The stability problem involves assuming the sail is parked at an ALO by means of some orientation determined by the attitude vector $\boldsymbol{n}$, and observing the natural dynamics of the system, i.e. no control.

$$\begin{aligned}\delta\ddot{\boldsymbol{r}}_{\boldsymbol{1}} + 2\boldsymbol{\omega}^{\times}\delta\dot{\boldsymbol{r}}_{\boldsymbol{1}} + \boldsymbol{\omega}^{\times}\boldsymbol{\omega}^{\times}(\boldsymbol{r_{1e}} + \delta\boldsymbol{r_1}) + \frac{(1-\mu)(\boldsymbol{r_{1e}} + \delta\boldsymbol{r_1})}{(r_{1e} + \delta r_1)^3} \\ + \frac{\mu(\boldsymbol{r_{2e}} + \delta\boldsymbol{r_2})}{(r_{2e} + \delta r_2)^3} = \mathcal{B}\frac{1-\mu}{(r_{1e} + \delta r_1)^2}cos^2(\beta_e + \delta\beta)\boldsymbol{n}_e.\end{aligned} \tag{2.3.4}$$

Linearizing equation 2.3.4 by the 1st order Taylor Series expansion gives the result,

$$\begin{aligned}\delta\ddot{\boldsymbol{r}}_{\boldsymbol{1}} + 2\boldsymbol{\omega}^{\times}\delta\dot{\boldsymbol{r}}_{\boldsymbol{1}} + \Bigg[\boldsymbol{\omega}^{\times}\boldsymbol{\omega}^{\times} + \frac{(1-\mu)}{(r_{1e})^3}\left(\boldsymbol{I} - 3\boldsymbol{p_1}\boldsymbol{p_1}^T\right) + \frac{\mu}{(r_{2e})^3}\left(\boldsymbol{I} - 3\boldsymbol{p_2}\boldsymbol{p_2}^T\right) \\ + \mathcal{B}\frac{1-\mu}{(r_{1e})^3}cos\beta_e(2cos\beta_e\boldsymbol{n}_e\boldsymbol{p_1}^T - \boldsymbol{n}_e\boldsymbol{n_e^T})\Bigg]\delta\boldsymbol{r_1} = \boldsymbol{0},\end{aligned} \tag{2.3.5}$$

where

$$\boldsymbol{p_1} \triangleq \frac{\boldsymbol{r_{1e}}}{r_{1e}}, \tag{2.3.6a}$$

$$\boldsymbol{p_2} \triangleq \frac{\boldsymbol{r_{2e}}}{r_{2e}}, \tag{2.3.6b}$$

and the following five terms are the external forces exerted on the solar sail in the rotating frame;

Centrifugal;
$$\boldsymbol{\omega}^{\times}\boldsymbol{\omega}^{\times} = \begin{bmatrix}-1 & 0 & 0\\ 0 & -1 & 0\\ 0 & 0 & 0\end{bmatrix} \tag{2.3.7}$$

Coriolis;
$$2\boldsymbol{\omega}^{\times} = \begin{bmatrix}0 & -2 & 0\\ 2 & 0 & 0\\ 0 & 0 & 0\end{bmatrix} \tag{2.3.8}$$

Sun Gravity;
$$\Psi_{SG} = \frac{(1-\mu)}{(r_{1e})^3}(\boldsymbol{I} - 3\boldsymbol{p_1}\boldsymbol{p_1}^T) \tag{2.3.9}$$

Earth Gravity;
$$\Psi_{EG} = \frac{\mu}{(r_{2e})^3}(\boldsymbol{I} - 3\boldsymbol{p_2}\boldsymbol{p_2}^T) \tag{2.3.10}$$

SRP; $$\Psi_{srp} = \mathcal{B}\frac{1-\mu}{(r_{1e})^3} cos\beta_e (2cos\beta_e \boldsymbol{n}_e \boldsymbol{p}_1^T - \boldsymbol{n}_e \boldsymbol{n}_e^T) \quad (2.3.11)$$

Let the sum of the four-term coefficient of $\delta \boldsymbol{r_1}$ be defined by the 3×3 gravity-radiation gradient matrix **Γ.** The linearized matrix equation of motion can now be written in the form of a standard second order matrix/vector linear differential equation describing a mechanical system:

$$\delta \ddot{\boldsymbol{r}}_1 + 2\boldsymbol{\omega}^{\times}\, \delta \dot{\boldsymbol{r}}_1 + \boldsymbol{\Gamma}\, \delta \boldsymbol{r}_1 = 0. \quad (2.3.12)$$

2.4 Stability of ALOs

2.4.1 State Space Model

The linearized equations of motion reveal the nature of the ALOs of the nonlinear system within a particular range. This range has been experimentally determined to extend to approximately 150,000km for most ALOs[33]. In this section, the stability of the linear, time invariant (LTI) system is determined by first rewriting the linearized equations of motion in state space. By doing this, the stability properties of the system can be easily determined. First, it is necessary to define what is means by a stable, unstable, and marginally stable system[34]:

1. A linear, time-invariant system is stable if the natural response approaches zero as time approaches infinity.
2. A linear, time-invariant system is unstable if the natural response grows without bound as time approaches infinity.
3. A linear, time-invariant system is marginally stable if the natural response neither decays nor grows but remains constant or oscillates as time approaches infinity.

The stability of the equilibrium solutions is obtained by examining the eigenvalues of the system's characteristic polynomial. To do this, the system must be represented in *state space*. The state space representation of a system allows one to represent the state of the system as a vector in Euclidean space. It is also a useful way to express a linearized system of n^{th} order differential equations as a system of first order differential equations. Consider the linear, time-invariant system

$$\dot{\boldsymbol{x}} = \boldsymbol{A}\boldsymbol{x} + \boldsymbol{B}\boldsymbol{u}, \tag{2.4.1.1}$$

where $\boldsymbol{x} \in \mathbb{R}^{\boldsymbol{n}}$ is the *state vector*, $\boldsymbol{A} \in \mathbb{R}^{\boldsymbol{n}\times\boldsymbol{n}}$ is the *dynamics matrix*, $\boldsymbol{B} \in \mathbb{R}^{\boldsymbol{n}\times\boldsymbol{n}}$ the *control/input matrix*, and $\boldsymbol{u} \in \mathbb{R}^{\boldsymbol{m}}$ is the *control vector*, or *control trajectory*. The dynamics of the system can be very quickly and simply determined for state space systems by looking at the location of the eigenvalues (or, system poles) of the dynamics matrix on the complex plane. Both the real and imaginary parts of the poles reveal information about the nature of the system. By rewriting equation 2.3.12 as a system of first order differential equations, the characteristic polynomial is given by the determinant of the 6×6 dynamics matrix

$$\boldsymbol{A} = \begin{bmatrix} \boldsymbol{0} & \boldsymbol{I} \\ -\boldsymbol{\Gamma} & -\boldsymbol{2\omega}^{\times} \end{bmatrix}. \tag{2.4.1.2}$$

2.4.2 Stability Properties

The dynamics matrix $\boldsymbol{A}$ reveals much about the system's stability properties. There are six system poles associated with this matrix. The location of all six poles on the complex plane reveal whether or not the system is asymptotically stable, marginally stable, or unstable. The Stability Theorem for LTI systems is as follows[34,35]:

1. A system is asymptotically stable if all poles of the dynamics matrix have negative real parts.
2. A system is marginally stable if it has one or more distinct poles on the imaginary axis, and any remaining poles have negative real parts.
3. A system is unstable if any pole has a positive real part, or if there are any repeated poles on the imaginary axis.

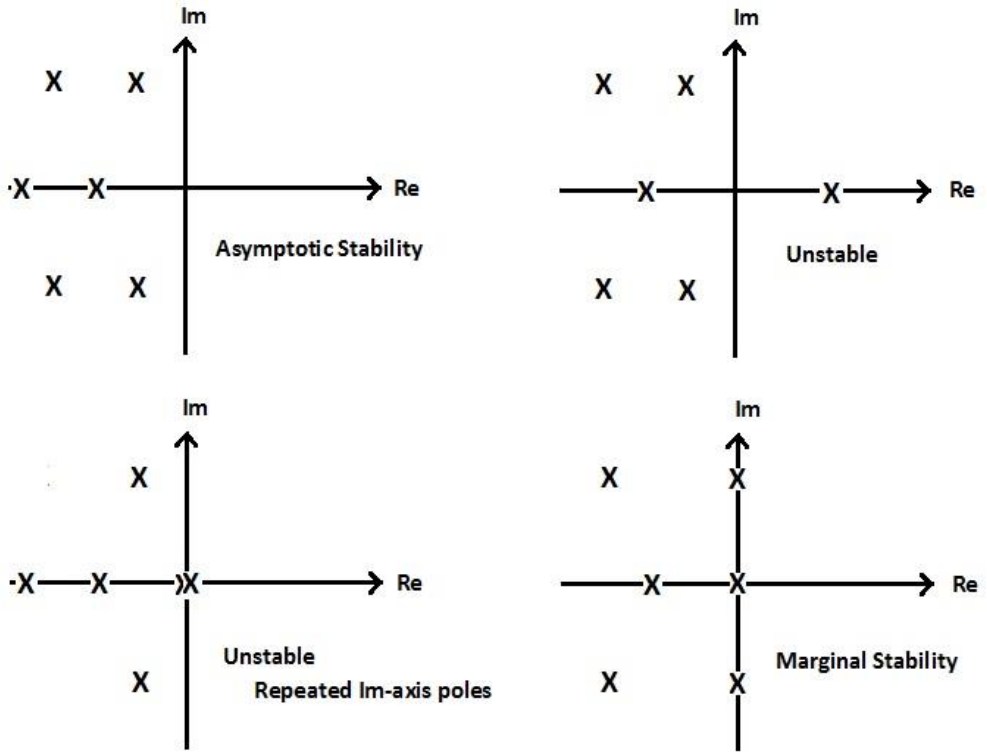

Figure 2.4.1 System Pole Location on the Complex Plane

Figure 2.4.1 shows the effects of pole location (on the complex plane) on the stability of the equilibrium points. The distance of the pole from the imaginary axis is an indication of how fast the corresponding time-domain exponential grows or decays. Since poles are roots of the characteristic polynomial, they are expressed as either exponentials or sinusoisoidals in the time domain. For example, if an eigenvalue of the characteristic polynomial has a positive real part, the natural response of the system is to grow without bound, indicating an unstable system. If an eigenvalue has a negative real part, the natural response of the system is to decay towards the equilibrium point, indicating a stable system. If an eigenvalue is purely imaginary, then the natural response of the system is to oscillate about the equilibrium point.

2.4.3 Stability Criterion

There are an infinite set of equilibrium solutions to the MCRTBP, each with its own unique set of eigenvalues. In order to determine the general stability of ALOs in the Earth-Sun system, the Routh-Hurwitz criterion is used. This method allows one to determine whether or not there are

unstable system poles in the characteristic polynomial without having to actually solve for the eigenvalues[34,35]. However, the eigenvalues will be computed for specific ALOs in Chapter 3 in order to see how stable/unstable the ALOs are.

Given a polynomial in s with constant, real coefficients:

$$a_0 s^6 + a_1 s^5 + a_2 s^4 + a_3 s^3 + a_4 s^2 + a_5 s + a_6 = 0. \quad (2.4.3.1)$$

The Routh-Hurwitz criterion states that any coefficient that is either zero or negative in the presence of at least one positive coefficient means that there must exist either a root, or roots, that are imaginary or have positive real parts[28,33]. The characteristic polynomial of the linear system derived in the previous section has the following coefficients:

$$a_0 = 1 \quad (2.4.3.2a)$$
$$a_1 = 0 \quad (2.4.3.2b)$$
$$a_2 = \Gamma_{11} + \Gamma_{22} + \Gamma_{33} + 4 \quad (2.4.3.2c)$$
$$a_3 = 2(\Gamma_{21} - \Gamma_{12}) \quad (2.4.3.2d)$$
$$a_4 = \Gamma_{11}\Gamma_{22} + \Gamma_{11}\Gamma_{33} + \Gamma_{22}\Gamma_{33} - \Gamma_{23}\Gamma_{32} - \Gamma_{13}\Gamma_{31} - \Gamma_{12}\Gamma_{21} + 4\Gamma_{33} \quad (2.4.3.2e)$$
$$a_5 = 2\Gamma_{33}(\Gamma_{21} - \Gamma_{12}) + 2(\Gamma_{32}\Gamma_{13} - \Gamma_{23}\Gamma_{31}) \quad (2.4.3.2f)$$
$$a_6 = \Gamma_{11}(\Gamma_{22}\Gamma_{33} - \Gamma_{23}\Gamma_{32}) - \Gamma_{12}(\Gamma_{33}\Gamma_{21} - \Gamma_{23}\Gamma_{31}) - \Gamma_{13}(\Gamma_{22}\Gamma_{31} - \Gamma_{21}\Gamma_{32}) \quad (2.4.3.2g)$$

The coefficients $a_0 = 1$ and $a_1 = 0$ of the characteristic polynomial reveal that asymptotic stability can be ruled out via the Routh-Hurwitz stability criterion since at least one eigenvalue does not lie in the left-hand complex plane. The condition for marginal stability, determined by substituting purely imaginary eigenvalues, $s = j\omega$ into the characteristic polynomial yields,

$$-\omega^6 + a_2\omega^4 - ja_3\omega^3 - a_4\omega^2 + ja_5\omega + a_6 = 0. \quad (2.4.3.3)$$

In order for Equation 2.4.3.3 to hold, both the real and imaginary parts must equal zero. However, equations 2.4.3.4 shows this to be false.

$$Re: \quad -\omega^6 + a_2\omega^4 - a_4\omega^2 + a_6 = 0 \quad (2.4.3.4a)$$
$$Im: \quad j\omega(a_5 - \omega^2 a_3) = 0 \quad (2.4.3.4b)$$

Unless $a_5 = 0$ and $a_3 = 0$, the solutions are not consistent[28,33]. This leads to the conclusion that the artificial Lagrangian orbits are generally unstable. Numerical simulations show that most ALOs have four poles that are extremely close to the imaginary axis and two real mirrored poles. It is the positive real pole that determines how unstable the ALO is, and it will be shown in Chapter 3 that this pole causes difficulty in control.

It is also well-known that the collinear Lagrange points have a decoupled, marginally stable z-component[36]. Like the five classical Lagrange points, all artificial Lagrange points which lie on the ecliptic plane have stable z-components. The bounded z component comes from the purely imaginary eigenvalues of the uncoupled subsystem shown in Equations 2.4.3.6. The 6×6 dynamics matrix is defined in section 2.4, and the control matrix and input vector are defined in section 3.2.

$$\begin{bmatrix} \delta\dot{x} \\ \delta\dot{y} \\ \delta\dot{z} \\ \delta\ddot{x} \\ \delta\ddot{y} \\ \delta\ddot{z} \end{bmatrix} = \begin{bmatrix} 0 & 0 & 0 & 1 & 0 & 0 \\ 0 & 0 & 0 & 0 & 1 & 0 \\ 0 & 0 & 0 & 0 & 0 & 1 \\ -\gamma_{xx} & -\gamma_{xy} & 0 & 0 & 2\omega & 0 \\ -\gamma_{yx} & -\gamma_{yy} & 0 & -2\omega & 0 & 0 \\ 0 & 0 & -\gamma_{zz} & 0 & 0 & 0 \end{bmatrix} \begin{bmatrix} \delta x \\ \delta y \\ \delta z \\ \delta\dot{x} \\ \delta\dot{y} \\ \delta\dot{z} \end{bmatrix} + \begin{bmatrix} 0 & 0 & 0 \\ 0 & 0 & 0 \\ 0 & 0 & 0 \\ n_{xe} & n_{ye} & 0 \\ n_{ye} & -n_{xe} & 0 \\ 0 & 0 & 1 \end{bmatrix} \begin{bmatrix} \frac{\delta A}{A} \\ \delta n_a \\ \delta n_b \end{bmatrix} \tag{2.4.3.5}$$

$$\delta\dot{x} = \delta\dot{x} \tag{2.4.3.6a}$$

$$\delta\dot{y} = \delta\dot{y} \tag{2.4.3.6b}$$

$$\delta\dot{z} = \delta\dot{z} \tag{2.4.3.6c}$$

$$\delta\ddot{x} = -\gamma_{xx}\delta x - \gamma_{xy}\delta y + 2\omega\delta\dot{y} + n_{xe}\frac{\delta A}{A} + n_{ye}\delta n_a \tag{2.4.3.6d}$$

$$\delta\ddot{y} = -\gamma_{yx}\delta x - \gamma_{yy}\delta y - 2\omega\delta\dot{x} + n_{ye}\frac{\delta A}{A} - n_{xe}\delta n_a \tag{2.4.3.6e}$$

$$\delta\ddot{z} = -\gamma_{zz}\delta z + \delta n_b \tag{2.4.3.6f}$$

3. Relative Controllability

In control theory, there does not exist one concrete way to determine the degree of controllability of a system, simply due to the nature of the problem. Asking how controllable a system is can be compared to asking how well a plane can fly. This cannot be answered simply by examining the plane's service ceiling, maneuverability, or speed. Although these factors may contribute to the answer, the question itself is dependent on factors like the mission objective. This chapter explores various methods for determining the controllability of a system, beginning first with a very common binary approach, and then a more appropriate quantitative method. A very well-known measure will be used to determine the relative controllability of a solar sail in ALOs followed by several examples to help verify the numerical results obtained.

3.1 The Condition for Controllability

3.1.1 A Binary Approach

The concept of controllability, as first introduced by Rudolf E. Kalman, plays a fundamental role in control theory. Controllability is the property of a system ensuring that the state can be steered from an arbitrary initial state to a desired final state over a finite period of time using the appropriate control input(s)[34,35]. If all states of the system are controllable, then the system is said to be *completely controllable.* This condition is indicated by a simple rank test. There are several ways to determine whether a system is controllable; since many of these methods are fundamentally similar, only one method is discussed in this section to give the reader some background on the subject. In order to derive the condition for controllability, the analysis begins with the solution to the state space equation introduced in Chapter 2[35].

$$\boldsymbol{x}(t) = e^{\boldsymbol{A}t}\boldsymbol{x}(0) + \int_0^t e^{\boldsymbol{A}(t-\tau)}\boldsymbol{B}u(\tau)d\tau. \tag{3.1.1}$$

Without loss of generality, it can be assumed that the final state is the origin of the state space, i.e. the state vector $\boldsymbol{x}(t) = 0$. Equation 3.1.1 is then rewritten as

$$\boldsymbol{x}(0) = -\int_0^t e^{-\boldsymbol{A}\tau}\boldsymbol{B}u(\tau)d\tau. \tag{3.1.2}$$

One method for determining the matrix exponential is by the *Cayley-Hamilton theorem*, which states that every matrix satisfies its own characteristic equation[35]. This means that an analytic function of a matrix, such as a matrix exponential, can be expressed as a polynomial of degree $(n-1)$ or less. Therefore, the exponential $e^{-\boldsymbol{A}\tau}$ can be rewritten as

$$e^{-\boldsymbol{A}\tau} = \sum_{k=0}^{n-1} \alpha_k(\tau)\boldsymbol{A}^k, \tag{3.1.3}$$

where the α_k's are determined by the set of equations given by the eigenvalues of the matrix $\boldsymbol{A}$. Substituting Equation 3.1.3 into Equation 3.1.2 yields

$$\boldsymbol{x}(0) = -\sum_{k=0}^{n-1} \boldsymbol{A}^k\boldsymbol{B}\int_0^t \alpha_k(\tau)u(\tau)d\tau. \tag{3.1.4}$$

The significance of this equation is that it reveals controllability is not dependent on time, it depends only on the dynamics and control matrices. If Equation 3.1.4 is true for any initial state $\boldsymbol{x}(0)$, then the system is said to be completely state controllable. The condition for complete state controllability is then summed up by a simple check on a well-known matrix called *Kalman's controllability matrix,*

$$\boldsymbol{\mathcal{C}} = \sum_{k=0}^{n-1} \boldsymbol{A}^k\boldsymbol{B} = [\boldsymbol{B} \quad \boldsymbol{AB} \quad \boldsymbol{A^2B} \quad \ldots \quad \boldsymbol{A^{n-1}B}]. \tag{3.1.5}$$

If the column vectors of the controllability matrix are linearly independent, or the matrix is full rank, the system is said to be completely controllable[37]. Although this is a necessary condition, it is not a practical measure of controllability. To understand why, the singular value decomposition (SVD) is introduced to reveal information about the "true" rank of the matrix.

The SVD of a matrix is one of the most important tools in numerical linear algebra, with applications in statistics, signal processing, and control theory. Very important and useful information about a matrix including rank and nearness to singularity is revealed through the use of the SVD.

Let $A \in \mathbb{C}^{m\times n}$ where $m \geq n$, then the singular value decomposition of A if given by:

$$A = U\begin{pmatrix}\Sigma\\0\end{pmatrix}V^T, where\ \Sigma = \begin{pmatrix}\sigma_1 & & \\ & \ddots & \\ & & \sigma_n\end{pmatrix}, and\ \sigma_1 \geq \cdots \geq \sigma_n \geq 0. \quad (3.1.6a)$$

If $m \leq n$,

$$A = U(\Sigma \quad 0)V^T, where\ \Sigma = \begin{pmatrix}\sigma_1 & & \\ & \ddots & \\ & & \sigma_m\end{pmatrix}, and\ \sigma_1 \geq \cdots \geq \sigma_m \geq 0. \quad (3.1.6b)$$

Where[38]

- $U \in \mathbb{C}^{m\times m}$ is called a left singular vector matrix
- $V \in \mathbb{C}^{n\times n}$ is called a right singular vector matrix
- U and V are unitary matrices
- The scalars σ_j are called the singular values.
- The number of singular values of an $m \times n$ matrix is $\min(m, n)$.
- $A \in \mathbb{C}^{n\times n}$ is nonsingular if and only if all the singular values are nonzero

The maximum and minimum singular values can provide important information regarding controllability. More specifically, they provide information about the two-norm of a matrix. If $A \in \mathbb{C}^{m\times n}$ and $m < n$, then

$$\sigma_1 = \|A\|_2 = max_{x\neq 0}\frac{\|Ax\|_2}{\|x\|_2}, \quad (3.1.7a) \qquad \sigma_m = \|A\|_2 = min_{x\neq 0}\frac{\|Ax\|_2}{\|x\|_2}. \quad (3.1.7b)$$

The matrix norm $\frac{\|Ax\|_2}{\|x\|_2}$ gives the gain of the matrix A along the direction, x. Hence, the largest singular value corresponds to the maximum gain direction, while the smallest singular value corresponded to the minimum gain direction. That is, the extreme singular values of a matrix A

reveal how much that matrix can stretch or shrink a unit-norm vector. To illustrate the relationship of singular values to controllability, the computing problem involved with implementing the rank test is discussed in the following section.

3.1.2 A Numerical Approach

One major problem arising from the use of the Kalman rank criterion – as a method of determining whether a system is controllable or not – is that it does not yield numerically effective tests for controllability. The rank of a matrix can be erroneously computed depending on the machine precision of the computer. The most numerically viable way to determine the true rank of a matrix is by computing its singular values[39]. Consider the rank function in MATLAB 2013, which returns only the number of singular values of a matrix that are larger than the default tolerance. The tolerance can be varied, but like any computer program, MATLAB also has a specific machine precision. Using the rank function in MATLAB (with default tolerance), the controllability matrix of the pair (A, B), where $A = diag(5^{-9}, 5^{-12}, 5^{-15})$ and $B = (1, 1, 1)^T$ is full rank (3), i.e. controllable. However, if the first element of the diagonal matrix A is changed to 5^{-10}, MATLAB computes the rank of the controllability matrix as rank 2. The three singular values of the latter controllability matrix are: 1.732, 8.197×10^{-8}, and 2.880×10^{-16}. Hence, the computer has erroneously concluded that the pair is uncontrollable. As previously mentioned, a system is full rank as long as all the singular values are strictly greater than zero, regardless of how close to zero they are. But these singular values have physical implications, which means that for most practical purposes (depending on the context), values very close to zero, may be considered equal to zero. Unless the elements of a matrix are known to infinite accuracy, the exact rank of the matrix cannot be obtained. Any singular matrix is arbitrarily close to a nonsingular matrix[40]. In other words, a controllable system may be only a small perturbation away from an uncontrollable system. Thus, controllability is best described as a spectrum rather than a binary opposition. In practice, knowledge of a system's nearness to rank deficiency is preferred over whether or not the system is "controllable". However, the computational problem remains somewhat ill-defined. Various algorithms have been developed on computing a measure of controllability based on a distance μ, of a controllable pair (A, B), to the nearest uncontrollable pair $(A + \delta A, B + \delta B)$. If the

distance is small, then the original controllable system is close to an uncontrollable system. If the distance is large, then the system is far from an uncontrollable system.

$$\mu(A,B) \triangleq minimum\|(\delta A, \delta B)\|_2 \; such\; that\; the\; system\; defined$$
$$by\; (A+\delta A, B+\delta B)\; is\; uncontrollable$$

This distance is sometimes used as a measure of controllability[40-42]. Returning to the discussion of singular values; the "distance to singularity" can be determined by the minimum singular value of the matrix. In the absolute sense, a nonsingular matrix is almost singular if its smallest singular values is close to zero. In the relative sense, a nonsingular matrix is almost singular if the largest and smallest singular values are far apart, i.e. $\sigma_{max} \gg \sigma_{min}$. The ratio of singular values of a matrix is known as the *condition number*,

$$\kappa(\boldsymbol{A}) = \frac{\sigma_{max}}{\sigma_{min}}. \tag{3.1.8}$$

A well-conditioned matrix has a condition number equal to 1, which represents a nonsingular matrix that is far from singular; in the relative sense. A poorly-conditioned matrix has a condition number that is much greater than 1, and can represent a nonsingular matrix that is very close to singular in both the absolute and relative sense. An attractive property of the singular values is that they are not very sensitive to changes in the matrix. Small perturbations in the matrix lead to small perturbation in its singular values. Thus, the singular values are "well conditioned" with respect to perturbations in the matrix[40, 43]. On the other hand, the eigenvalues of some matrices can be very sensitive to small changes in the matrix, and are said to be "ill-conditioned". It is therefore considered poor practice to use a system's eigenvalues in an attempt to determine its nearness to rank deficiency; it is the singular values which provide the best low-rank approximations.

The most common method used today for determining whether or not a system is completely controllable, is the binary rank test on the controllability matrix $\boldsymbol{\mathcal{C}}$. However, much work has been produced regarding quantitative measures of controllability; among the most well-known is

the work of Viswanathan, Longman, & Likins (1984) titled: *a definition for the degree of controllability*[44]. Motivation for the paper arose from the problem of choosing the optimal number and location of actuators on a flexible spacecraft that would provide the best control. The authors developed a simple method of calculating controllability for the case of a system for which the state space dynamics matrix has only distinct eigenvalues; a complementary paper was also published for the special techniques required for the case of repeated eigenvalues[45]. In developing such a definition for controllability, the authors examined a number of candidate definitions in order to highlight characteristics of a workable definition. One common quantitative measure for the DOC is the size of the minimum eigenvalue of the symmetric matrix $\mathcal{C}\mathcal{C}^T$. This measure reveals how close to rank deficient the system is based on how close the minimum eigenvalue is to zero; zero indicating an uncontrollable system. $\mathcal{C}\mathcal{C}^T$ is symmetric and positive semidefinite, so its eigenvalues coincide with the singular values. Viswanathan et al., *1984* examined five apparent difficulties with the aforementioned candidate definition for a meaningful measure of the DOC:

1) A transformation of coordinates affects the DOC since the eigenvalues are not invariant under changes in the state space representation.

2) There is no clear physical meaning attached to the size of the eigenvalues of $\mathcal{C}\mathcal{C}^T$ except for the minimum eigenvalue which is equal to zero when the system is uncontrollable.

3) A dependence on stability is not reflected properly. Control objectives influence the control system design, and this definition does not clearly reflect the control objective.

4) There is no dependence on the amount of time allotted to accomplish the control task. The system may be easier to control in some directions depending on when the control action is implemented.

5) This definition does not clearly reveal the amount of control effort required to accomplish the task. A system with very poor controllability is expected to require large control inputs for small maneuvers, and so control effort is a fundamental requirement for a good definition of controllability.

To resolve these five concerns, the authors introduced a *recovery region* which identifies all disturbed states that can be returned in some finite time using bounded controls. This definition

is based on an estimate, though an exact expression for the DOC has also been obtained for a constant, linear system, when the controls are bounded and the desired state is the origin[46]. The five issues were resolved into five essential requirements for a good definition of the degree of controllability

1. An uncontrollable system is represented numerically as zero.
2. Stability properties are examined.
3. A dependence on time is examined.
4. Control effort is properly defined.
5. Control objectives are included.

Although these five requirements are not all fulfilled in this study, they are used to help provide a more complete discussion on controllability. This thesis is not necessarily concerned with finding an exact or precise measure of controllability, since this requires looking at one equilibrium point and specifying a particular control task. Instead, attention is given to comparing the relative degree of controllability for all ALOs in the Earth-Sun system. This is achieved by the use of a metric that is derived from a more physically meaningful matrix than the controllability matrix, namely, the controllability *Gramian*, whose structure relates to energy notions of controllability. Controllability via Kalman's well-known rank condition was discussed earlier, but it is more informative to consider an energy-related metric as opposed to merely likening the controllability problem to that of a matrix rank deficiency problem. A more meaningful quantitative measure describes the input energy required to perform state transfers. To this effect, the symmetric positive semidefinite matrix is introduced:

Discrete time:

$$\boldsymbol{W_c = \mathcal{C}\mathcal{C}^T} = \left(\sum_{k=0}^{n-1} \boldsymbol{A^k B}\right)\left(\sum_{k=0}^{n-1} \boldsymbol{A^k B}\right)^T = \sum_{k=0}^{n-1} (\boldsymbol{A^k B B^T A^{Tk}}). \tag{3.1.9a}$$

Continuous time:

$$\boldsymbol{W_c} = \int_0^t e^{\boldsymbol{A}\tau}\boldsymbol{B}\boldsymbol{B}^T e^{\boldsymbol{A}^T\tau} d\tau \tag{3.1.9b}$$

Unlike the controllability matrix, the controllability Gramian is a function of time. The pair (A, B) is controllable if and only if the $n \times n$ controllability Gramian is positive definite over the interval (t_0, t_f). $\boldsymbol{W_c}$ is positive definite if and only if rank$(W_c) = n$. The controllability Gramian provides an energy-related quantification of controllability. The integral can be evaluated directly for stable systems because the state transition matrix e^{At} consists of decaying exponentials. However, the infinite-horizon $(t \to \infty)$ controllability Gramian is often obtained by solving the Lyapunov Equation for stable systems;

$$AW_c + W_cA^T + BB^T = 0. \tag{3.1.10}$$

Though the rank test on the controllability matrix implies that controllability is not a function of time, a good definition of controllability is in fact time dependent, and for obvious reasons. One drawback to the Gramian is the fact that it is not defined for unstable systems. However, there do exist alternative definitions and interpretations of the Gramian for unstable systems. One method for determining the steady state Gramian for unstable systems has been addressed by Lee and Park (2014)[47]. They derived a measure that is the sum of the two terms represented by the Gramian of the stable subsystem $\boldsymbol{W_s}$, and the Gramian of the unstable subsystem $\boldsymbol{W_a}$. Both Gramians are obtained by solving the two Lyapunov equations:

$$A_sW_s + W_sA_s^T + B_sB_s^T = 0 \tag{3.1.11a}$$

$$(-A_a)W_a + W_a(-A_a^T) + B_aB_a^T = 0 \tag{3.1.11b}$$

The assumption made in this paper is that there are no poles on the imaginary axis, since no energy is required to change the states of undamped modes in the infinite time period. Although

the infinite-horizon integral is only defined for asymptotically stable systems, the results of the finite time controllability Gramian apply more generally. In this thesis, an appropriate interval of integration for the Gramian is chosen to show how the singular values grow. It is more difficult to interpret absolute controllability this way, but by comparing these results to other equilibria, controllability in the relative sense is easily interpreted. The terms absolute and relative controllability here do not refer to the condition number of a matrix discussed earlier. Instead, they refer to the degree of controllability of various ALOs. In other words, the degree of controllability of one ALO relative to the degree of controllability of another ALO. An advantage to using the finite-horizon controllability Gramian is that it can be used for unstable systems without having to resort to more complex alternative methods[48]. The controllability Gramian is related to the input energy of state transfers, and the spectral norm of a matrix is related to the gain as a function of direction. This means that the larger the norm of the Gramian, the smaller the control effort required to influence the modes. Thus, minimizing control energy is equivalent to maximizing the norm of the Gramian, which is time independent. The trace of the Gramian is another measure related to the average energy of the Gramian. It is often interpreted as the average controllability in all directions. Maximizing the control energy is equivalent to maximizing the weighted trace of the Gramian. To see more clearly the application of singular values of the controllability Gramian, consider a geometric interpretation of the Gramian matrix. First, the use of a scalar metric is derived from the Gramian as an indication of input energy to move around in state space. Since controllability is dependent on input, the minimum energy is characterized by the input that steers the state from $x(0)$ to $x(t)$ and minimizes Equation 3.1.12. This is shown in discrete time for simplicity.

$$\sum_{\tau=0}^{t-1} \|u(\tau)\|_2^2. \tag{3.1.12}$$

Equation 3.1.12 describes the least-norm input for controllability. Among all inputs that steer x_{init} to x_{des}, the one that minimizes Equation 3.1.12 is given by:

$$\boldsymbol{u_{ln}} = \begin{bmatrix} u_{ln}(t-1) \\ \vdots \\ u_{ln}(0) \end{bmatrix} = \mathcal{C}^T(\mathcal{C}\mathcal{C}^T)^{-1}x_{des}. \tag{3.1.13}$$

$\boldsymbol{u_{ln}}$ is called the least-norm or minimum energy input that effects the state transfer. An important scalar, known as the minimum "average" energy – ε_{min}, can then be derived from the least-norm approximate solution. ε_{min} is a measure of how difficult it is to reach a desired state x_{des} from an initial state. The following equations describe the relationship between the controllability Gramian and the minimum energy through the least-norm approximate solution:

$$\varepsilon_{min} = \sum_{\tau=0}^{t-1} \|u(\tau)\|_2^2 \tag{3.1.14}$$

$$\varepsilon_{min} = (\mathcal{C}^T(\mathcal{C}\mathcal{C}^T)^{-1}x_{des})^T(\mathcal{C}^T(\mathcal{C}\mathcal{C}^T)^{-1}x_{des}) \tag{3.1.15}$$

$$\varepsilon_{min} = x_{des}^T(CC^T)^{-1}x_{des} \tag{3.1.16}$$

$$\varepsilon_{min} = x_{des}^T(\sum_{k=0}^{n-1}(\boldsymbol{A}^k\boldsymbol{B}\boldsymbol{B}^T\boldsymbol{A}^{Tk}))^{-1}x_{des} \tag{3.1.17}$$

The minimum energy control signal can now be written as:

$$\boldsymbol{u_{ln}}(\tau) = \boldsymbol{B}^T(e^{A\tau})^T\boldsymbol{W_c}^{-1}x_{des};\ \ \tau \in [0, t]. \tag{3.1.18}$$

where $x_{des} = x_f - e^{\boldsymbol{A}\tau}x_0$. This measure, though not a true measure of energy, is often used as an objective to compare the difficulty involved with various control trajectories. The singular values of the Gramian matrix take on a much more meaningful interpretation in the context of control. It has already been shown that the singular values of a matrix give information about the gain of a matrix in certain directions. The result of Equations 3.1.16 – 3.1.17 is an ellipsoid in state space where the eigenvectors and corresponding eigenvalues (or singular values) are the semi-axis directions and lengths of the ellipsoid. This ellipse describes all states that can be reached from an intial state $x_0 = 0$, using a specified amount of energy and time. The size of the ellipse is dictated by the singular values. The smallest singular value corresponds to a worst case metric

that is inversely related to the amount of energy needed to transfer the system along the direction in state space that is most difficult to control. The largest singular value corresponds to directions in state space that are more easily controlled. The weighted trace of the Gramian can also be obtained as the sum of the singular values of the controllability Gramian[49]. Consider a two dimension system in state space, the set of reachable states with a bounded input $\|u\| \leq c$, is determined by the following ellipse.

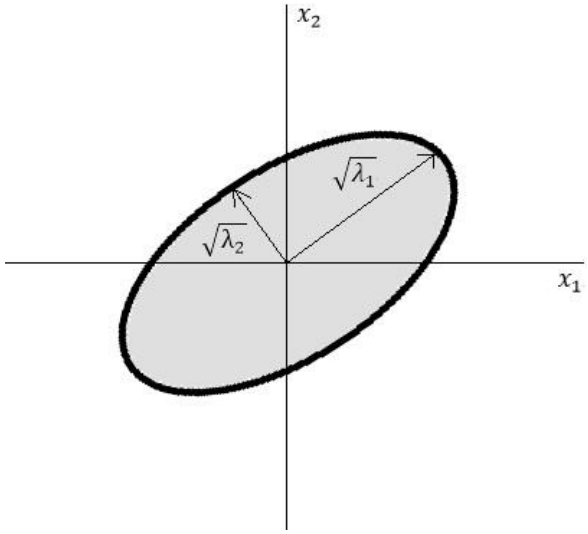

Figure 3.1.1 Controllability of States

Each singular value is a representation of energy contributions in a particular direction in state space, while the sum of singular values represents contributions to the total energy.

3.2 Controllable Configurations

Controllability is one of the most important properties of dynamical systems. It is the property which determines how a system can be steered from some initial physical state $x(0)$ to a desired state $x(t)$ by manipulating the system's dynamics. In Chapter 2 it was shown that ALOs are generally unstable for sailcraft, which means that left to its own dynamics, a solar sail will drift from equilibrium following some disturbance. A good understanding of the controllability of a sail is essential for future sail missions.

As discussed in the previous section, a very popular check for controllability is the rank test on Kalman's controllability matrix, but such a binary definition of control can be misleading, as it gives the impression that all state transfers for a controllable system are possible given the appropriate input. Though theoretically true, it may not necessarily be true for practical purposes. Physical constraints on energy and time could make some possible state transfers impossible. This is why it is necessary to consider other measures of controllability, and preferably, one which includes the five requirements for a workable definition discussed in section 3.1.2. Before that can be done, the insufficient but necessary rank condition on Kalman's controllability matrix must be checked in order to determine if the control configuration of the system satisfies the fundamental condition for controllability.

Though the purpose of this section is to examine the feasibility of controlling ALOs, the sail area – characterized by the sail quality parameter, $\mathcal{B}$ – is not excluded as a viable control input. Varying $\mathcal{B}$ during flight may be considered impractical due to the design complexity of such a mechanism, but the addition of a control element that could potentially increase controllability of the orbit is worth examining. Beginning with the xz plane of the rotating frame (see Figure 2.2.2), the sail angle and area are displaced about the equilibrium position to linearize the control term. Since the sail attitude is a unit vector, it follows that

$$\boldsymbol{n}_e^T \delta \boldsymbol{n} = 0, \tag{3.2.1}$$

where $\delta \boldsymbol{n}$ and $\boldsymbol{n}_e^T$ have the form:

$$\delta \boldsymbol{n} = \begin{bmatrix} n_{ze}\delta_a \\ \delta_b \\ -n_{xe}\delta_a \end{bmatrix}, \tag{3.2.2a}$$

$$\boldsymbol{n}_e = \begin{bmatrix} n_{xe} \\ 0 \\ n_{ze} \end{bmatrix}. \tag{3.2.2b}$$

δ_a, corresponds to perturbations in sail orientation along the xz components, and δ_b is a perturbation in the y-component; Figure 3.2.1 is provided as a visual aid. The control vector $u(t)$ can now be defined as

$$\boldsymbol{u}(t) = \begin{bmatrix} u_1(t) \\ u_2(t) \\ u_3(t) \end{bmatrix} \triangleq \begin{bmatrix} \frac{\delta A}{A}(t) \\ \delta n_a(t) \\ \delta n_b(t) \end{bmatrix} \tag{3.2.3}$$

The control inputs presented in Equation 3.2.3 include changing the area of the sail film $u_1(t)$, and the two angles determining sail orientation, $u_2(t)$ and $u_3(t)$. The linear control term acceleration $\boldsymbol{a_c}$ is obtained by perturbing the sail orientation and area about the equilibrium point using the first order Taylor Series expansion,

$$\boldsymbol{a_c} = \frac{f_c}{m} = \frac{2P}{m} A cos^2(\beta_e)\delta \boldsymbol{n} + \frac{2P}{m} cos^2(\beta_e)\boldsymbol{n_e}\delta A \tag{3.2.4}$$

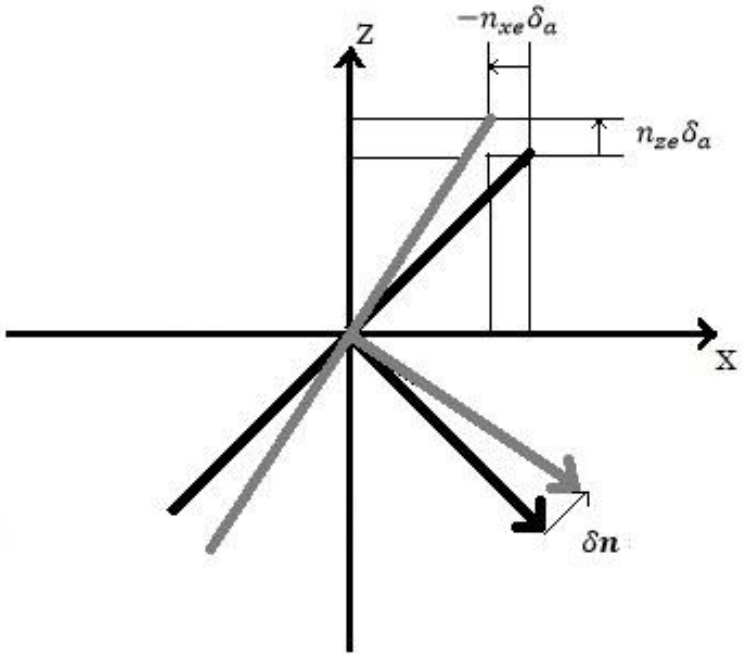

Figure 3.2.1 Inputs to Sail Attitude in the xz-plane

Equation 3.2.4 is simplified by letting

$$\mathfrak{V} \triangleq \frac{2P}{m} cos^2(\gamma_e). \tag{3.2.5}$$

$$\boldsymbol{a}_c = \frac{\boldsymbol{f}_c}{m} = \mathfrak{V} A \delta \boldsymbol{n} + \mathfrak{V} \boldsymbol{n}_e \frac{\delta A}{A}. \tag{3.2.6}$$

The state space input/control matrices for the xz and xy planes are

$$\boldsymbol{B'}_{\mathbf{xz}} = \Gamma \mathrm{A} \begin{bmatrix} n_{xe} & n_{ze} & 0 \\ 0 & 0 & 1 \\ n_{ze} & -n_{xe} & 0 \end{bmatrix}; \tag{3.2.7a}$$

$$\boldsymbol{B'}_{\mathbf{xy}} = \Gamma \mathrm{A} \begin{bmatrix} n_{xe} & n_{ye} & 0 \\ n_{\mathrm{ye}} & -n_{\mathrm{xe}} & 0 \\ 0 & 0 & 1 \end{bmatrix}. \tag{3.2.7b}$$

Where $\boldsymbol{B'}_{\mathbf{xz}}$ **and** $\boldsymbol{B'}_{\mathbf{xy}}$ are the control matrices corresponding to the planar solutions. The linear state space system can now be written with the control term $\boldsymbol{Bu}(t)$, where $\boldsymbol{B}$ is the 6×3 input matrix

$$\boldsymbol{B} \equiv \begin{bmatrix} \mathbf{0}_{(3\times3)} \\ \boldsymbol{B'} \end{bmatrix} \tag{3.2.8}$$

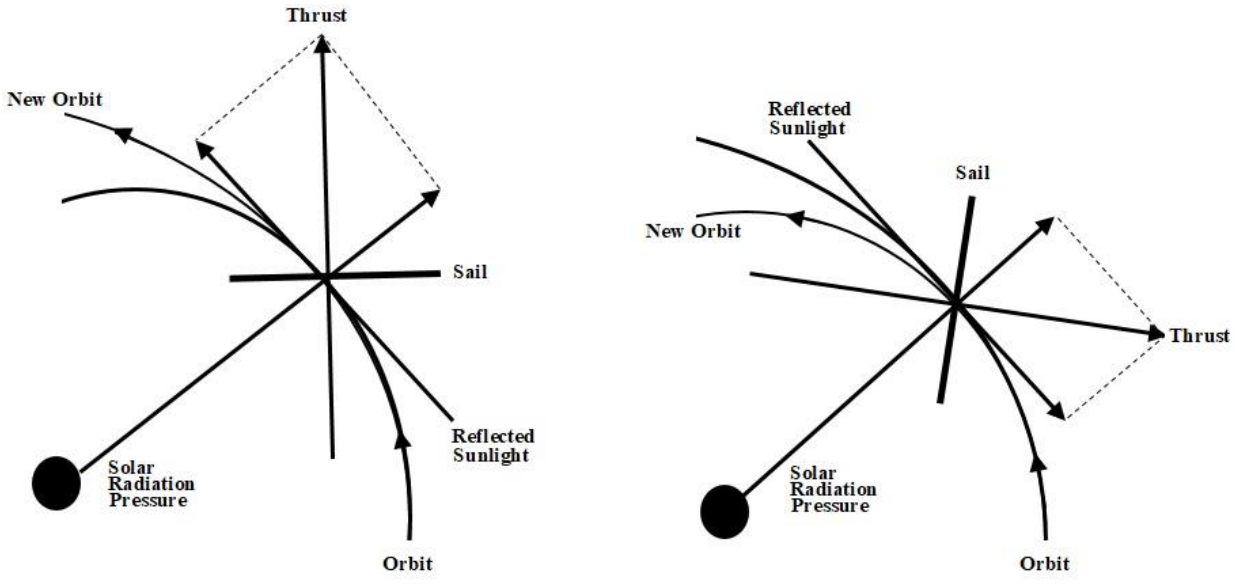

Figure 3.2.2. Solar Sail Orbital Altitude Maneuvering

The condition for complete controllability is given by the rank test on the 6×18 controllability matrix $\boldsymbol{\mathcal{C}} = \begin{bmatrix} \boldsymbol{B} & \boldsymbol{AB} & \boldsymbol{A^2B} & \boldsymbol{A^3B} & \boldsymbol{A^4B} & \boldsymbol{A^5B} \end{bmatrix}$. Numerical results show that the system is completely controllable for all ALOs, as $\text{rank}(\boldsymbol{\mathcal{C}}) = 6$ for the derived control configuration. Furthermore, numerical simulations reveal that ALOs in the xz plane are completely controllable for all possible control configurations of sail attitude and area. That is, the system is full rank using any one of the three control elements, or a combination of any two inputs. In the xy plane, full rank is only achieved when using at least two inputs, where one of those inputs is $\delta n_b(t)$. However, the idea that a sail is truly controllable using only one of the three inputs defined is suspect. Though it is not entirely impossible for the xz plane, it is very impractical. The centripetal acceleration of the rotating frame is the means by which the sail changes its orbital altitude. The force on the sail causing its orbital altitude to rise or fall (with respect to the Sun) is a result of the additive thrust vector component in the directions along the orbital velocity; this is illustrated in Figure 3.2.2. This is not the only way to decrease or increase the sail's orbital altitude. The force from SRP is completely avoided by varying the sail angle such that its normal vector is perpendicular to the Sun-line. The sail can then be drawn inwards towards the Sun via the Sun's gravity. For obvious reasons, this method of control is far weaker than the former, especially near the Earth. For these reasons, it is suspected that control using only single single

inputs drastically increases control difficulty. This cannot be verified unless a continuous metric is used for controllability. The merit of various control configurations is evaluated in section 3.2.2. It is true that adding a control element does not decrease controllability, but in some cases it can have little or no effect on the system's degree of controllability. Most, if not all, of the major contributions to the investigation of the controllability of solar sails in ALOs to date do not extend past the binary approach discussed in section 3.1.1, but includes the implementation of controllers developed for specific tasks for validation[28,33,50]. In the applications of controlling ALOs, this condition was assumed to be sufficient, and simulations were produced as a general "proof-of-concept". This chapter explores controllability as a metric, using well-developed methods to demonstrate relative controllability. Recall the five essential requirements for a workable definition of controllability:

1. An uncontrollable system is represented numerically as zero.
2. Stability properties are examined.
3. A dependence on time is examined.
4. Control effort is properly defined.
5. Control objectives are included.

The first requirement, that an uncontrollable system be represented numerically as zero, is fulfilled by the symmetric matrix $\boldsymbol{\mathcal{C}\mathcal{C}^{\mathrm{T}}}$, or better yet, the singular values of the controllability Gramian, as it provides us with more physically meaningful values. It has already been shown that the controllability matrix is full rank for the sail angle and area inputs, which means the minimum singular value is not equal to zero. Questions to be asked include: how close to zero is considered close enough to be uncontrollable? The machine precision is not a good candidate since its purpose is to compute values as close to zero as possible. It is difficult to establish how close to rank deficient the system is by looking at the smallest singular. For example, when compared to a minimum singular value of 10^{-8}, the singular value 10^{-3} seems relatively far from rank deficient. Singular values smaller than one are said to be attenuated, while singular values larger than one are amplified. The accuracy of the control signal, or rather, the limit for an acceptable minimum singular value, is not explored in this thesis since this is an experimental

problem. Instead, the singular values of some ALOs will be compared to the singular values of other ALOs in order to demonstrate relative control difficulty.

The second requirement has also been investigated in Chapter 2. This requirement directly affects the system's degree of controllability and is related to the control objective. Asymptotic stability works well for state regulation because the system's dynamics help steer the state to zero in a finite amount of time. If an asymptotically stable system is required to steer away from the equilibrium point, then it must fight against its natural dynamics. Therefore, the degree of controllability is also dependent on the nature of the ALO. A highly unstable system is more difficult to regulate than a system whose instability contains poles which are closer to the imaginary axis. The eigenvalues of the linearized system show that the ALOs are generally unstable; exactly how unstable each ALO is depends on it the exact location o fthe poles on the complex plane.

The dependence on time given to complete a control task influences controllability. An asymptotically stable system requires little to no control effort to regulate the state if the control task does not require the state transfer take place over a specified period of time, but allows the system to do so leisurely. This is because the natural dynamics of the system will eventually drive the state to zero, so no control effort is required unless the regulation time specified for the state transfer differs from the time it takes the system to naturally regulate the state. This passive type of control is used in gravity gradient stabilization for attitude control.

The finite-horizon controllability Gramian will be used to compare the condition number of various ALOs. This value will be used to draw some conclusions on relative controllability. Though this method does not give an explicit dependence on time, it can be used to compare the increasing condition numbers corresponding to ALOs in less controllable regions. This is done by integrating the Gramian over only a fraction of the orbital period. An appropriate orbital integration time is chosen experimentally and presented later in this chapter.

In the case of solar sails, the control effort is defined by the orientation of the sail normal vector with respect to the Sun. For example, when a control task requires the Sun-line to be parallel to the sail normal, or the sail area to be completely unfurled, the control effort is said to be large

because it requires as much SRP incident on the sail as possible. On the other hand, if the control task requires the Sun-line to be perpendicular to the sail normal, no control effort is required since no SRP is incident on the sail. Different control objectives will require different degrees of control effort. One way to look at this definition for controllability is the minimum energy ellipse introduced in section 3.1.2. The ellipse size and shape is a good indication of controllability as it represents state transfers for a fixed amount of time and energy. Since all real applications have physical constraints, standardizing energy and time is important, and makes relative controllability more apparent.

3.2.1 Dependence on Time

The inputs used for solar sails to maneuver affect the sail's orbital position and velocity in the rotating frame over generally long periods of time due to the faint but constant presence of SRP. Therefore, the control of solar sails is best described as a small input over a long period of time. It maybe impossible to perform even the simplest maneuvers without a sufficient amount of time for very large flexible sails with more complex dynamics. The time selected over which the controllability Gramian of the ALOs was integrated was determined by numerical results that are well within the computer's precision. Since all unstable systems have Gramians that grow without bound, the relative speed at which the ratio of singular values diverge is related to controllability. Since controllability can be defined by the condition number of the Gramian over a finite horizon, a system whose Gramian is controllable over a longer period of time is, in a relative sense, more controllable than a system whose Gramian remains nonsingular for a shorter period of time. Three ALOs are somewhat arbitrarily chosen and presented in Tables 3.2.1 to show the effect of the orbital integration time on the Gramian's singular values. The ALO positions are described in astronomical units (au) in the rotating frame defined in section 2.1. For example, $(0.7, 0, 0.001)$ is the position of an ALO that exists on the xz plane, which is perpendicular to the ecliptic and passes through the Sun and Earth. The distance $0.7\ au$ is $7/10^{th}$ the distance from the Sun to the Earth, and $0.001\ au$ is $1/1000^{th}$ the distance from the Sun to the Earth. The singular values corresponding to the ALO are computed by evaluating the controllability Gramian integral over various time periods. The numerical results presented in Tables 3.2.1 show that integrating the orbit over $100 - 200$ days provides a reasonable ratio of Gramian singular values for comparing the controllability of ALOs. Note the effect on the

maximum and minimum singular values, σ_1 and σ_6, respectively. The maximum singular value grows exponentially with time while the remaining singular values, including the minimum singular value, grow much slower. Hence, the cause of the nonsingular matrix growing near rank deficient is due to an increase in the ratio of singular values in the relative sense, and not in the absolute sense. The minimum singular value remains less than one with increasing time, which is often interpreted as attenuation, though not much more can be said about its physical meaning. It can not be used to compare a degree of controllability with the remaining ALOs since they are all very similar for a finite period of time.

Table 3.2.1a. Singular Values of the Controllability Gramian for 400 days (xz plane)

ALO (au)			Controllability Gramian Singular Values					
x	y	z	σ_1	σ_2	σ_3	σ_4	σ_5	σ_6
0.7	0	1.00E-03	4.20E+05	3.9946	3.2983	2.7008	1.2261	0.0206
0.8	0	1.00E-03	1.09E+05	5.1162	4.5501	3.5075	1.7267	0.0375
0.9	0	1.00E-03	2.04E+04	10.7606	6.1065	3.4835	2.4353	0.0715

Table 3.2.1b. Singular Values of the Controllability Gramian for 300 days (xz plane)

ALO (au)			Controllability Gramian Singular Values					
x	y	z	σ_1	σ_2	σ_3	σ_4	σ_5	σ_6
0.7	0	1.00E-03	7.83E+03	2.9321	2.4447	1.9273	0.9302	0.0197
0.8	0	1.00E-03	3.61E+03	3.6488	3.3626	2.7693	1.2155	0.0362
0.9	0	1.00E-03	1.42E+03	8.1846	4.5974	2.4854	1.9458	0.0645

Table 3.2.1c. Singular Values of the Controllability Gramian for 200 days (xz plane)

ALO (au)			Controllability Gramian Singular Values					
x	y	z	σ_1	σ_2	σ_3	σ_4	σ_5	σ_6
0.7	0	1.00E-03	132.017	2.0821	1.6142	1.1978	0.6259	0.0179
0.8	0	1.00E-03	121.4906	2.528	1.8735	1.7605	0.8235	0.0225
0.9	0	1.00E-03	137.1154	5.8233	1.9836	1.2236	1.0447	0.0221

Table 3.2.1d. Singular Values of the Controllability Gramian for 100 days (xz plane)

ALO (au)			Controllability Gramian Singular Values					
x	y	z	σ_1	σ_2	σ_3	σ_4	σ_5	σ_6
0.7	0	1.00E-03	5.642	0.8103	0.802	0.3149	0.1074	0.0011
0.8	0	1.00E-03	7.2112	1.0229	0.7448	0.4687	0.0856	0.0011
0.9	0	1.00E-03	8.37	1.1762	1.0174	0.4231	0.075	0.001

3.2.2 Dependence on Inputs

It is also interesting to note the effect on singular values with the number of inputs. The xy plane will now be used to compare two and three inputs, while the xz-plane ALOs that were used in Tables 3.2.1 will be used to compare single inputs. It is not important which planes are used here, as the Gramian's condition number is generally the same for ALOs in this region – see Figures 3.3.1. Tables 3.2.2 show the singular values for one, two, and three inputs using an interval of integration corresponding to 150 days. Table 3.2.2a shows the Gramian singular values when all three inputs are used, and is taken here as an objective to compare the effect of both the number and type of inputs used on the singular values. Tables 3.2.2a and 3.2.2b show that the singular values σ_1 to σ_5 are only slightly affected by the removal of the sail area input, implying no significant impact on control. However, the minimum singular value decreases by a factor of 10 for all three ALOs when using only two inputs. This tendency to rank deficiency may not be large enough to physically represent a decrease in controllability, but it does show that there is in fact a decrease in relative controllability with the removal of a more critical control element. This is demonstrated very clearly in Tables 3.2.2c-e, which show that not only does the minimum singular value diminished for single inputs – in comparison to Tables 3.2.2a-b – but other singular values are also strongly affected by the removal of a second control element. It is very clear that a real physical hindrance on controllability exists for solar sails using only one control element. It was shown earlier that the system is completely controllable for single inputs based on Kalman's controllability matrix, but demonstrated here is a substantial increase in rank deficiency of the controllability Gramian. It can be argued that for all practical purposes, the true rank of the controllability matrix is less than 6 for single inputs. Therefore, in regards to the Gramians corresponding to the single inputs δn_a, δn_b, and $\frac{\delta A}{A}$, it is more practical to treat these systems as though their Gramian matrix ranks are in fact 2, 4, and 4, respectively. As discussed

earlier, the difficulty in controlling a solar sail using only one input, based solely on intuition, is confirmed by the numerical results presented in these tables.

Table 3.2.2a. Singular Values of the Gramian for Three Inputs (sail area + sail attitude)

ALO (au)			Controllability Gramian Singular Values (150days)					
x	y	z	σ_1	σ_2	σ_3	σ_4	σ_5	σ_6
0.7	1.00E-03	0	56.1338	1.9808	1.3991	1.2667	0.389	0.0645
0.8	1.00E-03	0	51.9251	2.5068	1.5622	1.4367	0.584	0.076
0.9	1.00E-03	0	57.498	5.059	1.2412	1.0073	0.9741	0.0817

Table 3.2.2b. Singular Values of the Gramian for Two Inputs (sail attitude)

ALO (au)			Controllability Gramian Singular Values (150 days)					
x	y	z	σ_1	σ_2	σ_3	σ_4	σ_5	σ_6
0.7	1.00E-03	0	21.5118	1.3991	1.0266	0.9556	0.389	0.0081
0.8	1.00E-03	0	31.6504	1.8677	1.4367	0.5922	0.584	0.0076
0.9	1.00E-03	0	41.937	2.873	1.2412	0.9741	0.4097	0.0071

Table 3.2.2c Singular Values of the Gramian for the single Input $\delta n_a(t)$

ALO (au)			Controllability Gramian Singular Values (150 days)					
x	y	z	σ_1	σ_2	σ_3	σ_4	σ_5	σ_6
0.7	0	1.00E-03	1.3991	0.389	5.54E-06	1.33E-06	1.63E-08	1.86E-12
0.8	0	1.00E-03	1.4367	0.584	8.18E-06	1.03E-06	5.88E-11	8.50E-15
0.9	0	1.00E-03	1.2412	0.9742	8.87E-06	8.12E-07	2.16E-08	1.61E-12

Table 3.2.2d Singular Values of the Gramian for the single Input $\delta n_b(t)$

ALO (au)			Controllability Gramian Singular Values (150 days)					
x	y	z	σ_1	σ_2	σ_3	σ_4	σ_5	σ_6
0.7	0	1.00E-03	21.5117	1.0266	0.9556	0.0081	2.70E-08	7.25E-10
0.8	0	1.00E-03	31.6503	1.8677	0.5922	0.0076	8.11E-09	1.40E-10
0.9	0	1.00E-03	41.9387	2.873	0.4097	0.0071	2.06E-09	3.43E-11

Table 3.2.2e Singular Values of Gramian for the single Input $\frac{\delta A}{A}(t)$

ALO (au)			Controllability Gramian Singular Values (150 days)					
x	y	z	σ_1	σ_2	σ_3	σ_4	σ_5	σ_6
0.7	0	1.00E-03	35.2552	0.3992	0.2711	0.0182	2.77E-08	1.33E-09
0.8	0	1.00E-03	21.0531	0.4857	0.4069	0.0065	9.22E-09	5.22E-10
0.9	0	1.00E-03	17.08	1.0579	0.2786	0.0011	4.87E-09	1.52E-10

It is interesting to note the difference in how time and input affect the singular values of the Gramian. The integration time primarily affects the maximum singular value, while the input(s) primarily affect the minimum singular value. In both cases the ratio of singular values is affected, revealing the degree of controllability in a relative sense.

3.3 Relative Controllability of ALOs

One way to show relative controllability for the set of ALOs presented in Figure 2.2.2 is to plot them as a function of the controllability Gramian's condition number at each equilibrium point. This is demonstrated in Figures 3.3.1. Since the size of the Gramian's condition number is an indication of control difficulty, a plot of the ALOs as a function of their Gramian's condition number is a good respresentation of relative control difficulty with respect to the location of each ALO in the rotating frame. Since there is an infinite set of ALOs in the Earth-Sun system, and therefore a large range of condition numbers to plot, Figure 3.3.1 divides the ALOs into three distinct regions indicating closeness of the Gramian to rank deficiency. The Gramians corresponding to each unstable equilibrium point are integrated over an interval of 150 days – this number was determined experimentally to be the most meaning interval of time over which to integrate the Gramian. In Figures 3.3.1, ALOs with relatively well conditioned Gramians are considered to have condition numbers $\leq 10^4$.

$\times$ $\kappa(W_c) \leq 10^4$

$+$ $10^4 < \kappa(W_c) \leq 10^6$

$\bullet$ $\kappa(W_c) > 10^6$

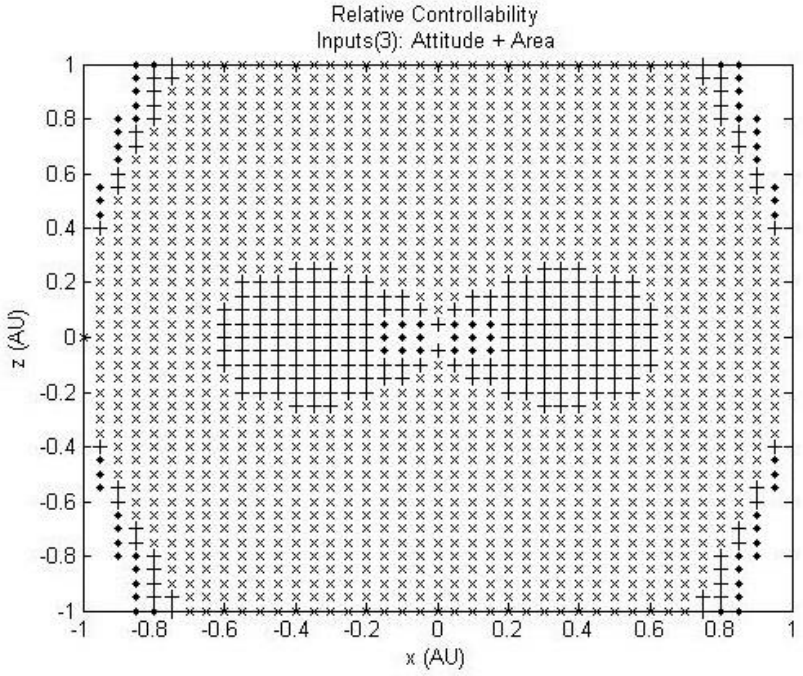

Figure 3.3.1a. Relative Controllability of ALOs in Earth-Sun System (xz-plane)

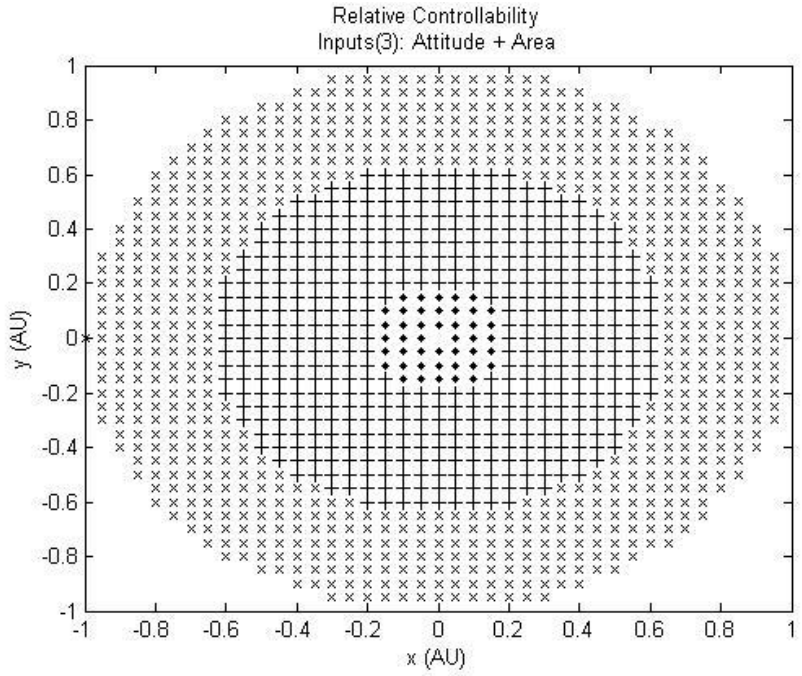

Figure 3.3.1b. Relative Controllability of ALOs in Earth-Sun System (xy-plane)

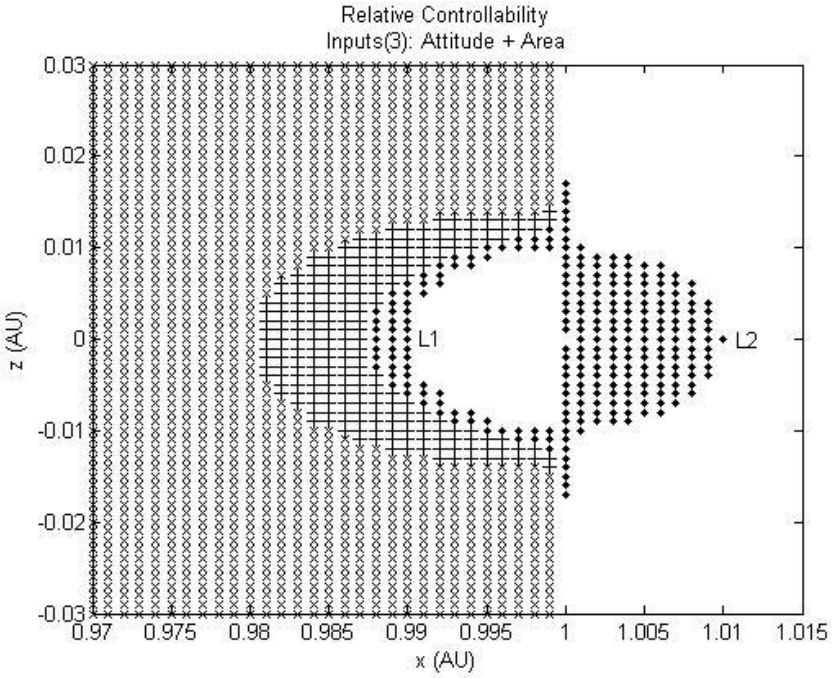

Figure 3.3.1c. Controllability of ALOs in Earth's Vicinity (xz-plane)

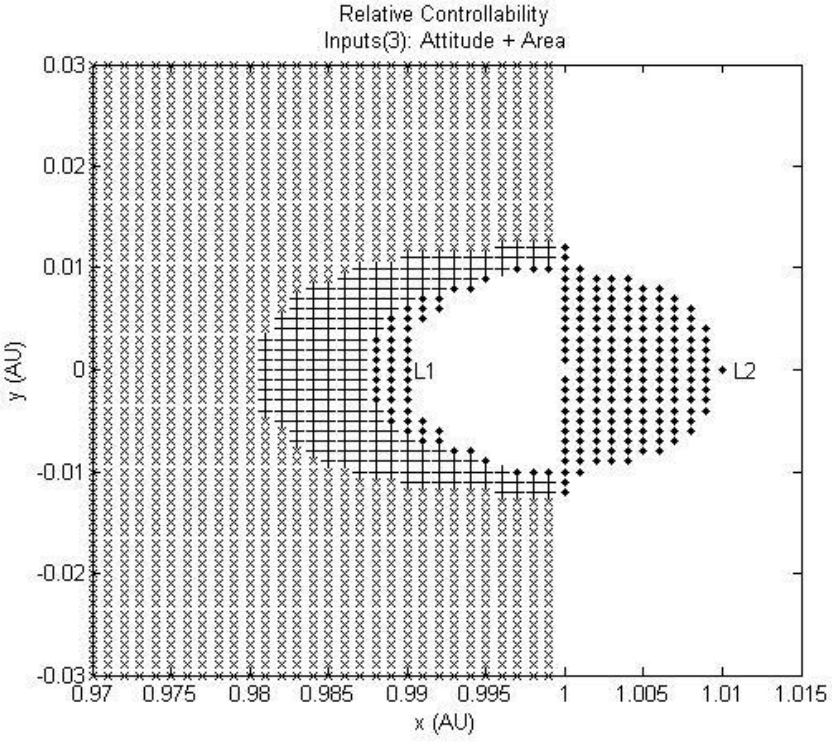

Figure 3.3.1d. Controllability of ALOs in Earth's Vicinity (xy-plane)

The control of states is most difficult with increasing proximity to either of the primaries due to the effect of gravity, which also grows by the inverse square of the distance. This is reflected in Figures 3.3.1 as poorly conditioned controllability Gramians near the Earth. There are other external forces not accounted for in this model such as gravitational forces from the moon, as well as albedo, which can have considerable effects on solar sails[51]. Figures 3.3.1c-d indicate that the ALOs near the Earth are relatively difficult to control. For example, the well-known Lagrange point $L1$ is where the Sun gravity and centripetal acceleration is balanced by Earth's gravity, while $L2$ is where the centripetal acceleration offsets both the Earth and Sun's gravitational pull[52]. Control difficulty grows with increased instability caused by both centrifugal and gravitational forces. This is evident from Figures 3.3.1b and 3.3.1d, as Earth's gravity only affects the condition number of the controllability Gramian for ALOs near the Earth, i.e. near $(1, 0, 0)\ au$. Outside the Earth's vicinity (more than 1.5 million km) the Gramian's condition number appears homogenous. As previously mentioned, the condition number alone is not a perfect indication of controllability; it is primarily a measure of the uniformity of control with regards to directions in state space. By looking at the Gramian's individual singular values a more thorough interpretation of controllability in state space can be obtained. The Gramian's singular values (for $t = 200$ days) at both Lagrange points, $L1$ and $L2$ are:

$$\sigma_{L1} = \begin{matrix} 2.539e6 \\ 2.282 \\ 1.840 \\ 0.762 \\ 0.396 \\ 0.017 \end{matrix}, \qquad \sigma_{L2} = \begin{matrix} 2.158e6 \\ 2.277 \\ 1.835 \\ 0.787 \\ 0.404 \\ 0.017 \end{matrix}$$

Based on the singular values of the controllability Gramian, control difficulty of the sail at the $L1$ and $L2$ points is virtually identical. The ratio of singular values is quite large here in comparison to the ratio of singular values of the non-collinear Lagrange points – $L4$ and $L5$ – which are located in regions where $\kappa(\boldsymbol{W_c}) \leq 10^4$. Relative to these points, controllability of a sail at $L1$ and $L2$ is more anisotropic – in the context of a minimum energy state space ellipse. This means that there are fewer directions in state space that can be reached without great effort. It should be emphasized here that the large condition number of $L1$ and $L2$ does not mean they are

uncontrollable, as successful control of orbits in the vicinity of $L1$ and $L2$ has been demonstrated in other studies[33]. In this context, the condition number is an indication of relative control difficulty. Figure 3.3.1 indicates that less control effort is required to perform state transfers by moving further away from the Earth in any general direction where ALOs exist. It also shows that radial Sun-side directions from Earth that are further away from the x axis point to more controllable ALOs at closer distances to the Earth. In other words, in order to minimize the control effort for near Earth missions, it is more feasible to park a sail in an ALO that does not lie on the ecliptic plane if the desire is to be as close as possible to the Earth.

3.4 Minimum Energy Control Effort

As per the five requirements for a workable definition of controllability, it is important to consider specific control tasks for a more complete definition. This section demonstrates the difficulty involved with performing regulation of the state as a specific control task, as in some cases it may be desirable to park the sail at an ALO. This section is used to compare the results obtained from different control configurations. The two most practical configurations as demonstrated in section 3.2.2 are; two inputs (sail attitude), and three inputs (sail attitude and area). Figures 3.4.1a-b plot the minimum energy/effort required to regulate the sail at a relatively well conditioned ALO, $\mathcal{L}_A = (0.6, 0.5, 0.4)\ au$, first using all three control inputs, then again for only two inputs.

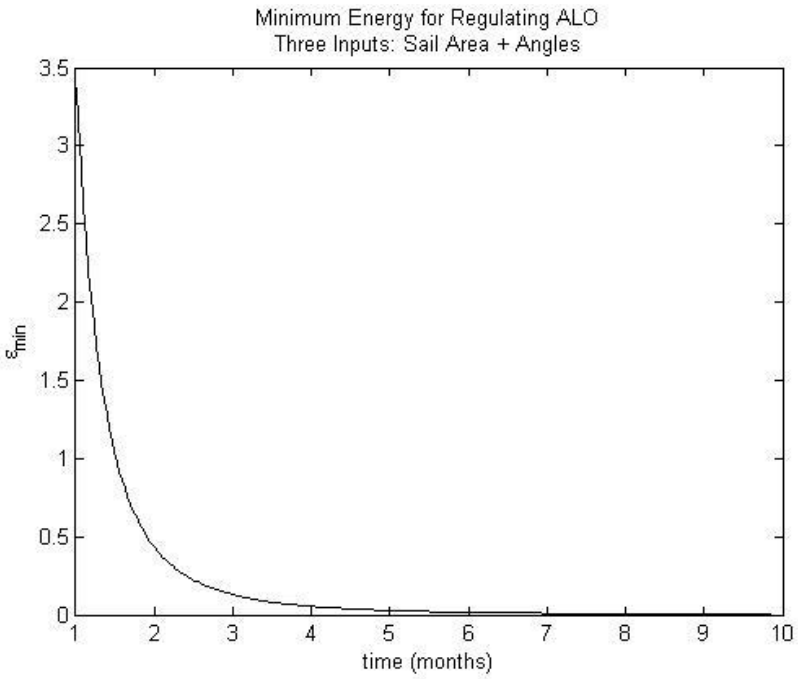

Figure 3.4.1a. Minimum Energy (Three Inputs)

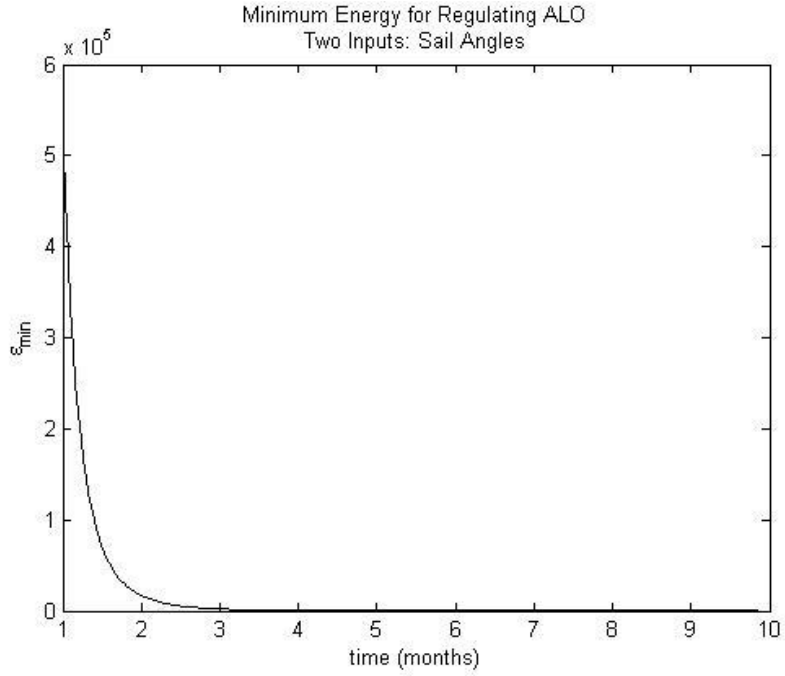

Figure 3.4.1b. Minimum Energy (Two Inputs)

There is a significant increase in control effort with the removal the of sail area as a control element; the minimum energy required to regulate the sail differs by a factor of 100,000 in the first few months, but approaches zero in both cases due to the unstable controllability Gramian. Though sail area variation presents a very difficult design problem, it does in fact minimize control effort. For this reason, the examples explored in this thesis involve both sail orientation and area. Figure 3.4.1 also indicates that the energy required to regulate the sail eventually approaches 0, which is not true in any case. Theoretically speaking, $\varepsilon_{min} = 0$ means that the desired state is reached by riding the system's instability using inputs with very little energy as "kicks" in the appropriate direction. In a more practical sense this is not true, and even less likely for solar sailing since impulsive inputs are not characteristic of how solar sails operate.

3.5 Controllability Ellipse

In this section, the singular values will be shown to affect the control each state in state space. Given that the LTI system is six dimensional (having six states), only three dimensions of state space will be considered, i.e. the three positional components. Recall from section 3.1.2 that the minimum energy ellipse reveals expensive directions in state space, as well as directions which can be reached with little effort. Beginning from a zero-state initial condition at some ALO - and a fixed value of energy and time - the relative size of the ellipse for various ALOs reflects the range of reachable states. The 'flatness' of the ellipse is a physical representation of the condition number. The controllability ellipse for three different ALOs are presented in Figures 3.5.1 for a fixed value of time and energy. The minimum energy was computed using Equation 3.1.17 for a period of time corresponding to 150 days. These are arbitrarily selected values which clearly demonstrate control difficulty in the relative sense based on the results of Figures 3.3.1. The

relative shape of the ellipse is a physical representation the Gramian's nearness to rank deficiency. The more elongated the ellipse, the more near rank deficient the Gramian is.

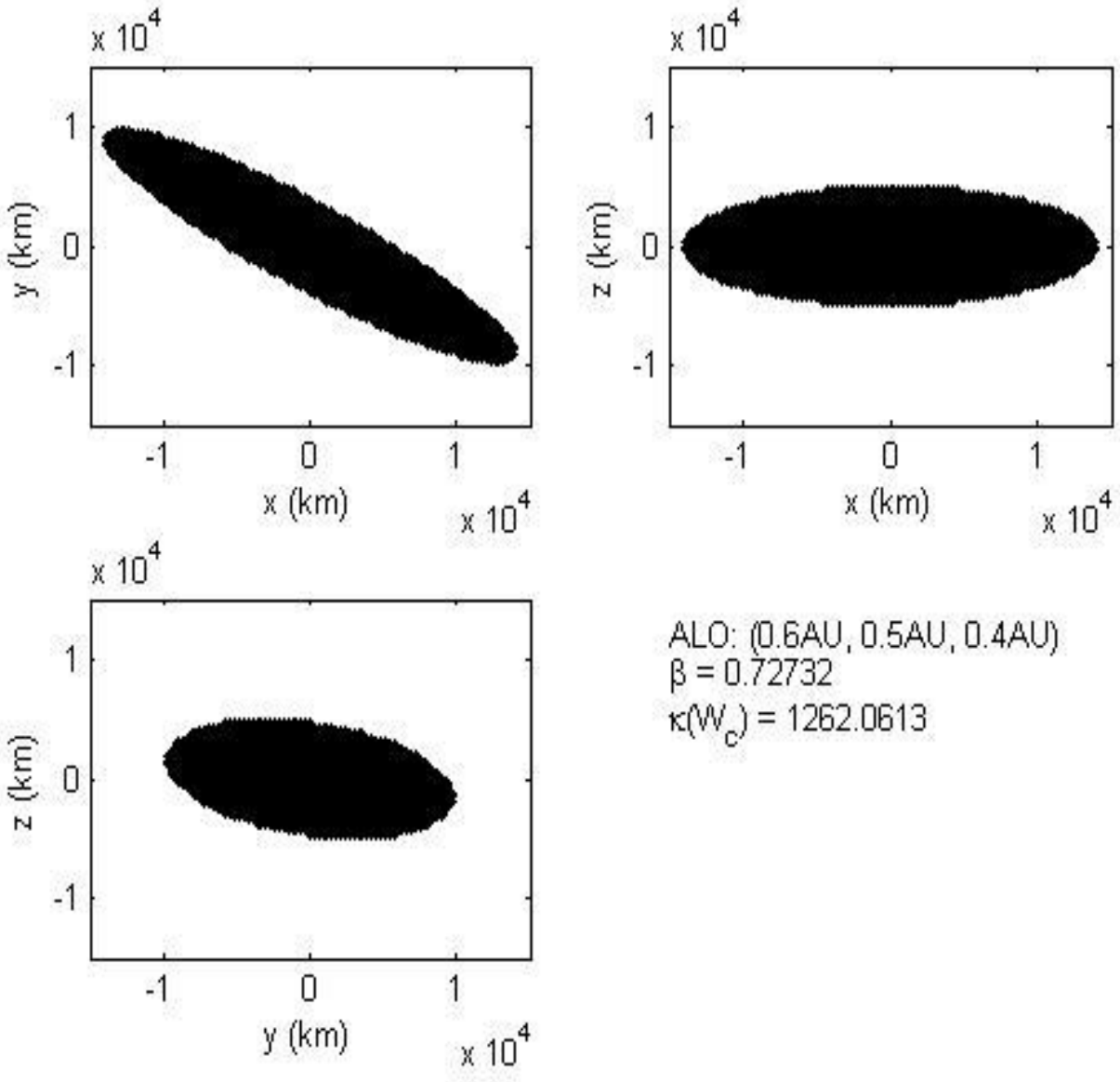

Figure 3.5.1a. Reachability of Orbital Positions $\mathcal{L}_A$

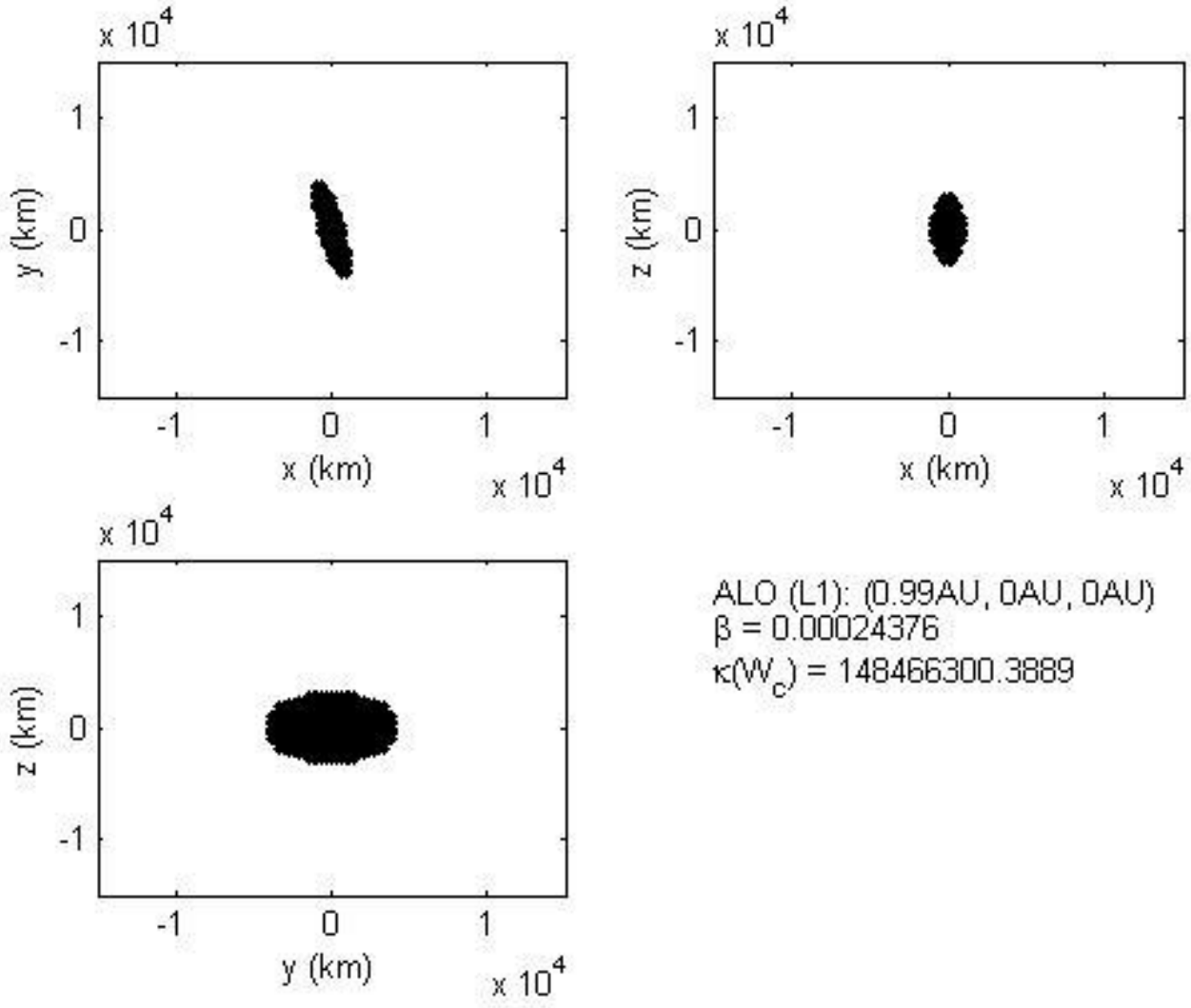

Figure 3.5.1b. Reachability of Orbital Positions at $L1$

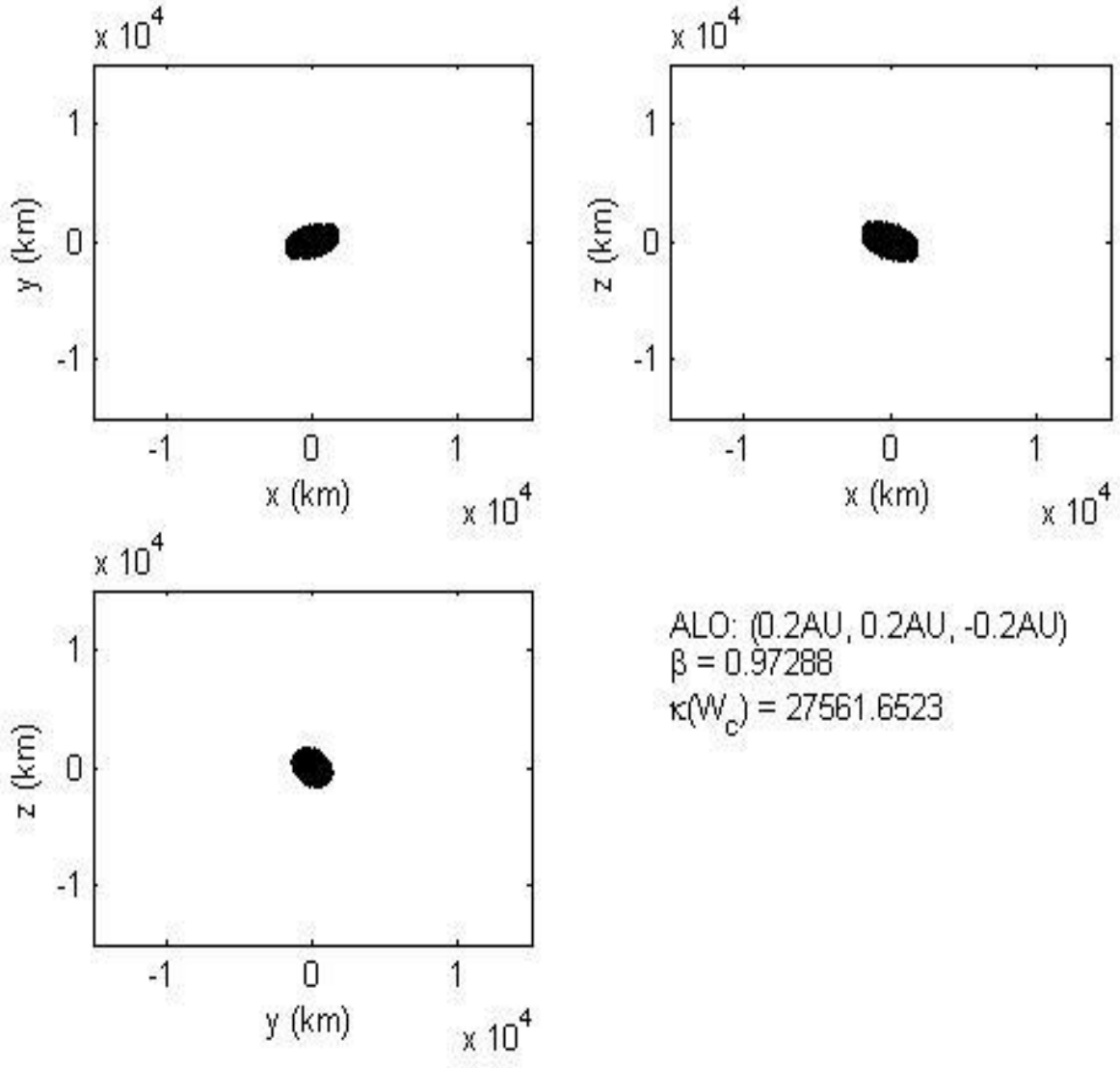

Figure 3.5.1c. Reachability of Orbital Positions at $\mathcal{L}_B$

Figures 3.5.1a – 3.5.1c show that the ellipse size and 'flatness' is largely dependent on sail proximity to the Earth and Sun, which confirms Figures 3.3.1. There is a large demand in energy to control states for ALOs near the primaries when compared to ALOs that are millions of kilometers away from them. The ellipse covers all states that can be reached with a bounded value of energy; states outside the ellipse require more energy than this bound. Another observation to make from Figures 3.5.1 is the ellipse orientation. Figure 3.5.1.a shows that

controllability of the orbital position at $\mathcal{L}_{\mathrm{A}}$ along the x and y axes is much easier than along the z-axis. This is illustrated by the range of values covered by the ellipse:

$$\mathcal{L}_{\mathrm{A}}: (-13{,}500 \lessapprox x \lessapprox 13{,}500;\ -10{,}000 \lessapprox y \lessapprox 10{,}000;\ -5000 \lessapprox z \lessapprox 5000)km$$
$$L1: (-1500 \lessapprox x \lessapprox 1500;\ -4000 \lessapprox y \lessapprox 4000;\ -3500 \lessapprox z \lessapprox 3500)km$$
$$\mathcal{L}_{\mathrm{B}}: (-1500\ \lessapprox x \lessapprox 1500;\ -2000 \lessapprox y \lessapprox 2000; -2000 \lessapprox z \lessapprox 2000)km$$

Figure 3.5.1.b shows that for $L1$, it is the z and y states which are more controllable than the x component, and that the range of states that are reachable in all directions is much less than the range of states at $\mathcal{L}_{\mathrm{A}}$. Figure 3.5.1c shows that for an ALO near the Sun, the ellipse is more isotropic than the previous two examples. However, the size of the ellipse is smaller, indicating that even fewer states can be reached in this case. This could not be seen in the condition number alone, but by examining the size of each singular value. In the next section, the regulation of solar sails is simulated for each of the three ALOs shown here, including examination of their controllability Gramian singular values, as well as the corresponding system eigenvalues.

4. Simulations

There are various controllers that can be used to simulate the regulation of solar sails in ALOs; for example, PID controllers have successfully been used to simulate the control of solar sails using variations in sail attitude[33]. In this section the initial condition and input responses of the sail's position and velocity in the rotating frame are simulated using inputs to the sail area and attitude using the minimum energy controller derived in the previous chapter. A minimum energy controller drives the system to a desired state with a minimal expenditure of energy. By definition, any other controller performing the same task would require more energy. The type of controller used is not necessarily important; the effect of the singular values on the system's output is more central to this study. This will also be compared to the natural response of the system, since the nature of the equilibrium point is directly related to its degree of controllability. The ALOs used for simulating orbital regulation here are the same ALOs that were used in the controllability ellipse examples in Chapter 3. Once again, these ALOs are chosen specifically to compare relative controllability following the results of Figure 3.3.1, to show the difference in control difficulty between ALOs both near to and far from either primary.

4.1 A Well-Conditioned Gramian

The control task simulated in this section is the regulation of a sail's position at an ALO with a relatively well conditioned controllability Gramian. The controller is implemented using the minimum energy required to regulate a solar sail at the ALO over a period of 200 days, which is also enough time for the ratio of singular values to begin an aggressive divergence for less controllable ALOs. The sail quality parameter required for each ALO is also shown, along with controllability Gramian's condition number and singular values for further analysis of the simulation. The eigenvalues of the dynamics matrix corresponding to the ALO is also included for investigation of the system's stability through the simulation of the natural (initial condition) response. The initial conditions place the solar sail just outside of the equilibrium point with a non-zero velocity so that the stability conditions of the ALO can be observed through the trajectory of the solar sail over time. These initial condition are given an appropriate distance from the equilibrium point such that the linear approximation remains valid; this distance has

been determined experimentally to be roughly 150,000km[5]. This section begins with the initial condition response of the solar sail position and velocity vectors:

ALO; $\mathcal{L}_A = (0.6\text{au}, 0.5\text{au}, 0.4\text{au})$

Initial State; $x(0) = \begin{bmatrix} 100{,}000km \\ -100{,}00km \\ 100{,}000km \\ 10m/s \\ 10m/s \\ -1m/s \end{bmatrix}$

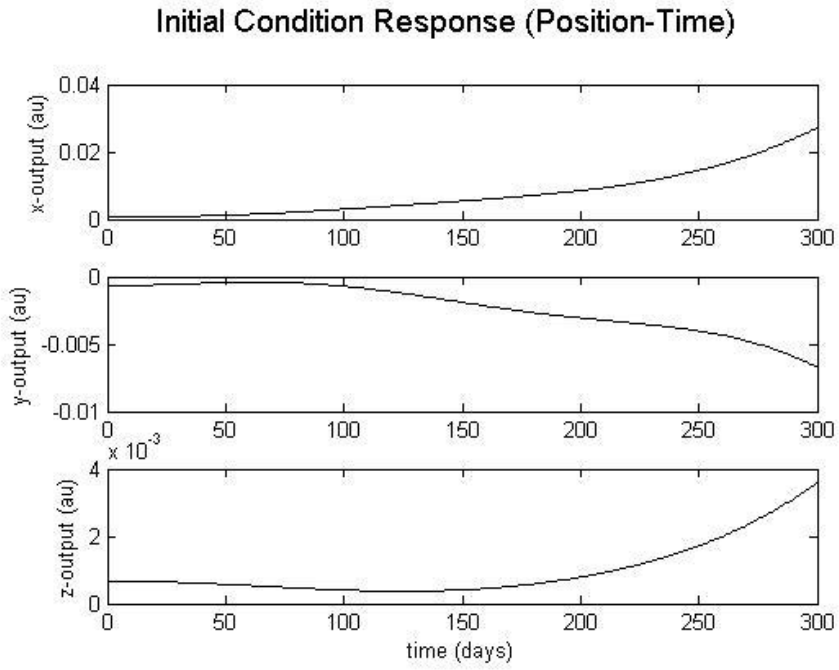

Figure 4.1.1a. Zero-Input Response at $\mathcal{L}_A$ (Position-Time)

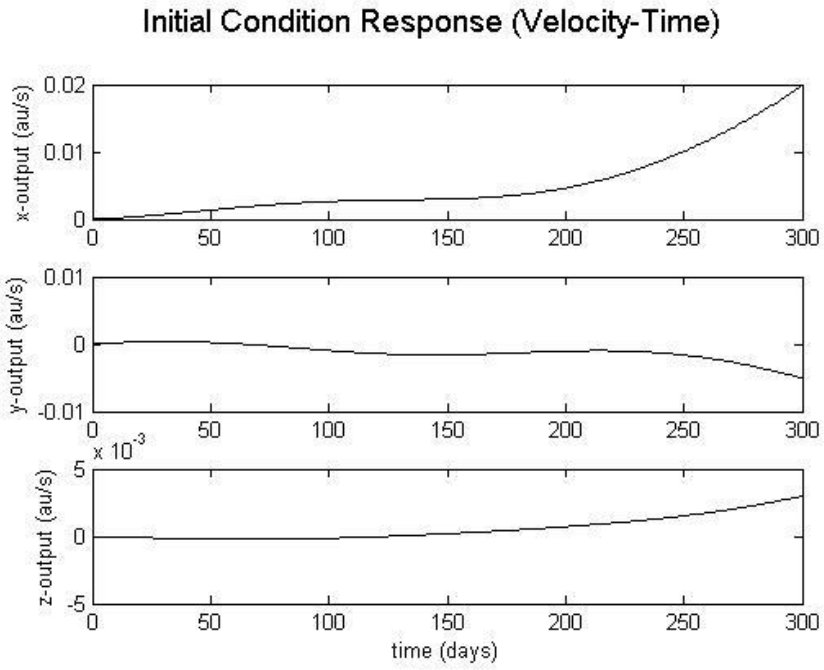

Figure 4.1.1b. Zero-Input Response at $\mathcal{L}_A$ (Velocity-Time)

The six components of the initial state vector, $x(0)$, correspond to the components of the sail's orbital position and velocity. The solar sail position is defined with respect to the ALO by shifting the origin of the rotating frame (described in Chapter 2) to the position of the ALO, $\mathcal{L}_A$. Figure 4.1.1a illustrates how the positional components of an uncontrolled solar sail in the vinicity of an ALO drifts over time as a result of the unstable nature of the equilibrium point. Recall, that an LTI system is unstable if the natural response grows without bound as time approaches infinity, and marginally stable if the natural response neither decays nor grows but oscillates as time approaches infinity. In Chapter 2 it was shown that the system is unstable because of the systems pole location on the complex plane. The eigenvalues of this system – shown in Figure 4.1.1e – contain both positive real parts and are very close to the imaginary axes.

The simulation shows that the y and z components of the system response are not immediately unbounded, but appear to oscillate for some time before becoming exponential. The x component

is the most unstable, and the solar sail immediately diverges from the ALO along this component. In the first 100 days, the y component shows marginal stability as the solar sail motion appears to oscillate for one period about the y axis. After 100 days, the component's instability is manifested and the solar sail's motion becomes unbounded. The motion of the solar sail along the z component also appears to indicate marginal stability for the first 100-150 days. After ~150 days, the solar sail trajectory along the z component also becomes exponential. The behviour of the sail shown by the simulations in this section are not exact for several reasons. One of the reasons the simulation may not display the accurate behaviour of the system is because the time response of unstable systems is unbounded, and physical systems have physical bounds. For example, the exponential response implies that the velocity of the sail increases without bound. The arbitrarily selected initial conditions also play a role in the large velocity components. If initial conditions are selected much closer to the equilibrium point, the velocity remains much smaller for a longer period of time. The simulations are valid in demostrating the instability of the ALO, which is why they are used here. However, the physical trajectory of the sail and the rate of divergence in these simulations should be ignored.

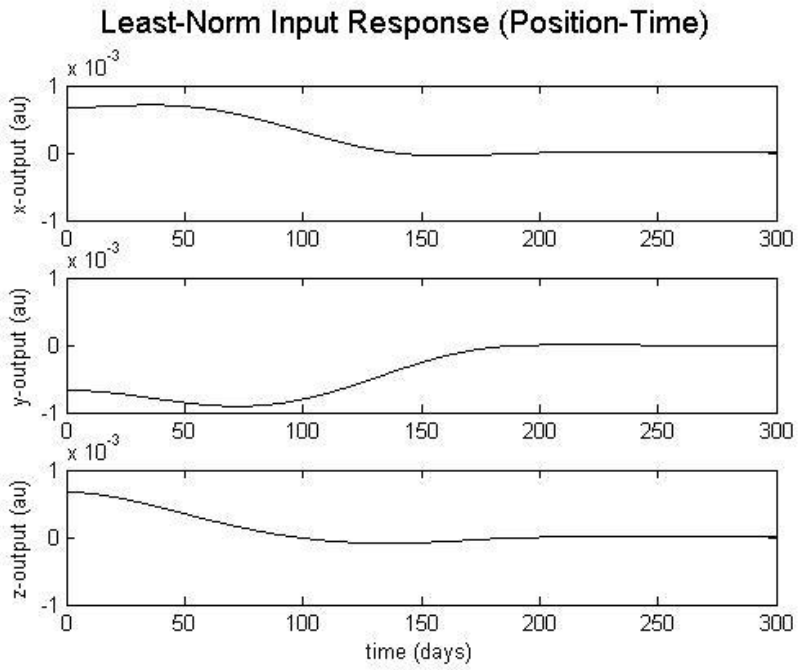

Figure 4.1.1d. Regulation at $\mathcal{L}_A$ (Position-Time)

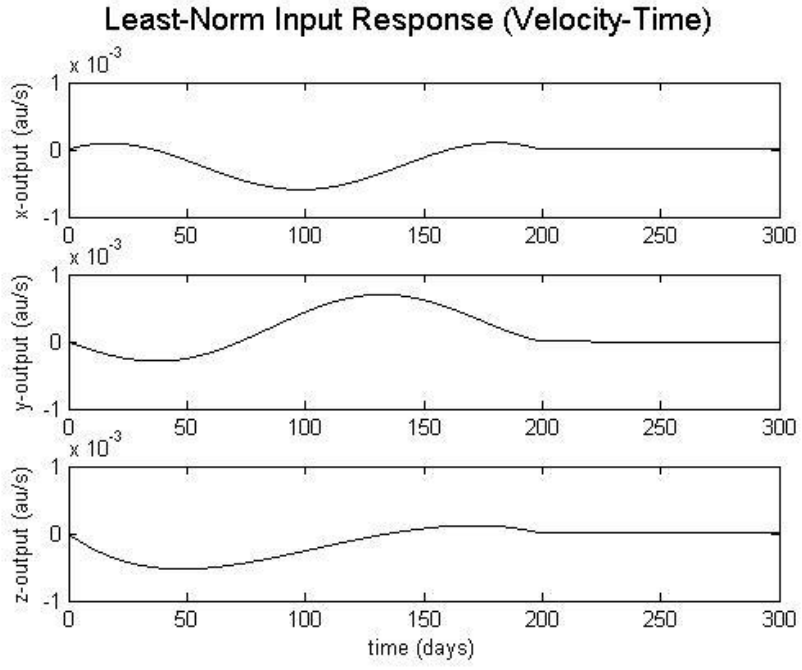

Figure 4.1.1e. Regulation at $\mathcal{L}_A$ (Velocity-Time)

Figure 4.1.1c shows successful orbital regulation of a solar sail using the minimum energy controller over a period of 200 days. The same trajectory is shown from another perspective in Figure 4.1.1e, and includes information on the sail quality, eigenvalue, and condition number of the Gramian. Again, this simulation does not accurately describe the true behavior of a sail, it only confirms that sail regulation is possible. The physical constraint on the inputs are not taken into account here. In other words, the rate are which the spacecraft is physically able to furl and unfurl its sail is not considered. Similarly, the mechanism involved with varying the sail attitude is not taken into account, so the rate at which the sail is able to vary its cone and clock angles is undefined. This minimum energy controller assumes there is no bound on these physical components, but describes the maneuvers required to regulate the sail using minimal energy over a period of 200 days. The velocity components were also successfully regulated, though the same comments apply here.

It is also important to take into consideration the integration of the controllability Gramian. The interval of integration was experimentally chosen to be 200 days for reasons explained in Chapter 3. Changing this interval directly affects the simulation in Figures 4.1.1c-d because the ratio of singular values decreases. However, like the initial conditions, the same interval of integration is used in succeeding examples to show how solar sails behave in different ALOs – at least in a relative sense. The ALO in Figures 4.1.1 is far enough from both primaries such that its controllability Gramian appears relatively well conditioned. The eigenvalues of the system's dynamics matrix $\boldsymbol{A}$ at this equilibrium point are also very close to the imaginary axis, which means the equilibrium point is not highly unstable in comparison to the following two examples. The magnitude of the individual singular values are somewhat attenuated in the directions corresponding to σ_5 and σ_6, though the simulations indicate that this has no significant impact on the control of any particular state, as predicted in Chapter 3. Compared to the values presented in Tables 3.2.1-3.2.2, the singular values corresponding to the controllability Gramian at $\boldsymbol{\mathcal{L}_A}$ are relatively controllable. For this reason, this ALO will be used as the standard for comparing controllability with respect to the remaining two examples in this chapter.

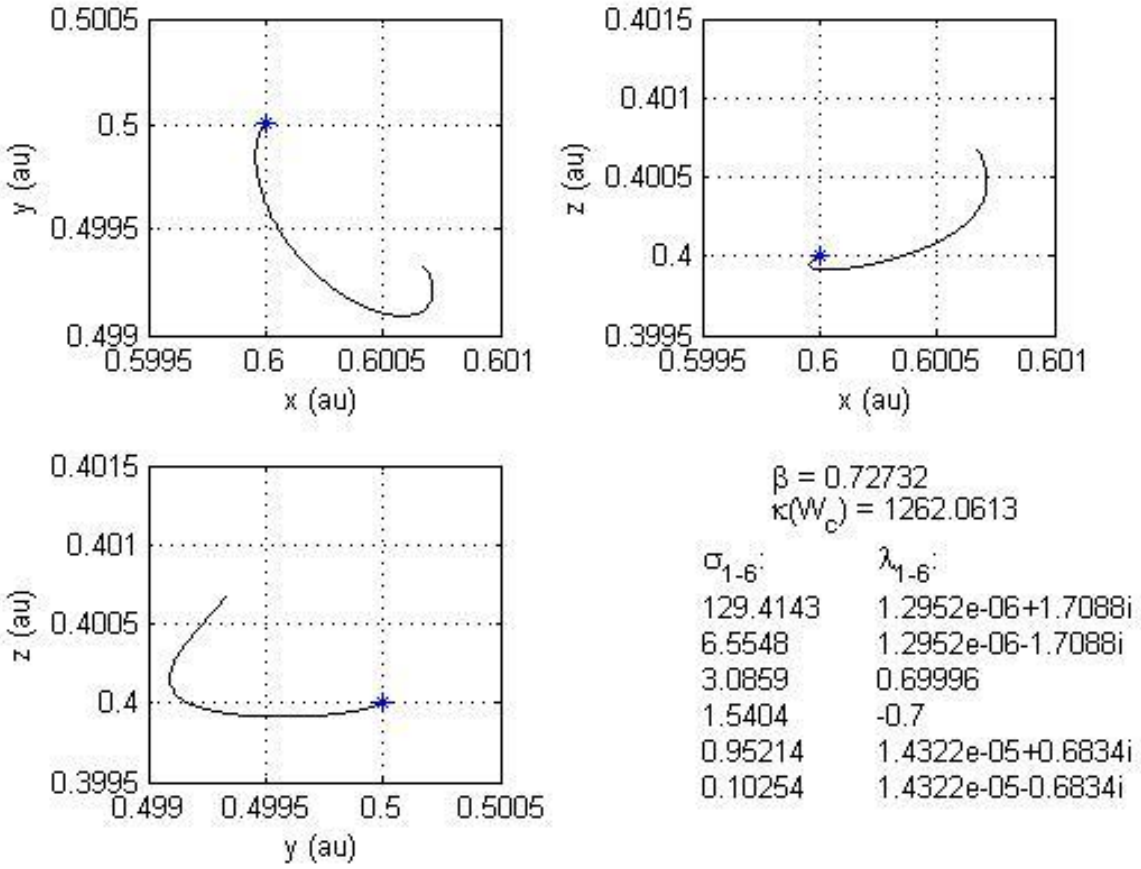

Figure 4.1.1c. Regulation of Sail Position at $\mathcal{L}_A$

4.2 ALO Near the First Primary

The ALO explored in this example is closer to the Sun and could ideally be used for a Solar Polar Imager mission. A sail flying this close to the Sun experiences a larger gravitational pull, but also a larger push from solar radiation pressure. It would be interesting to study more thoroughly the true behavior of a sail this close to the Sun compared to a sail much further away. In this example, it is expected that the ALO would be more unstable as a result of its nearness to the first primary. More importantly, the condition number of the controllability Gramian here implies more energy is required for sail regulation than in the previous example. According to Figures 3.3.1a-b, this ALO falls in a region that is less controllable than $\mathcal{L}_A$. The initial condition

response, as well as the least-norm input response for position and velocity, are compared to that of Figures 4.1.1a-e. The same initial conditions are used here as in the previous example, as well as the same interval of integration for the corresponding controllability Gramian and minimum energy. The only change which has been made here is the location of the equilibrium point in the Earth-Sun system.

ALO; $\mathcal{L}_B = (0.2\text{au}, 0.2\text{au}, 0.2\text{au})$

Initial State; $$x(0) = \begin{bmatrix} 100{,}000km \\ -100{,}00km \\ 100{,}000km \\ 10m/s \\ 10m/s \\ -1m/s \end{bmatrix}$$

As in the previous example, the solar sail position is defined with respect to the ALO by shifting the origin of the rotating frame to the position of the ALO, $\mathcal{L}_B$. It should immediately be noted that the scale size of the position axis in Figure 4.2.1a-b is much larger than the scale size of Figure 4.1.1a-b. This is because the exponential grows much faster in this example than in the previous one, indicating that the positive real part of the eigenvalues in this system are further from the imaganiry axis, which means that $\mathcal{L}_B$ is more unstable than $\mathcal{L}_A$. It is not easy to see oscillations in the first few months in this example because the scale size is too large. however, the exponential is clearly visible as in the last example for all three components after roughly the same time period (~150 days). The components appear stable for the first ~150 days, but that is only because the scale size is so large; if decreased the exponential would appear to grow much sooner. Similarly, the velocity-time plot shows the same kind of behaviour. Once again, both simulations do not accurately desribe the true behaviour of the solar sail near the ALO for the same reasons that were mentioned in the previous section.

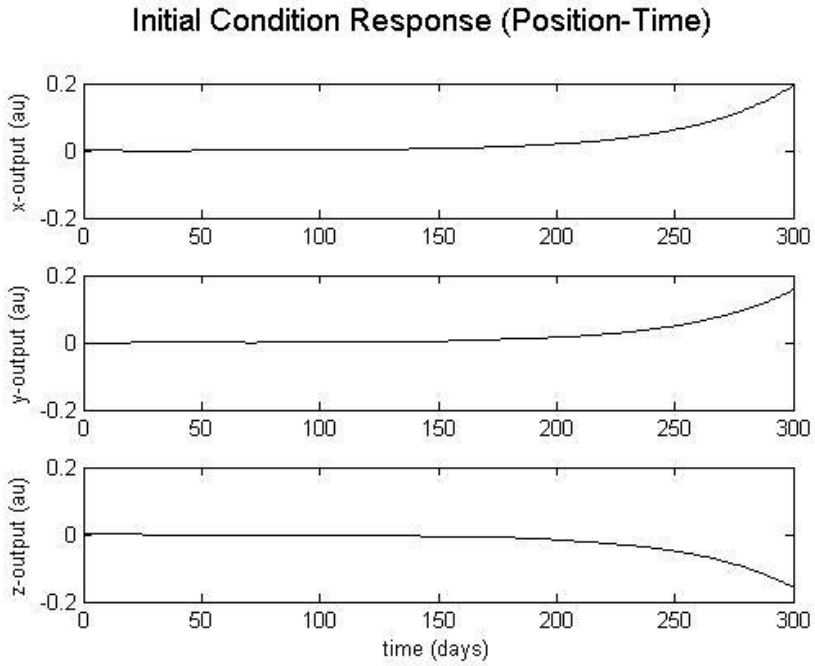

Figure 4.2.1a. Zero-Input Response at $\mathcal{L}_B$ (Position-Time)

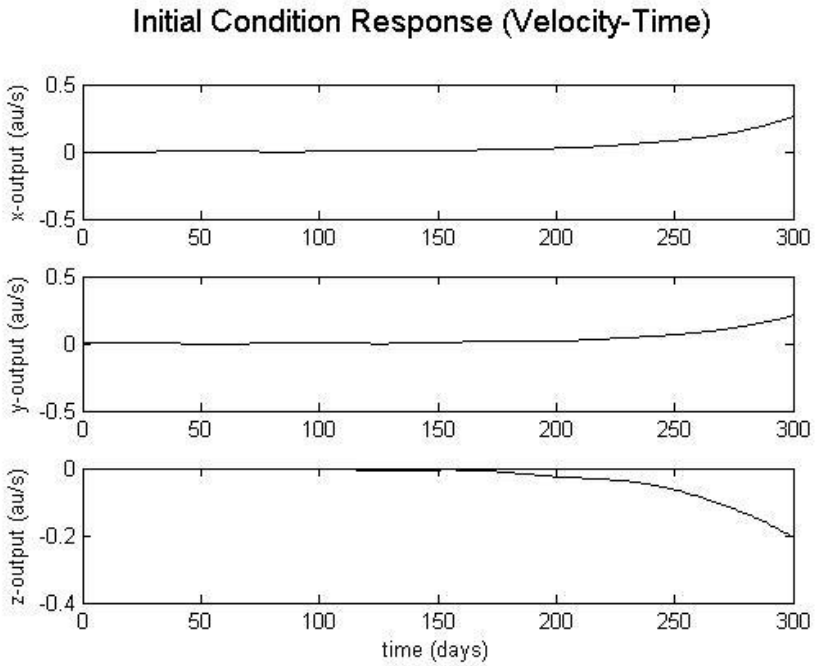

Figure 4.2.1b. Regulation at $\mathcal{L}_B$ (Position-Time)

Figure 4.2.1c shows successful regulation of the solar sail at $\mathcal{L}_B$ over a period of 200 days. This response is much more oscillatory than in Figure 4.1.1c. Since the minimum energy controller is implemented over the same period as in the previous example, the solar sail reaches steady state in 200 days even though the response is more underdamped. This response is a good indication that $\mathcal{L}_B$ is more difficult to control than $\mathcal{L}_A$ because it would take more energy to dampen the response so that it resembles Figure 4.1.1c. It is also important to consider whether or not the solar sail is physically capable of performing such maneuvers. This is not examined here, but the larger the frequency of oscillations in the transient response, the more difficult the system is to control. Figure 4.2.1d shows that the velocity-time response behaves similarly in that the direction or course of the solar sail changes very quickly. This may not be possible even if the magnitude of the velocity is decreased, the orientation of a large sail is difficult to meaneuver in short time periods. The rate at which the sail can perform these maneuvers is not covered in this thesis, but would also be interesting to examine, as it is also directly related to controllability.

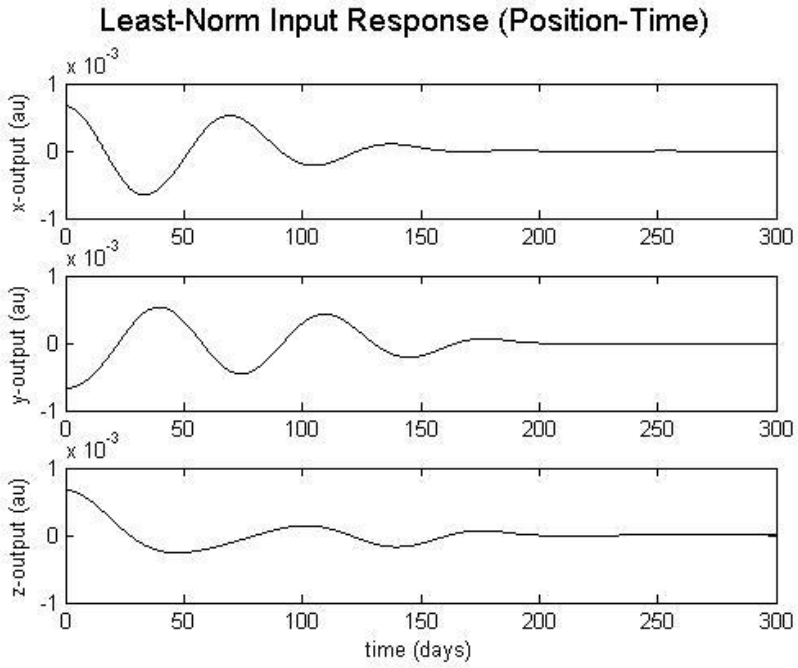

Figure 4.2.1c. Regulation of Sail Position at $\mathcal{L}_B$

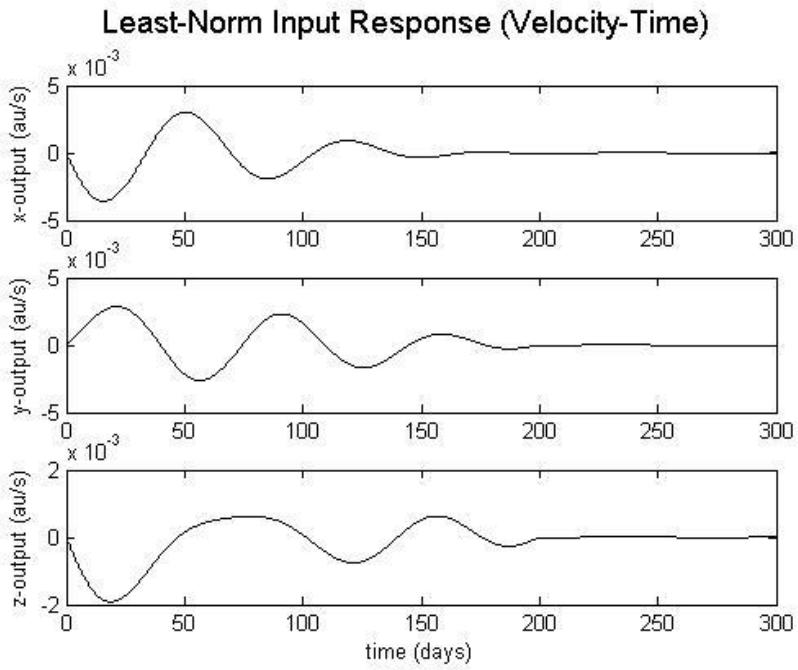

Figure 4.2.1d. Regulation of Sail Velocity at $\mathcal{L}_B$

The condition number for the Gramian at $\mathcal{L}_\mathrm{B}$ is an order of magnitude larger than the condition number of the Gramian at $\mathcal{L}_\mathrm{A}$ due to the singular values $\sigma_4 - \sigma_6$ being an order of magnitude smaller than the corresponding singular values at $\mathcal{L}_\mathrm{A}$. This was illustrated in Figure 3.4.1c using the minimum energy ellipse in comparison to the size and shape of Figure 3.4.1a. Here, the effect on the simulation is an increase in the number of oscillations before steady state is achieved, which is another demostration of relative control difficulty. If the minimum energy is increased together with a decrease in the time over which the controller is implemented, (refer to Figure 3.4.1b) this would result in a response that is less oscillatory and more similar to the response seen for $\mathcal{L}_A$ in Figure 4.1.1c-d. The reason for this is that the minimum energy is related to the singular values of the controllability Gramian and the period of time over which they diverge. The two real eigenvalues of the system shown in Figure 4.2.1e have a magnitude of 1.3336; about twice as large as that of the example for $\mathcal{L}_A$. As discussed earlier, this is likely due to the increased gravitational pull near the first primary. There is not enough information here to show how much more difficult this ALO is to control over $\mathcal{L}_A$, but enough to demonstrate – through simulations – that an increase in control effort is required to regulate the sail at $\mathcal{L}_\mathrm{B}$. The difference in the ratio of singular values of the controllability Gramian between the two

examples $\mathcal{L}_A$ and $\mathcal{L}_B$ is not huge, so although an increased difficulty in control is expected, it is not as concerning as other issues that arise near the Sun, such as temperature. The next example is for an ALO with a much larger condition number.

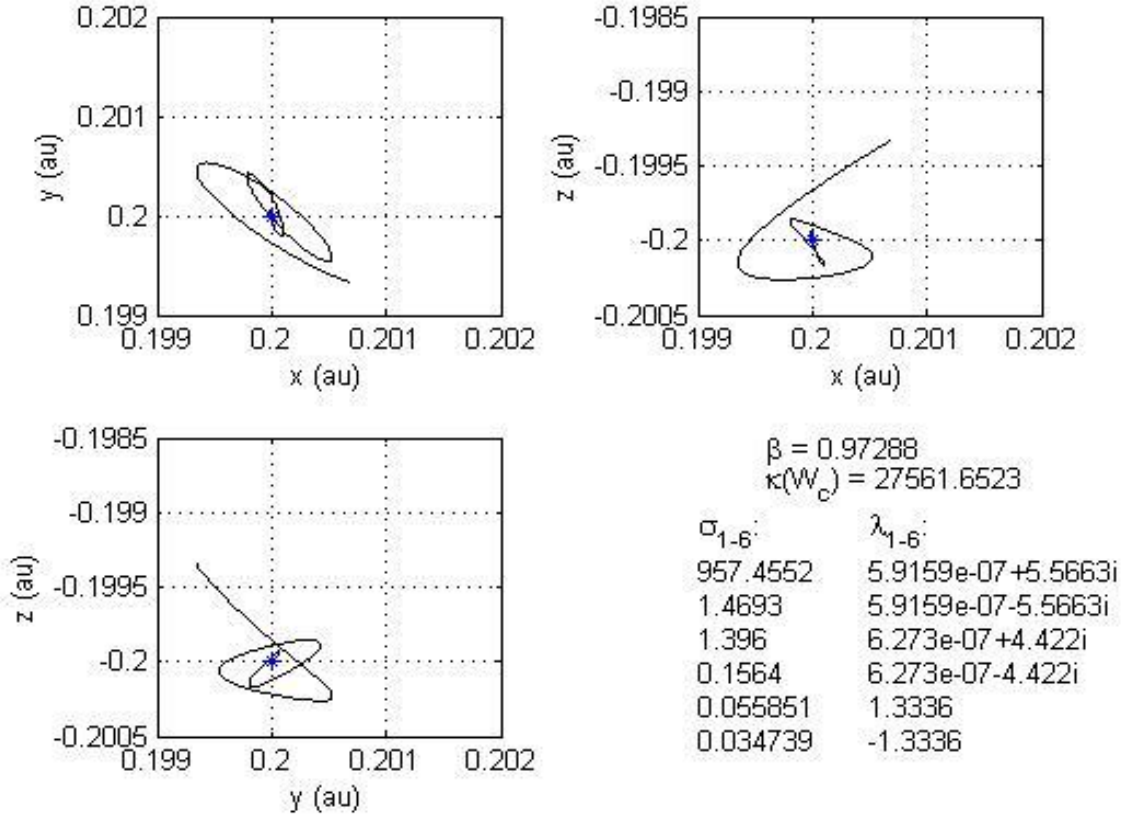

Figure 4.2.1e. Regulation of Sail Position at $\mathcal{L}_B$

4.3 ALO Near the Second Primary

The ALO explored in this example is a well-known Lagrangian point ($L1$) which exists in the Circular Restricted Three-Body Problem. $L1$ is a highly unstable ALO when compared to $\mathcal{L}_A$ and $\mathcal{L}_B$, but there are a number of artificial spacecraft operating in the vicinity of $L1$, including the Solar and Heliospheric Observatory (SOHO) – launched December 2nd, 1995. SOHO has been succesfully operating for over 20 years. It was designed to study the internal structure of the Sun, as well its atmosphere and solar wind[53]. $L1$ is located on the ecliptic plane roughly 1.5 million km Sun-side from the Earth; this location is ideal for early warning space weather systems.

The relative instability of this ALO is a result of the system's large, real positive eigenvalue, $\lambda = 2.5225$ – which is nearly twice that of $\mathcal{L}_B$ and four times that of $\mathcal{L}_A$. There are two possible cases which are expected to result from this simulation. The first case is that the transient response would be much more underdamped than the previous example, indicating that more energy is required to dampen the transient. The second case is that the system requires so much more energy to regulate the sail that the simulation would produce a response that is nonsensical and completely meaningless. In either case, this would be true for only two out of the three components of the system – recall that for equilibrium points on the ecliptic, the z component is decoupled and marginally stable. The simulations shown in Figures 4.3.1 show that for libration point control, the second case is true. The exponential response of the x and y components grow so fast that it is completely irrational. Control of the unstable x and y components requires much more energy than what was used to regulate the sail's orbit in the previous two examples. It is interesting to note that although the condition number at $L1$ is a factor of 10^5 times larger than that of $\mathcal{L}_A$, the controllability matrix at $L1$ is full rank, which means that it is possible – in theory – to regulate a sail at $L1$. Information on how practical that is, is available through the condition number of the Gramian. Similar to the previous example for $\mathcal{L}_B$, the initial condition response shown in Figures 4.3.1a-b are not practical or physically possible. The simulation is only useful in showing that relative to the previous two examples, $L1$ is highly unstable in the x and y components and requires much more energy to control. Figures 4.3.1a-b also show that the decoupled z component is oscillating about -100,000km to +100,000km. It is the only component that can be regulated using the same minimum energy controller that was used in the previous two examples.

ALO; $L1 = (0.99\text{au}, 0\text{au}, 0\text{au})$

Initial State; $$x(0) = \begin{bmatrix} 100{,}000km \\ -100{,}00km \\ 100{,}000km \\ 10m/s \\ 10m/s \\ -1m/s \end{bmatrix}$$

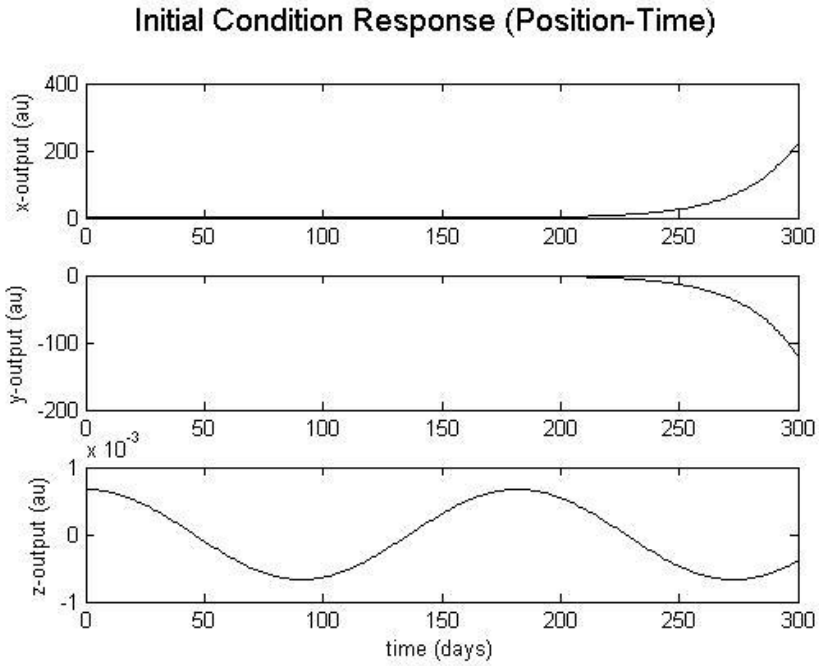

Figure 4.3.1a. Zero-Input Response at $L1$ (Position-Time)

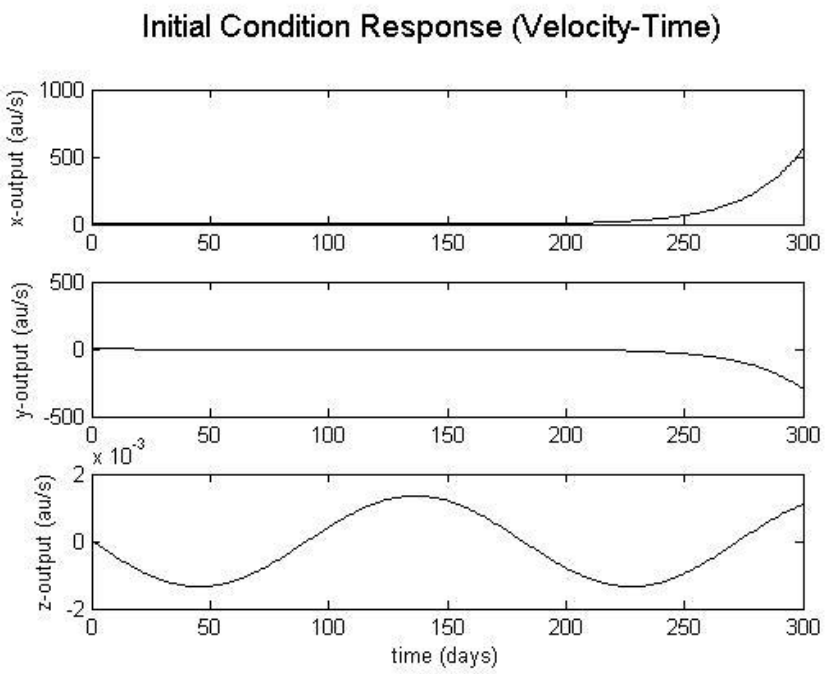

Figure 4.3.1b. Zero-Input Response at $L1$ (Velocity-Time)

Figures 4.3.1c-d show that the minimum energy controller is unable to regulate the x and y components of the sail orbit after 200 days. However, the controller is able to regulate the uncoupled z component with less energy than the z component of the sail at $\mathcal{L}_B$; this is apparent because the z component regulation at $\mathcal{L}_B$ is more underdamped than in this example. $L1$ has a positive real eigenvalue of 2.5225, and purely imaginary eigenvalues which are very close to each other ($\pm\, 2.0803i$ and $\pm 2.0089i$). This implies that the equilibrium point in this example is more unstable, and therefore more difficult to control than the previous examples. As discussed in Chapter 3, the reason for the increased instability of the equilibrium point is due its proximity to the Earth. Given that the ecplitpic plane guarentees a marginally stable z component, it can be argued that the most relatively controllable ALOs lie on the eclpitic plane in the range of $x = 0.6\ au$ to $0.9\ au$ (refer to Figure 3.3.1). The range of singular values of the controllability Gramian for ALOs in this region is smallest, and the ALOs on the ecliptic are marginally stable. There is potential for solar sails in this region to operate as Sun observation satellites. However,

L1 should not be ruled out, these simulation results only imply that controlling a sail at an ALO on the ecliptic that is further out from the Earth than L1 would be less expensive.

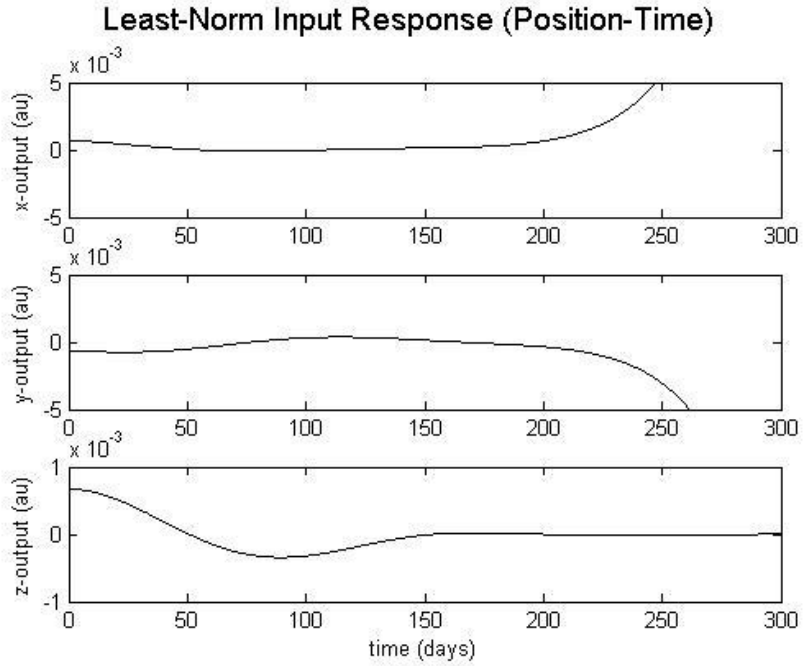

Figure 4.3.1c. Failed Regulation at $L1$ (Position-Time)

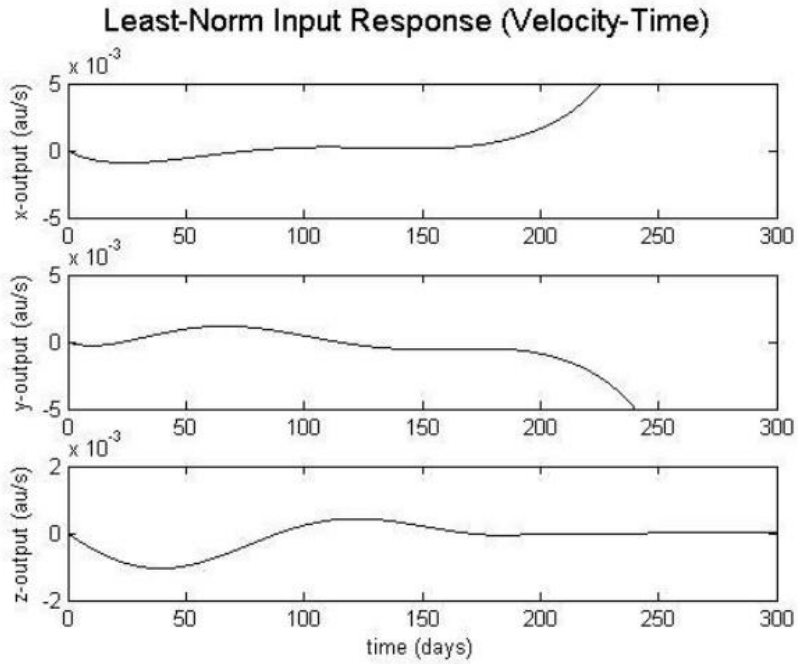

Figure 4.3.1d. Failed Regulation at $L1$ (Velocity-Time)

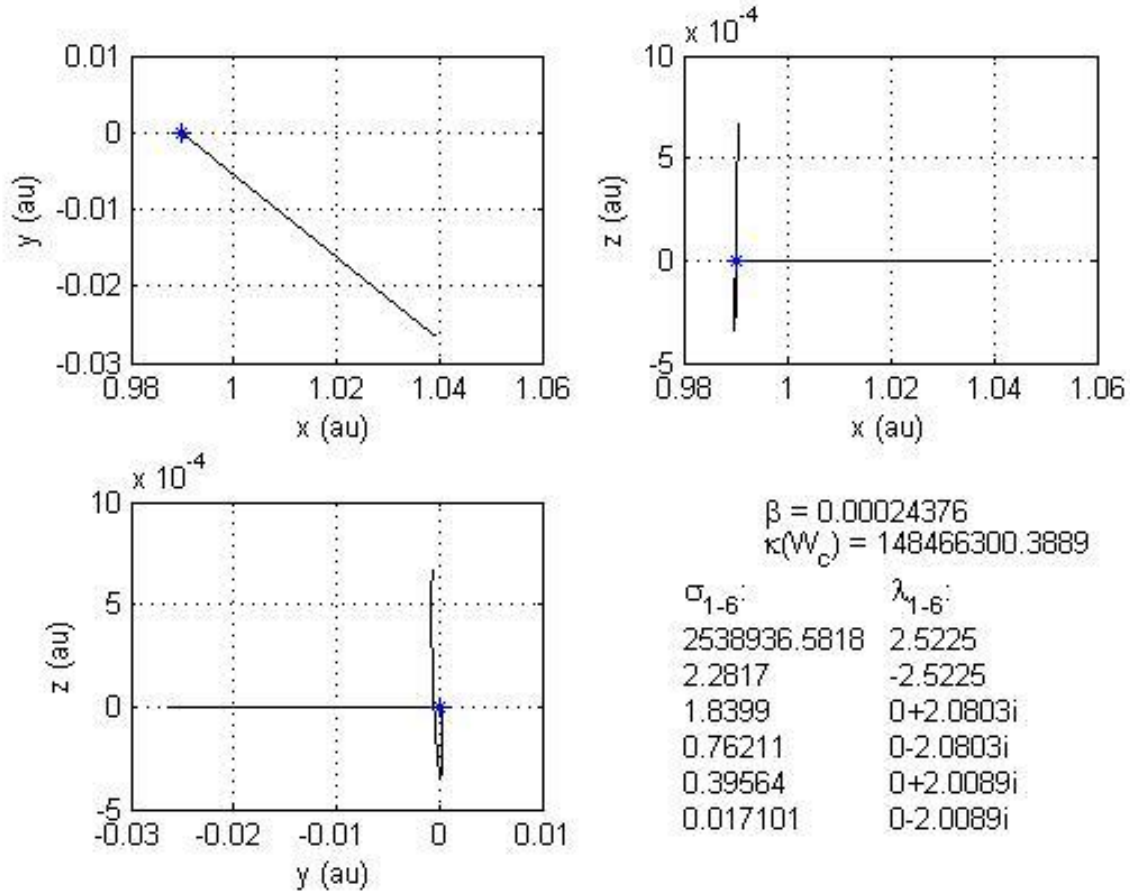

Figure 4.3.1e. Failed Regulation of Sail Position at $L1$

Figure 4.3.1e shows the condition number of the Gramian at $L1$. This is significantly larger than the condition number of the previous two examples, and the impact this value has on the system is demonstrated clearly through the simulations. As discussed in Chapter 3, the increased condition number is primarily due to the incease in the maximum singular value, and not the minimum singular value. The minimum singular value in each example looked at in this Chapter has only changed by a factor of 10, while the maximum singular value has grown by a factor of 1000. Recall, that a descrease in the minimum singular value often implies attenutation of the signal corresponding to that direction in state space. An increase in the singular value is often desirable, but only if all singular values maintain the same relative size. The failed regulation of the solar sail at $L1$ is primarily due to the fact that unstable system's Gramian grows too fast. In Chapter 3, it was shown that the integral of the controllability Gramian of the unstable system

grows without bound over time. This rate of growth is also related to how unstable the system is. Given that $L1$ is the most unstable ALO considered in this Chapter, it is expected that the least-norm input response of the system would reflect the rate of growth of the Gramian's maximum singular value. In order to force a successful regulation in this simulation, the interval of integration needs to be decreased to a time before the ratio of singular begins to aggresively diverge; this is demonstrated in Figures 4.3.2. By decreasing the interval of integration to 100 days (and the minimum energy controller to 100 days), the x and y components can be successfully regulated.

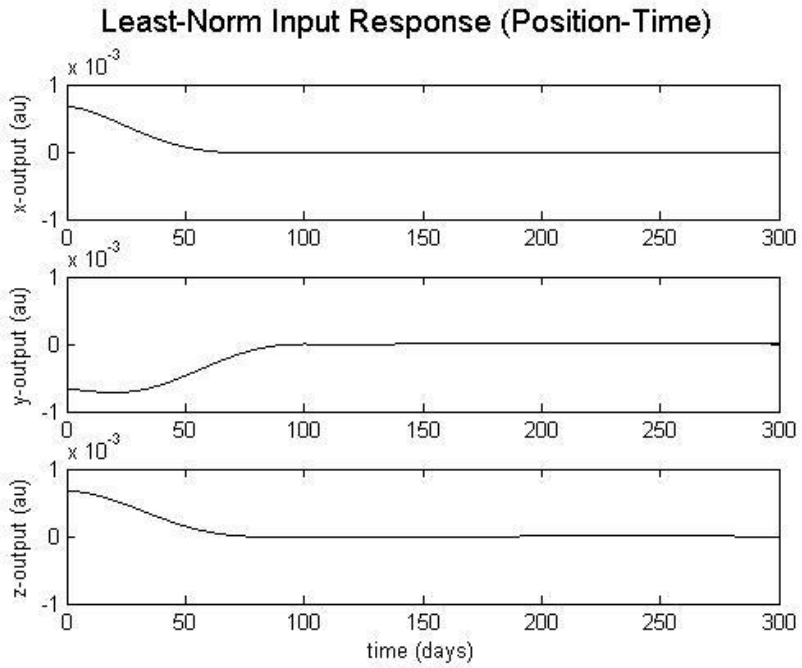

Figure 4.3.2a. Orbital Regulation at $L1$ Position (100 days)

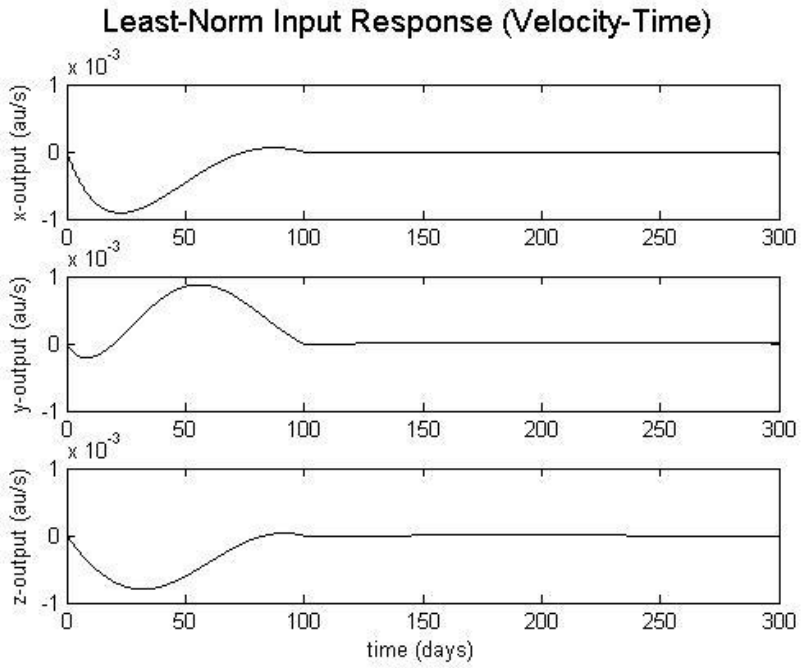

Figure 4.3.2b. Orbital Regulation of *L*1 Velocity (100 days)

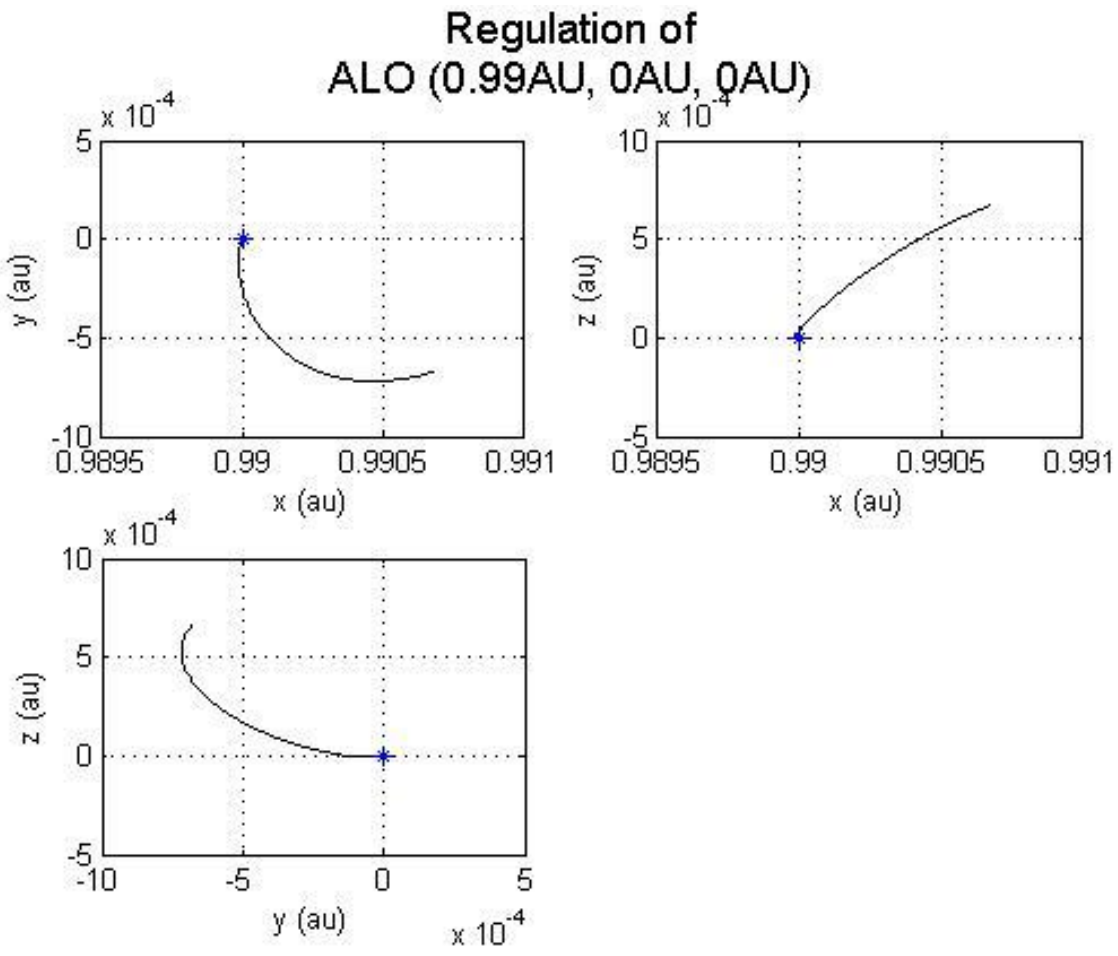

Figure 4.3.2d. Successful Regulation of ALO at $L1$

This Chapter has investigated the controllability of a sail at various ALOs based on the condition number of the controllability Gramian using simulations of the system's natural and controlled response. The difficulty of controllability – in terms of minimum energy – was investigated based on the size of the condition number of the controllability Gramian corresponding to an ALO, as well as the location of the ALO – whether on the ecpliptic, or near a primary. A minimum energy controller was used to show that the energy required to regulate a sail is dependent on the size of the ratio of singular values of the controllability Gramian corresponding to the equilibrium point. Since the unstable Gramian is unbounded, the interval of integration is used to illustrate the rate of growth at which the singular values of the Gramin diverge, based on how unstable the equilibrium point is, and therefore how difficult it would be to control. A relative, quantitative measure of controllability can therefore be represented by the rate at which

the ratio of singular values grow over the Gramians interval of integration – as shown in these simulations. The simulations themseleves do not reflect the true behviour of the sail, but are used to illustrate the relative behaviour of the sails at various ALOs. This chapter is not meant to discuss the absolute controllabiliy of a sail at each ALO, but the relative controllability. It was shown that the closer the Gramian's condition number is to a value of 1, the more controllable the sail orbit .

5. Conclusion

5.1 Summary

The main objective of this thesis is to demonstrate the relative degree of controllability of solar sails in various artificial Lagrangian orbits using an energy-related measure. To do this, the modified circular restricted three-body problem was introduced for the Earth-Sun system, which included the acceleration of the sail due to solar radiation pressure. After demonstrating the existence of ALOs in Chapter 2, a linear model was derived so that the system could be rewritten in state space, and the local behavior of the system (near each equilibrium point) could be revealed through the location of the system's eigenvalues on the complex plane. The Routh-Hurwitz critereon was used to show that asymptotic stability is not possible and that the system is generally unstable. The six system poles were shown to be located very close to the imaginary axis, with the exception of two mirrored poles, which grow further from the imaginary axis for ALOs existing closer to the primaries. The linear model derived in Chapter 2 does not account for two factors which may have a significant effect on the dynamics of the problem near the Earth, i.e., gravitational effects from the moon, as well as albedo effects from both the Earth and Moon. These effects would be manifest in the near Earth ALOs and could increase instability. In Chapter 3, various methods used in control theory to determine the degree of controllability of a system were explored. A method involving the singular values of the well-known controllability Gramian was chosen because it has a physical meaning of minimum input energy, which satisfies the objective of this study. Various possible control configurations were demonstrated to provide complete controllability in the xz and xy planes via the rank test for controllability. However, the practicality of these configuration awas revealed in the ratio of singular values of the controllability Gramian. It was shown that although the system is full rank for any controllable configuration (one, two, or three inputs), the degree of controllability – based on the condition number of the controllability Gramian – is significantly weakened by the removal of any two of the three control elements introduced in Chapter 3. If only one element is used to control the sail, the true rank of the controllability matrix is 4, and not 6. In other words, the system is – for all practical purposes – not controllable. The ratio of singular values were also used to demonstrate control difficulty in terms of energy requirements with regards to various

ALOs in the xz and xy planes. The minimum energy required to regulate the sail orbit using the same initial conditions showed a huge decrease in energy required for state transfers when including the sail area as a control element, as opposed to only the sail attitude (see Figures 3.4.1). The condition number was then represented as a minimum energy ellipse produced by the controllability Gramian, and revealed controllable directions in state space. The results presented in Figures 3.5.1 are consistent with the results of Figures 3.3.1. Finally, Chapter 4 demonstrated orbital regulation of a sail at three ALOs, using a fixed controllable configuration (sail attitude + sail area) and bound on energy. Simulations were produced using the minimum energy controller in order to show which ALOs require more energy to regulate a sail. Again, the results obtained through the simulations were consistent with what was shown in Figures 3.3.1 and 3.5.1. The simulations revealed control difficulty increasing near the primaries; especially along the axes that joins the two primaries. The investigation of other types of controllers reveal libration point control is possible at $L1$, but the purpose of using the minimum energy controller in this thesis was to demonstrate relative control difficulty. It is very clear that controllability decreases greatly near the Earth, and it was shown that control difficulty can be significantly reduced by choosing the appropriate ALO.

The purpose of this study was to examine the relative degree of controllability of solar sails in the modified circular restricted three-body problem using the well-known energy-related controllability Gramian. This was succesfuly done by demostrating that the ratio of singular values of the linear dynamical system's controllability Gramain vary greatly depending on the location of the ALO, as well as the control elements of the sail. Prior to this study, the relative controllability of a sail in ALOs was not known because the rank test of controllability does not reveal quanitative information on a system's degree of controllability. This thesis is a first step in the direction of detemining the absolute degree of controllability for solar sails in artificial Lagrangian orbits.

5.2 Recommendations

Following the results of this thesis, there are many directions to proceed with. A clear indication of control difficulty exists for various ALOs as represented by the condition of the Gramian matrix; especially if control is limited to only sail angles. Many definitions for the degree of

controllability of a system have been developed and can be used to confirm the results presented here, as well as provide a more fundamental measure of controllability. The difference in controllability due to the addition of the sail area control element should also be further examined with regards to its merit. This may only be necessary for very unstable ALOs that require greater control effort. A more thorough examination would include directions in state space that become more controllable with the addition of this element. For near Earth ALOs it would be worthwhile to examine the difference in controllability of the altered, but still unstable ALOs, when albedo effects are included.

The on-axis libration points are also important for missions involving Sun observations, and so further examining their controllability is encouraged. As shown in Chapter 2, the entire ecliptic plane has a stable z-component, and it has been shown that regions of marginal stability exist in the ecliptic. It would be interesting to examine the controllability of such ALOs as their stable dynamics could make regulation much simpler for solar sails.

It is most important however, to note that the true physical meaning of what the magnitude of singular values represents in this thesis is unknown. Perhaps a minimum singular value with a magnitude as small as 1×10^{-6} corresponds to a direction in state space that is in fact controllable. Ideally, this would be investigated experimentally but perhaps it can also be determined indirectly by comparing the results of this problem to the results of a similar, more well-known problem.

5.3 Concluding Remarks

Solar sailing is a novel technology that is still in its infancy, with great potential for a large number of missions that are not possible with conventional spacecraft. There is much still to learn about the dynamics and control of solar sails. Many constraints on solar sailing applications are due to mechanical designs that must first be resolved. Solar sailing missions have been abandoned in the past, primarily due to the fact that they have not been proven to be a well-developed technology.

This study has succesfully demonstrated the relative degree of orbital controllability of solar sails in artificial Lagrangian orbits using energy related measures of control. The condition number of the controllability Gramain is only one of many methods that can be used to demonstrate relative controllability.

References

[1] Levin, E. (1968). *Solar radiation Pressure Perturbations of Earth Satellite Orbits*. AIAA Journal, 6(1), 120-126.

[2] Solar Sail Propulsion. (2005, April). Retrieved June, 2016, from *https://www.nasa.gov/pdf/134645main_solar_sail_fs.pdf*

[3] Friedman, L., Carroll, W., Goldstein, R., Jacobson, R., Kievitt, J., Landel, R., Layman, W., Marsh, E., Ploszaj, R., Rowe, W., Ruff, W., Stevens, J., Stimpson, L., Trubert, M., Varsi, G., and Wright, J., "*Solar Sailing-The Concept Made Realistic*", AIAA-78-82, 16th AIAA Aerospace Sciences Meeting, Huntsville, AL, January 1978.

[4] Lior, N. (2013). *Mirrors in the sky: Status, sustainability, and some supporting materials experiments.* Renewable and Sustainable Energy Reviews, 18, 401-415.

[5] Sci/Tech | Znamya – *what went wrong?* (1999, February 05). Retrieved March 22, 2016, from http://news.bbc.co.uk/2/hi/science/nature/273220.stm

[6] Tsuda, Y., Mori, O., Funase, R., Sawada, H., Yamamoto, T., Saiki, T., Endo, T., Yonekura, H., and Kawaguichi, J., "*Achievement Of Ikaros – Japanese Deep Space Solar Sail Demonstration Mission*", 7th IAA Symposium On Realistic Near-Term Advanced Scientific Space Missions, Aosta, Italy, 2011.

[7] JAXA | Small Solar Power Sail Demonstrator "IKAROS". (n.d.). Retrieved January 31, 2017, from http://global.jaxa.jp/projects/sat/ikaros/topics.html

[8] Johnson, L., Whorton, M., Heaton, A., Pinson, R., Laue, G., & Adams, C. (2011). *NanoSail-D: A solar sail demonstration mission*. Acta Astronautica, 68(5-6), 571-575.

[9] Alhorn, D., Casas, J., Agasid, E., Adams, C., Laue, G., Kitts, C., and O'Brien, S., "*NanoSail-D: The Small Satellite That Could*", 25th Annual AIAA/USU Conference on Small Satellites, Ogden, UT, 2011.

[10] *DeorbitSail Update and Initial Camera Image*. (2015, November 13). Retrieved February 01, 2017, from https://amsat-uk.org/2015/11/13/deorbitsail-update-and-initial-camera-image/

[11] *Solar Sail Demonstrator* ('Sunjammer'). (n.d.). Retrieved February 01, 2017, from https://www.nasa.gov/mission_pages/tdm/solarsail/index.html

[12] Wie, B., Thomas, S., Paluszek, M., and Murphy, D., "*Propellantless AOCS Design for a 160-m, 450-kg Sailcraft of the Solar Polar Imager Mission*," 41st AIAA/ASME/SAE/ASEE Joint Propulsion Conference and Exhibit, Tucson, USA, July 2005, AIAA Paper 2005-3928.

[13] Wie, B., "*Thrust Vector Control of Solar Sail Spacecraft*," AIAA Guidance, Navigation, and Control Conference, San Francisco, USA, August 2005, AIAA Paper 2005-6086.

[14] Dachwald, B., Ohndorf, A., & Wie, B. (2006). *Solar Sail Trajectory Optimization for the Solar Polar Imager (SPI) Mission*. AIAA/AAS Astrodynamics Specialist Conference and Exhibit.

[15] Waters, T.J., & McInnes, C. R. (2007). *Periodic Orbits Above the Ecliptic in the Solar-Sail Restricted Three-Body Problem*. Journal of Guidance, Control, and Dynamics, 30(3), 687-693.

[16] Wie, B. (2004). *Solar Sail Attitude Control and Dynamics, Part 1*. Journal of Guidance, Control, and Dynamics, 27(4), 526-535.

[17] Wie, B. (2004). *Solar Sail Attitude Control and Dynamics, Part Two*. Journal of Guidance, Control, and Dynamics, 27(4), 536-544.

[18] Price, H., Ayon, J., Buehler, M., Garner, C., Klose, G., Mettler, E., Nakazono, B., and Sprague, G. (2001). *Design for a Solar Sail Demonstration Mission*. Space Technology and Applications International Forum (STAIF 2001), Albuquerque, NM.

[19] West, J. L., and Derbes, B. (2000). *Solar Sail Vehicle System Design for the Geostorm Warning Mission*. AIAA Paper 2000-5326.

[20]Rogan, J., Gloyer, P., Pedlikin, J., Veal, G., and Derbes, B. (2001). *Encounter 2001: Sailing to the Stars*," Paper SSC01-II-2, Utah State University, Logan, UT, Aug. 2001.

[21]Cohen, D., Gloyer, P., and Rogan, J. (2002). *Preliminary Design of a High Performance Solar Sailing Mission*," Paper SSC02-II-5, Utah State University, Logan, UT.

[22] Murphy, D. M., Murphey, T.W., and Gierow, P. A. (2002). *Scalable Solar Sail Subsystem Design Considerations*. AIAA 2002-1703.

[23] Hutputtanasin, A. and Toorian, A., "CubeSat Design Specification - Revision 9," http://cubesat.atl.calpoly.edu/ media/Documents/Developers/CDS%20R9.pdf, 2005, [Online; accessed 25-April-2007].

[24] Moore, J., "*SRS Technologies — Solar Sails*," http://www.stg.srs.com/atd/Solar_Sail.htm, 2000, [Online; accessed 25-April-2007].

[25] Edwards et al. (2004). *Electron Radiation Effects on Candidate Solar Sail Material*. High Performance Polymers, 16(2), 277-288.

[26] Bate, R. , Mueller, B. , white, J. (1971*). Fundamentals of Astrodynamics*. Dover Publications, Inc. New York.

[27] George, L.E. , Kos, L.D. "Interplanetary Mission Design Handbook: Earth to Mars Opportunities and Mars to Earth Opportunities, 2009-2024". NASA/TM 1998-208533.

[28] McInnes, C. R. (1999). *Solar Sailing : Technology, Dynamics and Mission Applications*. Chichester, UK: Springer-Praxis.

[29] Schaub, H., & Junkins, J. L. (2003). *Analytical Mechanics of Space Systems*. Reston, VA: American Institute of Aeronautics and Astronautics.

[30] Arnold, V. I., Kozlov, V. V., & Neishtadt, A. I. (1993). *Mathematical Aspects of Classical and Celestial Mechanics (2nd ed)*. Berlin: Springer-Verlag.

[31] Curtis, H. D. (2005*). Orbital Mechanics for Engineering Students (3rd ed.).* Amsterdam: Elsevier Aerospace Engineering Series.

[32] McInnes, C. R., & Simmons, J. F. L. (1992). *Solar Sail Halo Orbits I: Heliocentric Case*. Journal of Spacecraft and Rockets, 29(4), 466-471.

[33] McInnes, A. I. S. (2000). *Strategies for Solar Sail Mission Design in the Circular Restricted Three-Body Problem*.

[34] Nise, N. S. (2011). *Control Systems Engineering* (6th ed.). Hoboken, NJ: John Wiley & Sons, Inc.

[35] Ogata, K. (2010). *Modern Control Engineering (5th ed.)*. Boston, MA: Prentice-Hall

[36] Greenspan, T. (2014). *Stability of the Lagrange Points, L_4 and L_5*.

[37] Kalman, R. E. (1960). *Contributions to the theory of optimal control*, Bol. Soc. Mat. Mex. 2(5) 102-118.

[38] Ipsen, I. C. (2009). *Numerical matrix analysis: linear systems and least squares*. Philadelphia: Society for Industrial and Applied Mathematics.

[39] Datta, B. N. (2004). *Numerical Methods for Dense Problems*. Numerical Methods for Linear Control Systems. Retrieved February 26, 2017, from https://pdfs.semanticscholar.org/dfb7/d37ffc41c5d98f8c0312a2ff5939692b9043.pdfhttps://pdfs.semanticscholar.org/dfb7/d37ffc41c5d98f8c0312a2ff5939692b9043.pdf.

[40] Paige, C. (1981). *Properties of numerical algorithms related to computing controllability*. IEEE Transactions on Automatic Control, 26(1), 130-138.

[41] Eising, R. (1984). *Between controllable and uncontrollable*. Systems & Control Letters, 4(5), 263-264.

[42] Eising, R. (n.d.). *The distance between a system and the set of uncontrollable systems*. Mathematical Theory of Networks and Systems Lecture Notes in Control and Information Sciences, 303-314.

[43] Dooren, P. V. (1999). *Software for Control System Analysis and Design, Singular Value Decomposition*. Wiley Encyclopedia of Electrical and Electronics Engineering.

[44] Viswanathan, C. N., Longman, R. W., & Likins, P. W. (1984*). A Degree of Controllability Definition – Fundamental Concepts and Application to Modal Systems*. Journal of Guidance, Control, and Dynamics, 7(2), 222-230.

[45] Viswanathan, C. N., Longman, R. W., & Likins, P. W. (1984). *A Degree of Controllability Definition – Repeated Eigenvalue Systems and Examples of Actuator Placement*. The Journal of the Astronautical Sciences.

[46] Schmitendorf, W. E. (1984). *An Exact Expression for Computing the Degree of Controllability*. Journal of Guidance, Control, and Dynamics, 7(4), 502-504.

[47] Lee, H., & Park, Y. (2014). *Degree of Controllability for Linear Unstable Systems*. Journal of Vibration and Control, 22(7), 1928-1934.

[48] Summers, T. H., Cortesi, F. L., & Lygeros, J. (2016). *On Submodularity and Controllability in Complex Dynamical Networks*. IEEE Transactions on Control of Network Systems, 3(1), 91-101.

[49] Le, V., Li, X., Li, Y., Cao, Y., & Le, C. (2015). *Optimal placement of TCSC using controllability Gramian to damp power system oscillations*. International Transactions on Electrical Energy Systems, 26(7), 1493-1510.

[50] Bombardelli, C., & Peláez, J. *On the stability of the Artificial Equilibrium Points in the Circular Restricted Three-Body Problem*. Celest. Mech. Dyn. Astron.

[51] Grøtte, M. E., & Holzinger, M. J. (2016). *Solar Sail Equilibria with Albedo Radiation Pressure in the Circular Restricted Three-Body Problem*. Advances in Space Research.

[52] Montgomery IV, E. E., Garbe, G. P., & Heaton, A. F. (2003). *Places Only Sails Can Go*. Huntsville, AL: NASA Marshall Space Flight Center.

[53] Domingo, V., Fleck, B., & Poland, A. I. (1995). SOHO: *The Solar and Heliospheric Observatory*. The High Latitude Heliosphere, 81-84.